SEPT 1999 General

LIBRARY COPY

A SIMULATION MODEL FOR THE REGIONAL AQUIFER BENEATH THE PAJARITO PLATEAU

Progress report

2002

Elizabeth Keating, EES-5
Edward Kwicklis, EES-5
Marc Witkowski, EES-5
Tony Ballantine, EES-5

September 30, 1999

13303

Table of Contents

A SIMULATION MODEL FOR THE REGIONAL AQUIFER BENEATH THE PAJARITO PLATEAU 1

SUMMARY 4

Key model developments 4

Summary of model status 5

CHAPTER 1. OVERVIEW OF NUMERICAL FLOW MODEL IMPROVEMENTS 7

Numerical grid updates 8

Hydrostratigraphic Framework model updates 9

CHAPTER 2. ESTIMATING FLUXES AT MODEL BOUNDARIES 11

Summary of Previous Estimates of Recharge 12
- Chloride Mass-Balance Method 12
- Water-Budget Methods 14
- Ground-water modeling 16

Pre-Development Water Budget for the Los Alamos County area 17
- Precipitation and Evapotranspiration 18
- Streamflow 19
- Springflow 21
- Recharge Calculations 21

Recharge Estimates Used in This Work 25

CHAPTER 3. MODEL CALIBRATION 31

Steady-state calibration (predevelopment) 32
- Establishing Steady-State Calibration Targets 33
- Parameter Estimation 34
- Results 36
- Sensitivity 39

Transient simulations 41
- Compilation of hydrograph and pumping data 41
- Compilation of aquifer properties 42
- Simulating pumping 43
- Simulating water level changes since 1945 45

CHAPTER 4. MODEL EVALUATION 48

CHAPTER 5. SUGGESTIONS FOR FUTURE WORK 51

Hydrostratigraphic framework model 51

Permeability modeling 51

REFERENCES 53

LIST OF FIGURES 56

LIST OF TABLES 57

APPENDIX I. 71

Grid Generation Process for Orthogonal Structured Grids 71

Grid Generation Process to create Octree (OMR) grid 72

APPENDIX II. WITHDRAWAL DATA 73

Summary

This report describes the activities in FY99 relating to further development of a numerical model for the regional aquifer beneath LANL. In FY98, an initial geologic model for the Española Basin was generated, a steady-state flow model using FEHM was constructed, and preliminary calibrations were presented. The primary goals of the work in FY99 were to add improvements to the hydrostratigraphic framework model and boundary conditions, to refine the steady-state calibration, to simulate the transient response of the aquifer to pumping, and to increase the grid resolution in the vicinity of LANL to prepare for transport calculations. Two additional goals, to incorporate an updated geological model and to incorporate geochemical data, have been postponed to FY00.

Key model developments

1) Steady-state calibration. The steady-state simulations developed this year, in contrast to those presented in FY98, are focused on understanding pre-development conditions in the Española Basin. One result of this effort has been to provide much-improved estimates on fluxes into and out of both the basin model and the Pajarito Plateau. Adequately simulating fluxes are critical to both transient simulations and to transport calculations we expect to begin in the near future. Methods used to calculate fluxes for model calibration included a water budget calculation for the Pajarito Plateau, streamflow analysis for major streams within the basin, and chloride mass balance techniques for estimating recharge.

2) Transient calibrations. Much of the effort regarding transient simulations focused on compiling data, including pumping data, hydrograph data (for model evaluation), and pump test results. We also developed methodologies for accurately simulating pumping

on a numerical mesh using FEHM, explicitly incorporating information from the geological framework model to apportion withdrawals selectively to the most permeable units within a wellbore. Comparisons of predicted and observed water level changes in response to 50 years of pumping have shed new light on aquifer characteristics; the calibration process is ongoing.

3) Increased grid resolution on the Pajarito Plateau. It is our intent that the added benefits of using a basin modeling approach should not be offset by a diminished ability to model the fine details of flow and transport beneath the plateau. To achieve this, we imbedded a fine mesh within the relatively coarse basin model in the vicinity of LANL, resulting in a factor of four increase in resolution on the plateau. This allows more detail from the hydrostratigraphic model at the site scale to be incorporated into the flow model, and allows more detailed predictions of flow directions. The new numerical grid has required updating the steady state and transient flow calibrations; finalization of these calibrations awaits incorporation of the FY99 site-wide geologic model into the basin-scale model.

Summary of model status

To date, the bulk of model development has focused on compiling all available hydrologic and geologic data for the site and for the basin, developing a numerical framework that integrates these data, and a groundwater flow model that can be quantitatively evaluated based on comparisons with measurements. Our emphasis has been to provide a model that reflects our conceptual model to as full an extent as possible, based on decades of data collected within the LANL site and in the surrounding basin. The only category of data that has not been integrated is water chemistry data; this omission is important since much of the available data pertaining to the regional aquifer falls within this category. We intend to begin this integration immediately in FY00.

Once this process is complete, we are in good position to integrate more fully with the deep drilling program, by incorporating new permeability, water level and/or

geologic data quickly into the model and evaluate its significance in changing either the conceptual model upon which the numerical model is based and/or predicted flow directions or travel times. If requested, we can also use the model to inform data collection activities. We will also able now to provide transport calculations in support of risk assessment in the case that contaminants are discovered during drilling. The model has already been used to perform preliminary transport calculations of HE in the regional aquifer from TA-16 (Keating et al. 1999).

Chapter 1. Overview of numerical flow model improvements

We have made several significant improvements to our initial model (Keating et al. 1998) both to better represent the local hydrostratigraphy and hydrology and to develop the framework for simulating transport in the aquifer. (Keating et al. 1999). One category of model development relates to the hydrostratigraphic framework model, shown in Figure 1, and numerical grid. This year, we incorporated one update to the hydrostratigraphic framework model (January, 1999) that incorporated improvements to the deepest layers in the model. A second update, expected to be more significant than the first, is expected in October, 1999 (Bill Carey, EES-1, pers. comm.). We also incorporated two updates to the numerical grid. The first update, coincident with the geology update in January, implemented a change in the total depth of the model. The second update, August 1999, embedded high-resolution zones within the basin model to improve our ability to capture fine detail at the scale of the Pajarito Plateau. These changes to the hydrostratigraphy and numerical grid are described in more detail in a section below

A second category of model development is related to improving estimates of water flux at model boundaries. This work, described in detail in Chapter 2, consisted of compiling and interpreting hydrologic data from a variety of sources and calculating a water budget for the Pajarito Plateau. Application of these estimates to model calibration is described in Chapter 3.

The third category of model development is related to simulation of groundwater withdrawals in water supply wells. This activity required compiling a database of well locations, construction information, pumping history, and hydrographs documenting changes in water levels over 50 years. The process of mapping water supply wells onto a large numerical mesh and simulating pumping with FEHM required a substantial amount of code development, interfacing data files with FEHM input and output files. The development of this capability and subsequent transient flow model calibration is described in Chapter 3.

Numerical grid updates

Unfortunately, both the properties and the geometries of the hydrostratigraphic units within the saturated zone beneath the Pajarito Plateau are uncertain, due to sparse data below the water table. We have placed great emphasis, therefore, on building flow model and numerical grid generation capabilities that are independent of any particular model of hydrostratigraphy. With this capability, we can evaluate the response of flow and transport scenarios to various alternative conceptual models of plateau stratigraphy, and easily incorporate updates to the geologic model as the deep well drilling program proceeds. Our grid generation methods allow the stratigraphy to be honored in numerical grids of different resolution, so that comparison studies can be performed to test grid quality and to determine the resolution required for flow simulations.

As described in Keating (1998), generating a numerical grid for FEHM computations is a two-step process. First, a grid is generated to discritize the model domain (the saturated aquifer) with sufficient resolution to capture important stratigraphic and/or hydrologic details. Secondly, the hydrostratigraphic framework model is draped onto the grid using LaGrit software (Trease et al. 1996) and each node in the model domain is assigned to a hydrostratigraphic unit.

Our initial numerical grid, described in Keating et al. (1998), was an orthogonal structured grid. Dimensions and resolution of this grid are summarized in Table 1 (Version 6, 1998). Orthogonal grids are more efficient to compute on and are compatible with particle tracking algorithms, which are necessary for flow direction and transport calculations. This year, we made two improvements to this grid. The first, coincident with the first geologic update described below, consisted of removing all nodes deeper than 100m MSL (Table 1, Version 1, 1999). By comparing flow model results with those computed on the earlier grid (minimum depth = -1300m), we detected very little change. Our conclusion from this is that ignoring flow in the deepest third of the basin (below the deepest water supply wells) does not negatively impact our ability to simulate the flow in

the upper portion of the basin. This resulting decrease in the total thickness of the model allowed us, in a later version of the grid, to increase the x-y resolution in the model without reaching a prohibitively large total number of nodes in the problem.

A second grid update, August 1999, used Octree Mesh Refinement (OMR) methods to embed a high-resolution zone within the relative coarse basin grid (Table 1, Version 2, 1999). This grid is better suited to capture site-scale flow and transport process in areas of interest, while allowing boundary conditions from the regional model to be applicable without adversely affecting the computation time or the computer memory required to run the model. The outline of grid elements in the vicinity of LANL is depicted in Figure 2.

The x-y dimensions of the OMR were identical to previous grids, however, the total thickness of the model changed slightly. The OMR grid is 500 meters deeper and contains variable cell spacing in the vicinity of the Pajarito plateau and the Santa Fe well field. Outside these two areas, the x-y spacing is approximately 1 km; inside these areas grid resolution increases to 250 m. Vertical spacing is 50m above 1100m; 500m below. The lower z-resolution area is below the depth of the deepest water supply well in the basin. In total, the OMR grid contains 301,436 nodes and 1,688,457 elements. Further details of the grid generation process can be found in Appendix I.

Hydrostratigraphic Framework model updates

The initial hydrostratigraphic framework model for the basin was developed in 1998 using a combination of Stratamodel (Landmark 1998) and LaGrit software (Trease et al. 1996). This model contained 20 hydrostratigraphic units and was described in detail by Keating et al. (1998). Since then, one update has been incorporated. Hydrostratigraphy represented within Stratamodel was improved to better represent the deepest units in the model: the pre-Tertiary basement rocks. To improve their representation, we subdivided the unit into two separate units: a Precambrian unit which effectively serves as the impermeable basement to the flow system, and a Paleozoic/Mesozoic unit overlying the Precambrian in much of the western portion of the

basin. Stratamodel implementation was performed by EES-1 staff. One benefit to this separation is that includes better integration of geophysical data, which is critical to our understanding of the geometries of these deep units.

As described in Keating (1998), La Grit software was used to further subdivide three units within the Stratamodel representation (Precambrian, Paleozoic/Mesozoic, and Santa Fe group). The Santa Fe group was subdivided into six shallow units representing broad regions within the basin and one deeper unit (depth below 914 meters). All nodes within Precambrian and Paleozoic/Mesozoic units more shallow than 1214 were assigned to a separate unit to account for the possibility that more shallow rocks may be more fractured and hence more permeable than deeper rocks. These units are shown in Figure 3, along with information about the numerical grid resolution.

This year, additional subdivisions were added to the Santa Fe group in the vicinity of Pojoaque and Santa Fe to account for hydrogeologically significant permeability variations identified by Frenzel (1995). It was considered beyond the scope of this project to identify independent data to justify these new sub-divisions, since they were far from our primary area of interest, the Pajarito Plateau. We incorporated them into our model to improve calibration in the eastern portion of the basin.

In total, the current number of hydrostratigraphic units within the model is 21; 7 of these are relatively far from the Pajarito Plateau. All units are shown in map view in Figure 4. Table 2 describes the total volume of each hydrostratigraphic unit, for each of the three grids we have developed so far. Although, the largest-volume unit is the deep Precambrian basement, this unit is assigned a very low permeability and very thus only very small fluxes enter the basement. Other large volume units are the Santa Fe Group Rocks, which comprise the basin-fill sediments and serve as the regional aquifer for most of the basin, and the shallow crystalline rocks of the Sangre de Cristo Mountains. Many of the rock units on the Pajarito Plateau are very small in volume when compared to the basin as a whole.

Chapter 2. Estimating fluxes at model boundaries

Keating (1998) presented the rationale behind the regional flow model construction and specification of boundary conditions. To summarize, our model extends out to the natural boundaries of the regional flow system, which we define using a combination of structural, topographic, and hydrologic criteria. One advantage to this approach is that we can use regional data to better to define the large-scale flow system that will strongly affect local flow directions. More importantly, this approach allows us to place reasonable bounds on the total amount of water flowing through the system. This second point is discussed in greater detail below.

Correctly estimating the magnitude of fluxes through the aquifer beneath LANL is critical to our ability to assess fate and transport of contaminants, for several reasons: 1) recharge rates (flux from the unsaturated zone to the water table) will determine how quickly surface contaminants will reach the aquifer and how much dilution will occur, 2) fluxes within the aquifer will influence travel times, and 3) fluxes from the aquifer to discharge points (supply wells, springs, and outflow to the Rio Grande) will, in part, determine the potential risk to downstream users.

Through the process of flow model calibration, we evaluate the relationship between fluxes, water levels in wells, and permeability of aquifer materials. Of these three quantities, water levels in wells are usually the best known. Permeability is usually less well-known, in part due to sparse data and in part due to scaling issues, since permeability data is often collected at much smaller scales than typical model elements. If both fluxes and permeability are poorly constrained, there may be many models assuming various combinations of flux and permeability parameters that are equally consistent with observed water levels. This is problematic, especially if these models predict substantially different contaminant transport scenarios.

To address this problem of model non-uniqueness, we have devoted considerable effort to placing independent constraints on fluxes through the regional aquifer. The following section describes our efforts to place reasonable bounds on recharge rates and on groundwater discharge to streams within the basin. By incorporating independent

flux estimates into the model calibration process, we reduce the degrees of freedom in the problem and are able to focus more clearly on the validity of the hydrostratigraphic model and the relationship between permeability and water levels in the basin.

The boundaries of the Española Basin groundwater-flow model in large part follow topographic divides and, except for small areas near rivers entering or leaving the basin, are modeled as no flow boundaries (Figure 1). Consequently, recharge within the basin itself contributes most of the water to the flow system within the model area. Preliminary modeling of the basin has indicated that between 80 and 100% of the ground water within the Española Basin originates from local recharge (Keating et al., 1998, table 4). The likely dominance of local recharge in the water budget of the basin indicates that it may strongly affect values of other parameters estimated from the model such as hydraulic conductivity, ground-water fluxes, and ground-water travel-times and underscores the need for reliable recharge estimates. The purpose of this summary is to review published estimates of recharge that have been made for sub-areas within the basin and, if possible, develop a general model of recharge that can applied throughout the model area.

Summary of Previous Estimates of Recharge

Previous recharge estimates have been made using a variety of techniques. The basis for these techniques and the results of their application to areas within the Española Basin are described in the sections that follow.

Chloride Mass-Balance Method

Mountain-front recharge for the Santa Fe River, Rio Tesuque and Arroyo Hondo drainages on the western slope of the Sangre de Cristo Mountains was estimated by Anderholm (1994) using the chloride concentration of shallow ground water. Mountain-

front recharge includes focussed stream-channel recharge and diffuse bedrock recharge upgradient from the sampling location. Based on mass-balance principles, the concentration of chloride dissolved in precipitation relative to the chloride dissolved in ground water indicates the fraction of precipitation that escaped evapotranspiration to become net recharge. In areas with surface runoff, such as the drainages considered by Anderholm (1994), allowances can also be made for chloride that flows out of the drainage basin in surface runoff. Although simple in principle, application of the chloride mass-balance method was complicated by anthropogenic sources of chloride, such as septic system effluent and road salt, that may have been responsible for the highly variable ground-water chloride concentrations within the individual drainages (Anderholm, 1994, plate 1). The lower ground-water chloride concentrations within individual drainages were considered by Anderholm (1994) to be most representative of pre-development conditions. The chloride concentrations of ground water under pre-development conditions were estimated to be 4.0 mg/L in the Rio Tesuque drainage and 3.0 mg/L in the Santa Fe River and Arroyo Hondo drainages (Anderholm, 1994, p. 35), values which, when combined with an estimated effective chloride concentration in precipitation of 0.29 mg/L and estimated precipitation rates, were used to calculate recharge both with and without corrections for surface runoff. Corrected where necessary for surface runoff , the estimated recharge volumes were 2,320 acre-ft/yr for the Santa Fe River drainage, 690 acre-ft/yr for the Rio Tesuque drainage, and 830 acre-ft/yr for the Arroyo Hondo drainage (Anderholm, 1994, table 7), values that are 7.7, 3.2 and 9.7 percent of the total precipitation falling on these drainage basins (table 3).

In addition to estimating mountain-front recharge in the three drainages, Anderholm (1994) also estimated recharge rates in several arroyos and in low-elevation areas undissected by arroyos. Unsaturated-zone chloride and soil-moisture data from three boreholes in the undissected areas indicated recharge rates less than 0.1 mm/yr for the past 6,700 to 8,800 years and only slightly higher (1 to 2 mm/yr) recharge rates prior to these dates (Anderholm, 1994, fig. 7). The higher recharge rates indicated by the data from the deeper parts of the boreholes are presumed to represent pluvial conditions associated with the late Pleistocene. Similar unsaturated-zone data from beneath two arroyos gave average chloride concentrations for the soil water of 45.5 and 62.7 mg/L

(Anderholm, 1994, p. 24). Recharge estimates for the arroyos are difficult to make because the infiltration of runoff results in the application of an unknown amount of chloride at the ground surface. Assuming that the chloride in soil water beneath the arroyos resulted only from precipitation falling at the sampling sites, Anderholm (1994, p. 24) obtained lower-bound estimates of recharge in the arroyos of about 3 mm/yr. Anderholm (1994, p. 35) noted that ground water pumped from the regional discharge area at the Buckman well field had a chloride concentration of only about 5 mg/L, and therefore that arroyo recharge with an order-of-magnitude higher chloride concentration is probably insignificant to overall recharge within the Española basin. However, ground water from the Buckman well field has the most depleted deuterium and oxygen-18 values in the basin, indicating it may have been recharged under a climate that was cooler (and wetter) than the present-day climate (Anderholm, 1994, p.45). Thus, even if substantial arroyo recharge were occurring under the present climate, its absence in ground water at the Buckman field might be explained by the fact that it has not yet reached the discharge area. The presence of ground water with high chloride concentrations upgradient from areas with low chloride concentrations noted by Anderholm (1994, Plate 1) may be the result of one or more of several processes, including present-day arroyo recharge, or the variable depths of the flow paths taken by ground water recharged at different elevations combined with the variable depths of the sampling wells.

Water-Budget Methods

Water budgets were estimated for five drainage basins on the western slope of the Sangre de Cristo Mountains by Wasiolek (Wasiolek 1995). The basins included the Rio Nambe, Rio en Medio, Tesuque Creek, Little Tesuque Creek and Santa Fe River drainages. Recharge in these basins was calculated as the residual between measured or estimated values of precipitation minus the sum of surface runoff plus evapotranspiration.

Water budgets were calculated for winter, spring and summer/fall periods and summed to obtain annual totals. Effective precipitation was calculated for the winter months by adjusting the estimated precipitation to account for the sublimation of snow. Evapotranspiration was estimated with curves describing the seasonal relations between evapotranspiration and precipitation that had been established for the Rock Mountain region; these curves also accounted for the effects of slope aspect on evapotranspiration. Like Anderholm (1994), Wasiolek (1995) concluded that most recharge in the mountain drainages occurred during winter months, which were considered by Wasiolek to extend from October through February (Wasiolek, 1995, tables 7,11,15, 19 and 23). The estimated volumes of recharge and the percent of the total precipitation falling on the basins that becomes recharge are listed in table 3.

The recharge estimates made by Wasiolek (1995) for the Rio Tesuque and Santa Fe drainage basins are high compared to the estimates made by Anderholm (1994) for the same basins. Some of the discrepancy between the recharge estimates may by due to the fact that the two studies considered slightly different basin areas and precipitation amounts (Anderholm, 1994, table 7). More likely, the discrepancies for the recharge estimates for the two models arise from (1) the difficulty in choosing representative natural chloride concentrations when using the chloride-mass balance method and (2) the use of regional rather than site specific precipitation and evapotranspiration relations in the water-budget method. Wasiolek (1995, p. 13) stated that water-budget models based on climatic factors tend to overestimate the amount of actual recharge because they neglect the potentially limiting affects of bedrock permeability. On the other hand, Anderholm's (1994) selection of values of 3 to 4 mg/L as representative pre-development chloride concentrations was largely based on subjective judgement and would be difficult to reproduce objectively from the available data. Assuming that the representative pre-development chloride concentration of each basin considered by Anderholm (1994) is 2 mg/L and that other parameters are as given in table 7 of Anderholm (1994), the runoff-corrected recharge estimates are 3,780 acre-ft/yr in the Santa Fe River drainage, 2250 acre-ft/yr in the Rio Tesuque drainage basin and 1,240 acre-ft/yr in the Arroyo Hondo drainage basin. A pre-development chloride concentration of 2 mg/L is similar to spring surface runoff in the Santa Fe River drainage (Anderholm, 1994, Table 4), and is an

equally plausible value for a representative chloride value given the variability of the ground-water chloride concentrations.

Ground-water modeling

Ground-water flow in the southern part of the Española Basin was previously modeled by McAda and Wasiolek (1988) and by Frenzel (1995). The model of Frenzel was essentially a refinement of the model previously developed by McAda and Wasiolek (1988). Their model domains extended from near the city of Española on the north, La Cienaga on the south, the Pajarito Fault on the west and contact between the basin-fill materials and the Pre-Cambrian bedrock on the east. The authors of these studies compiled estimates that had been made for various components of the ground-water budget in the model area and integrated the estimates into their numerical models. A successful match between measured hydraulic heads within the model area and hydraulic heads simulated by the models using the estimated values for terms in the water budget indicated the reasonableness of the estimates. The water budget used for the predevelopment steady-state simulation by McAda and Wasiolek (1988) is shown in table 4. The value in Table 4 for east mountain-front and stream-channel recharge includes 4.3 cubic feet per second (cfs) in the upper reaches of the Rio Tesuque, a combined 4.0 cfs along the upper reaches of the Rio en Medio and Rio Nambe, 7.5 cfs along the upper reaches of the Santa Fe River, and 0.7 cfs for the upper reaches of the Arroyo Hondo (McAda and Wasiolek, 1988, fig. 9 and table 2) in addition to the diffuse recharge from the mountains entering along the eastern model boundary. These values of recharge were input as specified fluxes in the model. The lower reaches of Rio Tesuque, Rio en Medio, Rio Nambe and the Pojoaque River were predicted by the model to receive ground-water discharge totaling 7.3 cfs. Fluxes to the Rio Grande in the model were a function of the simulated heads. Ground water was predicted to discharge to the Rio Grande at all but the two southernmost nodes in the model area. Net discharge to the Rio Grande was 37.4 cfs for the approximately 26 mile reach of the of the Rio Grande extending from Española south to about 6 miles south of Frijoles Canyon. Areal recharge

was estimated to be 10.6 cfs or 14.4% of the total inflow to the model area, with rates ranging from 0.05 to 0.4 inches per year. In particular, areal recharge rates on the Pajarito Plateau were estimated by McAda and Wasiolek (1988, fig. 13) to be 0.15 inches per year. The nonzero recharge rates in the low elevation areas within the basin can be reconciled with the conclusion of Anderholm (1994) that recharge in the undissected areas is zero by noting that the low elevation areas are criss-crossed by numerous arroyos that probably contribute some recharge. Recharge rates used by Frenzel (1995, fig. 14) were generally smaller than recharge rates assumed by McAda and Wasiolek (1988). Frenzel (1995) assumed that recharge on the Pajarito Plateau was only 0.02 inches per year.

Pre-Development Water Budget for the Los Alamos County area

A pre-development water budget was calculated for the area bounded by Santa Clara and Frijoles Creeks, the Rio Grande, and the western boundary of Los Alamos County (Figure 5) using an approach similar to that described in Wasiolek (1995). The water-budget study area includes all of Los Alamos County as well as neighboring areas north, south and east of the county. The conceptual framework for the analysis is outlined in Figure 6. Recharge is assumed to equal the difference between precipitation and evapotranspiration minus the difference between surface-water outflow and inflow:

$$R = P - ET - (S_o - S_I)$$

Where P is precipitation, ET is evapotranspiration, and S_o is surface-water outflow from and S_I is surface-water inflow to the water-budget study area. When the term $(S_o - S_I)$ is positive, the net outflow from the area represents the runoff of local precipitation that becomes unavailable for recharge. When the term $(S_o - S_I)$ is negative, it represents the

net amount of water that has entered the area as streamflow and infiltrated into the stream channels. The equation implicitly assumes that the water that infiltrates beneath the channels does not evaporate, an assumption which is reasonable for perennial streams but which may not be valid for ephemeral streams where the streambed is periodically exposed to the atmosphere. The water balance equation may be further modified to account for springflow:

$$R = P - ET - (S_o - S_I) - Q_{sp}$$

where Q_{sp} is the total springflow discharging from perched springs within the area. Discharge from perched springs represents rejected recharge, that is, infiltration that escaped evapotranspiration but does not reach the water table because geologic controls on permeability force the water to the land surface. The possibility exists that springs could discharge water to streams and thereby be counted twice in the water-balance equation. However, as will be shown, values for the streamflow and springflow terms in the equation are small compared to the difference between P and ET. Additionally, most of the larger springs in the water-budget study area are downgradient from the gaging stations and are discharging from the regional ground-water system.

Precipitation and Evapotranspiration

To calculate the water balance, elevation classes were defined and the area falling within each elevation class was determined from topographic maps. These areas were then assigned to the average elevations within the classes (table 5). Precipitation was distributed with elevation using the correlation between precipitation and elevation presented in Figure 7, and seasonally, based on monthly precipitation averages calculated from data collected at Los Alamos between 1942 and 1998. It was assumed that monthly precipitation varied with elevation in the same way as the annual precipitation. The monthly precipitation in each elevation class was then summed according to season:

winter (October to February), spring (March to June), and summer/fall (July to September). The seasonal evapotranspiration was estimated using curves in Wasiolek (1995, figs. 6-8) which relate evapotranspiration to precipitation, thereby serving to distribute evapotranspiration with elevation as well as with season (Table 5). Evapotranspiration curves for east-west slope aspects were used in the calculations. Although east-trending canyons locally create slopes with north and south aspects, this level of detail was not considered in this analysis. Annual and seasonal totals for precipitation, evapotranspiration, and the difference between precipitation and evapotranspiration were calculated by summing the area-weighted values across elevation classes.

The results of Table 5 show that most precipitation falls in the summer/fall season and at higher elevations. However, except for elevations greater than about 8500 feet, all of the summer/fall precipitation, as well as some soil moisture originating from precipitation in the previous winter and spring, is consumed by evapotranspiration. The potential for recharge, indicated by a positive difference between seasonal precipitation and evapotranspiration, is greatest during winter when evapotranspiration is smallest, and at higher elevations. On an annual basis, the negative values for the difference between precipitation and evapotranspiration indicate that no net recharge is expected to take place below about 6500 feet. The total annual difference between precipitation and evapotranspiration is estimated to be 1.5 inches. This value represents the average depth of the recharge applied evenly across the water-budget study area, unadjusted for springflow or surface runoff.

Streamflow

The net amount of water entering or leaving the study area as streamflow ($S_o - S_I$) was calculated using the average annual streamflow totals from gaging stations located within the boundaries of Los Alamos National Laboratory for the water years 1995 to 1998 (Figure 8)(Shaull et al. 1996a; Shaull et al. 1996b; Shaull et al. 1998; Shaull et al.

1999). Based on precipitation data recorded at Los Alamos since 1942, these were years of about average annual precipitation. Although not all streams are gaged, it is assumed that flow on the ungaged streams is comparatively small. The differences between outflow and inflow along individual canyons traversing the laboratory are given in Table 6. When the headwaters of streams are within the water-budget study area, inflow is estimated to be zero even if gaging stations located upstream from the outflow station along a particular stream had recorded some flow for the year. The outflow from the laboratory boundaries totals 2.42 acre-feet/year and the inflow totals 231.4 acre-feet/year. The difference in these values, 229 acre-feet/year, is estimated to be the stream-focussed recharge within the laboratory boundaries. Most of this stream-focussed recharge occurs in Los Alamos Canyon (130.5 acre-feet/year) or Pajarito Canyon (90.1 acre-feet/year).

Streamflow measurements made near their mouths also are available for Frijoles Creek from 1982 to 1995 and for Santa Clara Creek from 1936 to 1993 (Reference). Average annual flow is 1543 acre-feet/year on Frijoles Creek and 2901 acre-feet/year on Santa Clara Creek. Treatment of the flow in these streams in the water-budget analysis is problematic because streamflow measurements on these streams are few near the upgradient boundaries of the water-budget study area and because parts of the drainage basins of these streams exist outside the boundaries of the study area. Based on streamflow measurements made during 1977 and 1978, Purtymun and Adams (1980) reported that base flow for Frijoles Creek primarily is from springs emerging from welded tuff as the canyon cuts into the slopes of the Sierra de los Valles near the boundary of the water-budget study area. Because of uncertainty regarding the source of the water for these springs and because no similar observations were known to the authors about the source of the baseflow in Santa Clara Canyon, flow on Frijoles and Santa Clara Creeks is treated several alternate ways in the water-budget analysis, as described in the section "Recharge Calculations".

Springflow

Springs within the water-budget study area discharge from both perched water and from the regional ground-water system. Most of the springs discharging from the regional ground-water system are located at low elevations near the Rio Grande. Purtymun (1980) estimated that 3 of the 15 cfs increase in flow between Otowi Bridge and Frijoles Canyon originated from springs discharging near the river, primarily in White Rock Canyon. Although these springs discharge above the elevation of the river, their outflow, for practical purposes, is part of the baseflow to the river. In contrast, the fate of the outflow of springs discharging from perched water high on the Pajarito Plateau is less certain. The total discharge of these springs is estimated to be 0.2 cfs (145 acre-feet/year) (Table 7), but this value should be viewed with caution. In many cases, the sampling frequency of the springs discharging from perched water may have been inadequate to fully characterize the temporal variability in flow rates that might be expected for these springs. Compared to the springs discharging from the regional ground-water system, springs discharging from perched water would be expected to have more variability in their flow rates because the elevation of the perched-water surface relative to the spring orifices could change rapidly as a result of infiltration from storm events and the relatively small volume of the perched water.

Recharge Calculations

Recharge under pre-development conditions was calculated in two ways in order to account for uncertainty in hydrological significance of the flow in Santa Clara (2901 acre-feet/year) and Frijoles (1543 acre-feet/year) Creeks. Although neither of these cases is considered to be completely realistic, they may serve to bound the possible recharge for the study area.

In the first case, flow in Santa Clara and Frijoles Creeks was treated as if the entire annual discharge of these streams originated from surface runoff or from the

discharge of perched water within the study area. For this case, the total discharge of these streams (4444 acre-feet/year) is added to the streamflow totals of the streams within the boundaries of LANL (-229 acre-feet/year):

$$R = 137{,}060 \text{ acre-ft/yr} - 123{,}122 \text{ acre-ft/yr} - 4215 \text{ acre-ft/yr} - 145 \text{ acre-ft/yr}$$

$$= 9{,}578 \text{ acre-ft/yr (1.0 inches/year or 26 mm/year).}$$

In the second case, flow on Santa Clara and Frijoles Creeks was ignored in the calculation, implying that the source of the measured flow on these streams was either outside the study area or, perhaps, that most of the flow in these streams originated as discharge from the regional aquifer system in the lower reaches of these streams where the flow measurements were made:

$$R = 137{,}060 \text{ acre-ft/yr} - 123{,}122 \text{ acre-ft/yr} - (-229 \text{ acre-ft/yr}) - 145 \text{ acre-ft/yr}$$

$$= 14{,}022 \text{ acre-ft/yr (1.5 inches/year or 38 mm/year)}$$

It can be noted that both of these estimates are high compared to the areal distributed recharge rate of 0.02 inches per year assumed by Frenzel (1995) and the rate of 0.15 inches per year assumed by McAda and Wasiolek (1988) for an area overlapping with the current water-budget study area. The water budget estimates also appear high based on analyses by Rogers et al. (1996), which noted that the volume of groundwater pumped on the Pajarito Plateau approximately equals the volume of the cones of depression associated with pumping fields on the Plateau. This observation indicated to Rogers et al. (1996) that little recharge had reached the regional ground-water system since pumping began in the 1940's. The plausibility of the estimates resulting from the water-budget analysis is further evaluated in the following paragraphs.

Chloride concentrations and discharge measured at twenty-three springs in White Rock Canyon in the early 1960's by Purtymun (1980) result in a discharge-weighted

chloride concentration for the springs of 4.2 mg/L. Twenty of the twenty-three springs were on the west side of the Rio Grande. The chloride concentrations of these springs may be an appropriate indicator of the average recharge in the water-budget study area because the springs mix and discharge water that was recharged over a large area. Furthermore, δ^2H and $\delta^{18}O$ data for the springs collected during subsequent studies indicates that most of the estimated recharge elevations are between 6500 and 9,800 feet (Blake et al., 1995, table 6), which places most of the recharge within the elevation range of the study area. Using the chloride mass-balance equation ($PC_p = RC_r$) and assuming an average precipitation for the study area of 14.75 inches per year, an average chloride concentration in precipitation (C_P) of 0.29 mg/L, as measured at Santa Fe airport by Anderholm (1994), and a chloride concentration for the recharge (C_r) of 4.2 mg/L gives a calculated recharge rate of

$$R = (14.75 \text{ inches/yr})\ (0.29 \text{ mg/L}) / (4.2 \text{ mg/L}) = 1.0 \text{ inches/year}$$

The recharge rate of 1.0 inch per year calculated from the chloride concentrations of the springs is consistent with the case1 water-budget estimate, but indicates that the case 2 water-budget estimate is too high.

A second check on the plausibility of the water-budget recharge estimates is provided by the gain in flow along the Rio Grande adjacent to the study area. Based on stream-gaging records from 1926 to 1969, the mean gain in January flow in the Rio Grande for the 26-mile reach between Otowi Bridge and Cochiti Reservoir is 13 cfs, or 0.5 cfs per mile (see section "Recharge Estimates Used in This Work"). Applying the same rate of gain to the entire 28-mile reach adjacent to the water-budget study area results in a gain of 14 cfs or 10,143 acre-feet per year. This does not account for the 1.2 cfs mean January discharge from Frijoles Creek. The Case 2 water-budget estimate for recharge of 14,022 acre-feet per year exceeds the total estimated gain to the river and is therefore discounted. The Case 1 water-budget estimate of recharge of 9,578 acre-feet per year for the study area indicates that about 94% of the gain in flow is due to recharge in the water-budget study area, with the remainder of the baseflow gain due to the discharge of groundwater recharged east of the Rio Grande and to the discharge of

groundwater flowing beneath the Pajarito Plateau from the Jemez Mountains west of the study area to the Rio Grande. The large disparity in the implied magnitudes of the discharge originating from west and east of the Rio Grande indicate that, despite the agreement with the chloride mass-balance analysis, the estimate of the Case 1 water-budget analysis is also too high.

One possible source of error in the water-budget analysis is the use of generic evapotranspiration/precipitation relations developed for alpine forests in the Rocky Mountains. These relations may be particularly inappropriate for lower elevation areas within the study area where desert vegetation such as juniper and gamma grass dominate. However, desert species are expected to be more conservative in their use of water than alpine species and the transpiration of desert vegetation would be less than assumed in the present analysis. In any event, Table 5 shows that the calculated annual difference between precipitation and evapotranspiration is already negative below about 6500 feet, indicating that no recharge occurs below this elevation in the analysis. Thus, the use of evapotranspiration relations more appropriate to desert species can only cause an increase in the estimated recharge below 6500 feet. The use of non-site-specific evapotranspiration/precipitation relations might also have introduced errors into the water-budget analysis. However, the use of site-specific evapotranspiration/precipitation relations based on data from Technical area 6 (TA-6) at LANL resulted in even higher recharge estimates than those described in this section, primarily because summer evapotranspiration rates were locally at least one-third lower than the maximum rates in the curves used by Wasiolek (1995). A third possible source of error, and possibly the most likely one given the dominance of winter recharge in the analysis, is the neglect of possible sublimation of snow, which effectively reduces the winter precipitation rates. Wasiolek (1995, p. 18) reduced precipitation by 50 percent in treeless areas to account for the greater importance of sublimation in areas more likely to be affected by strong winds. Winter precipitation was estimated to be reduced by 5 to 39 percent by sublimation, primarily at elevations above treeline. Although the Los Alamos County area does not extend above treeline, there are areas where trees are sparse and wind-enhanced sublimation might be an important factor.

Recharge Estimates Used in This Work

The lateral boundaries of the models used by McAda and Wasiolek (1988) and Frenzel (1995) coincided with the contact between the basin-fill sediments and the bedrock forming the surrounding mountains. In their models, high-elevation recharge in the mountains of the basin was represented by specified fluxes along the model boundaries corresponding to the basin fill/bedrock contact ("mountain-front recharge") and, therefore, not explicitly considered as areally distributed recharge. In contrast, the lateral boundaries of the present model generally correspond to topographic divides, which are assumed to also represent ground-water divides, and high- as well as low-elevation recharge is represented as specified fluxes along the upper boundary of the model. The benefit of the approach taken in the present model is that the model explicitly tracks the movement of water from the point of recharge; the drawback of this approach is that recharge estimates must be explicitly provided for a larger area, including areas for which no recharge data exist.

An important constraint on the total recharge to the basin is provided by measurements of flow in the Rio Grande and its tributaries at various locations throughout the basin. The Rio Grande and the low elevation reaches of its tributaries constitute the discharge areas for groundwater in the basin. Assuming that the ground-water system is at steady-state, the downstream increases in streamflow that arise because of discharge from the aquifer are equal to the recharge in upgradient areas in the basin. The component of the streamflow contributed by aquifer discharge, also known as baseflow, was calculated using data from the U.S. Geological Survey stream-gaging network shown in Figure 9. In general, baseflow along a particular reach was calculated by subtracting the sum of the flow at the upstream gaging station and any gaged tributaries along the reach from the flow measured at the downstream gaging station defining the reach. The calculations were done using mean streamflow data for January, a time when streamflow rates and absolute measurement error were low, and overland flow and evapotranspiration rates were at a minimum. It should be noted that for some small streams, such as those monitored by stations 83215000 and 8279000, there was no gaging station in the upstream parts of the reach. However, because the headwaters of

these streams are within the basin, flow into the basin along these streams are zero and, therefore, baseflow can simply be assumed equal to the January streamflow rate measured at the downstream station defining the reach.

The results for different reaches exhibit substantial year-to-year variability for the period of record (Figure 10). Nonetheless, the calculated mean differences for the defined reaches are consistently positive (Table 8) indicating that, as expected, discharge from the aquifer is augmenting flow along each individual reach. (Note that the discharges in figure 10 are in kilograms per second, the units used by he numerical model, whereas the summary statistics are given in cubic feet per second, the unit of stream discharge familiar to most hydrologists.) Neither the baseflow estimates nor their standard errors reflect the effects of ungaged tributaries along these reaches. Although most ungaged tributaries probably do not contribute much flow during January, this has not been verified by reconnaissance. The total gain is estimated to be 115.2 cfs with a total standard error of ±1.7 cfs. These values suggest that, at a 95 percent confidence level, total baseflow in the basin could be zero. However, most (71.7 cfs) of the total standard error is associated with the Española to Otowi reach. If this reach is neglected, the total gain for the remaining reaches becomes 83.8 cfs and the total standard error becomes 10 cfs, so that minimum recharge to the basin is between 60 and 100 cfs with a high degree of certainty. Not included in these baseflow totals are the 7.3 cfs estimated by McAda and Wasiolek (1988) to discharge along lower Pojoaque Creek and its tributaries.

Although the total recharge to the basin is known reasonably well from the streamflow gains, its areal distribution is less certain. Field characterization of recharge throughout the basin was beyond the scope of this study. However, several observations indicate that recharge throughout the basin depends strongly on elevation: (1) A strong correlation exists between precipitation and elevation (see Figure 7); (2) Vegetation zones are strongly correlated with elevation (Spiegel et al. 1963, p. 17); and (3) In local water balance studies within the basin, the difference between precipitation and estimated evapotranspiration increases with elevation (for example, Wasiolek, 1995). To account for the these observations and have a general recharge model that could be applied throughout the basin, an elevation-based recharge model similar to that described in Duffy and Al-Hassan (1988) was used:

$$R = P(z)\,\alpha \qquad \text{for } z > z_{max}$$

$$R = P(z)\,\alpha\,(z - z_{min})/(z_{max} - z_{min}) \qquad \text{for } z_{min} < z < z_{max}$$

$$R = 0 \qquad \text{for } z < z_{min}$$

Where

R = recharge;

Z = elevation;

P(z) = precipitation as a linear function of elevation;

α = the maximum fraction of precipitation reaching the water table;

z_{max} = elevation above which $R = P(z)\,\alpha$; and

z_{min} = elevation below which R = 0.

The equations indicate that recharge increases as a parabolic function of elevation between z_{min} and z_{max} and is a linear function of elevation above z_{max}. Various combinations of values of z_{max}, z_{min}, and α can be selected that reproduce the estimated total recharge to the basin of approximately 100 cfs. However, as described in the following paragraphs, different lines of evidence are inconclusive and even somewhat contradictory regarding the steepness of the recharge gradient.

Geochemical data tabulated in Blake et al. (1995) were examined in an attempt to characterize the relation between recharge and elevation and thereby constrain the range of possible parameters in the recharge model. Potentially useful data for this purpose are deuterium, oxygen-18, and chloride.

The condensation temperature strongly influences the isotopic content of hydrogen and oxygen in precipitation and causes the standardized ratios of deuterium (δ^2H) and oxygen-18 ($\delta^{18}O$) in precipitation to become more depleted, relative to seawater, at higher elevations. A correlation between recharge elevation and δ^2H and $\delta^{18}O$ content was established for the Jemez Mountains by Vautez et al.(1986) using data

from springs. This correlation was used by Blake et al. (1995, Table 4) to assign recharge elevations to surface-, spring- and ground-water samples in the basin. The data in Blake et al. (1995) were culled to remove samples that, based on Blake et al.'s (1995) criteria (NO_3^- > 5 mg/L, SO_4^{2-} > 20 mg/L, PO_4^{2-} > 0.1 mg/L, Pb > 0.01 mg/L, and ClO_3 > 0.11 mg/L) were likely to have been contaminated by human activities. After further discarding all surface water samples and subsurface water whose estimated recharge elevation was lower than their sampling elevation, a data set was obtained whose chemistry was likely to have be unaffected by anthropogenic sources and whose estimated recharge elevations were at least grossly consistent with their sample elevations. The chloride concentration of these samples are plotted against their δ^2H and $\delta^{18}O$ values in Figures 11a and 11b. The chloride concentrations do not show any obvious correlation with δ^2H or $\delta^{18}O$ and, except for a few outliers, are fairly constant over a relatively wide range in isotopic values. This observation implies that although recharge may increase because of increases in precipitation with elevation, the percentage of precipitation that becomes recharge is constant with elevation. These conclusions are illustrated in Figures 12a and 12b, which show the results of applying the chloride mass-balance method to data shown in the previous figures. The analysis assumes that the chloride concentration of precipitation is 0.29 mg/L (Anderholm, 1994), that precipitation is adequately described by the precipitation/elevation relation presented in Figure 7, and that the recharge elevation is the average of those estimated from δ^2H and $\delta^{18}O$ in Blake et al. (1995, table 4). Chemical analyses of the precipitation for the Pajarito Plateau reported by Adams et al. (1995) are also available, but were not used in this analysis. Although the use of these data is not expected to substantially alter the conclusions of the present analysis, this assumption needs to be verified.

No samples in figures 8a and 8b have estimated recharge elevations lower than 2000 m (6562 ft.) and few samples have estimated recharge elevations higher than 3000 m (9843 ft.). Although this could be interpreted to mean that recharge only occurs within a relatively narrow elevation range, an alternative explanation is that the inferred range in recharge elevations has been narrowed by mixing of groundwater either in the wellbore or as a result of hydrodynamic processes. The percentage of precipitation that becomes recharge generally varies between 1 and 20 percent with an average value of about 10

percent, and actual recharge is generally estimated to be less than 4 inches per year at any elevation. The assumption that recharge above 6500 feet is 10 percent of precipitation results in an estimated recharge of 235 cfs to the basin, more than twice the discharge estimated from the streamflow data. The recharge estimates based on chloride may be higher than the actual recharge because the estimates neglect the possible effects of surface runoff, which would result in less total chloride entering the soil zone than would be estimated from precipitation. However, this effect is probably small because most of the samples originate on the west side of the basin where streamflow volume is very low.

An attempt to calibrate the parameters of the recharge model also was made using the results of Wasiolek's (1995) water-budget analysis and her estimates of the elevation distribution within each of the drainage basins. A trial-and-error match to the data using z_{max} = 9,000 feet, z_{min}= 5,500 feet, and α=0.125 provided the best overall fit to her results (Fig. 13). Because these results were obtained by trial-and-error, it is possible that another set of recharge parameters would result in a match as good or better than the one presented. The result that recharge increases parabolically over much of the elevation range of the drainage basins is not surprising given the relations between precipitation and evapotranspiration Wasiolek (1995) used in the analysis. These relations indicate that with increasing precipitation rates (and correspondingly increasing elevations) a larger fraction of the precipitation escapes evapotranspiration. Using z_{max} = 9,000 feet, z_{min}= 5,500 feet, and α =0.125, recharge for the entire basin was estimated to be 224 cfs, which is again about twice the discharge estimated from the streamflow data. Either the recharge estimates made by Wasiolek (1995) are too high, as suggested above in the review of previous estimates, or the recharge model based on her results cannot be generalized to the rest of the basin.

The total recharge to the Espanola Basin is reasonably well-constrained by the estimated discharge to river and streams in the basin, although its distribution is only qualitatively known. Because of this uncertainty, three recharge models were selected for use in the calibration, each of which has a total recharge of approximately 97 cfs. Included in the total recharge is the approximately 16 cfs that is applied as focussed recharged along streams in the lower Sangre de Cristo Mountains. This estimate of the stream-focussed recharge was taken from McAda and Wasiolek (1988, table 2). The

remainder (approximately 81 cfs) was applied as diffuse recharge using equation (1). The recharge parameters for the three cases are given in Table 9. In case 1, recharge increases parabolically with elevation between 6,000 and 9,000 feet and linearly above 9,000 feet (Fig.14a). In case 2, recharge increases linearly with elevation throughout the elevation range of the basin above 6,000 feet (Fig 14b), which is consistent with the conclusion of the chloride analysis that recharge is a constant fraction of precipitation over a wide range of elevations. The rate of increase in recharge with elevation is slow and recharge is relatively uniformly distributed with elevation. In Case 3 (Fig. 14c) recharge at first increases slowly with elevation and then more abruptly at high elevations. The decrease in z_{min} to 5,500 feet (the lowermost part of the basin) in Case 3 is intended to qualitatively account for recharge along arroyos that was inferred by Anderholm (1994) from soil chloride profiles.

The areal distributions of recharge for the three cases are shown in Figure 15. The average recharge within the boundary of Los Alamos National Laboratory is 0.26 inches for the case 1 recharge model, 0.55 inches for case 2, and 0.29 inches for case 3. In the pre-development water-budget study area, the average recharge is 0.22 for the case 1 recharge model, 0.40 inches for case 2, and 0.24 inches for case 3.

Chapter 3. Model calibration

Our overall approach is to begin with a steady-state calibration of pre-development flow conditions within the basin, and then to simulate withdrawals from the aquifer due to pumping and evaluate response of predicted water levels. This comprises two separate flow modeling activities, although they were coupled since both models must assume identical aquifer characteristics such as permeability and the steady-state model provides the initial condition for the transient model.

A very common approach to model calibration is to allow all model parameters to vary freely with the intent to best match model predictions with observations. One example of this approach, is the model calibration presented by Frenzel (1995) who made adjustments to recharge rates and permeability zone definitions (placing small scale permeability zones around individual groups of wells) in order to better fit water level data. Little independent data was presented (geologic or otherwise) to support these changes. If executed successfully, this approach will produce excellent agreement between model predictions and observations. However, this approach suffers from the problem of non-uniqueness described above and is of limited value in shedding light on the fundamental processes and conceptual model upon which the model is based.

Two primary goals for our regional flow model development are 1) to accurately simulate the flow field in the vicinity of LANL, and 2) by integrating geologic and hydrologic data, serve as a quantitative tool for interpreting these data and evaluating various alternative conceptual models of flow and transport. As we collect new geologic and hydrologic data with the deep drilling program, we expect to gradually approach the first goal. To meet the second goal, our model must be process-based so that the degree of agreement or disagreement between model predictions and observations can be used to re-evaluate our conceptual model and to inform future data collection. This is a very different approach to the one described above. One implication of this approach is that both agreement and disagreement between model predictions and observations are valuable, in that they inform us about the strengths and weaknesses of our conceptual model for the regional aquifer and the adequacy of our hydrogeologic dataset.

The model calibrations described below should not be understood to be "final". Implementing the OMR grid recently (mid-August) required that we re-calibrate both the steady-state and transient flow models. The optimized parameter sets described below were, in fact, derived from calibrations on the older, coarser grid and are currently being updated through calibrations on the OMR grid. We expect residuals to decrease with this approach. In addition, we expect a new hydrostratigraphic model within a month (Carey, pers. comm.). Again, this will require re-calibration of the model and hence results may change.

Steady-state calibration (predevelopment)

Implicit in the calibration approach is the assumption that pre-development conditions, once adequately described, represent a steady-state condition. This assumption is difficult to evaluate because hydraulic head data from the pre-development period are too sparse to determine if heads throughout the basin were responding to either long-term or short- term climate fluctuations that existed in the past. The assumption that the flow system is at steady-state is a necessary one, however, because no quantifiable data exist concerning how recharge rates, streamflow, and ground-water levels in the past may have differed from those of the present. The assumption that the ground-water system is at steady-state is also a convenient one because, at steady-state, the flow system is independent of the storage of the aquifers and the effects of permeability on the flow system theoretically can be isolated from those of the storage terms.

The pre-development ground-water conditions in the Española Basin were estimated from the early part of the hydrologic record for the basin, which includes water-level measurements made in domestic and public water-supply wells and stream flow measurements made at various gaging stations in basin. Frenzel (1995) noted that, although the earliest part of the hydrologic record may provide the best approximation to pre-development conditions, the ground-water system may have already been substantially altered from its original state by the time enough data has been collected to

provide an adequate description of the system. Indeed, the estimated gains in streamflow attributed to ground-water discharge seem to show temporal trends that, although weak, may reflect the effects of ground-water development (see Fig 10). Another difficulty in estimating pre-development conditions relates to the fact that different parts of the basin were developed at different times, so that data in some parts of the basin were not available until after other parts of the basin had already undergone substantial development. In this study, the requirement that measurements reflect undisturbed conditions was balanced by the need for geographic coverage and the data from later periods also was used to characterize the pre-development conditions.

In summary, the data used to characterize the pre-development state of the flow system span different time periods. The water-level data used to create a map of the pre-development potentiometric surface generally were obtained in the 1940's and 1950's, except in the northern one-third of the basin, where the need for geographic coverage overrode requirements that the data represent undisturbed conditions, in which case data from a later period was used. Streamflow data were collected over various periods in the basin, as gaging stations maintained by the U.S. Geological Survey were added to or dropped from the network of stations in the basin. Baseflow estimates based on streamflow gains could be made only for periods in which data from all the relevant stations contributing to the calculation were available.

Establishing Steady-State Calibration Targets

Model calibration proceeded by adjusting values of permeability of different hydrogeologic units in the model within data-defined ranges until a reasonably good match between measured and simulated quantities that characterize the flow system was achieved. The measurements, hereafter referred to as observations, were replicated both through a trial-and-error approach and by using an automated optimization program named PEST (Watermark Computing 1994). The application of PEST will be discussed in the following section.

The observations used as calibration targets included (1) pre-development ground-water heads, (2) the estimated baseflow to various reaches of rivers and streams, and (3) permeability measurements of the hydrogeologic units. The pre-development ground-water heads used as observations are given in Table 10, along with other data relevant to the measurements. The potentiometric surface contoured from these data (fig. 16) indicates that ground water generally moves from the upland areas along the western, northern and eastern margins toward the rivers in the central part of the basin. The baseflow to a particular reach of a stream or river was assumed to be equal to the mean increase in January streamflow along the reach (Table 8). Estimates of the permeabilities determined from field-scale hydraulic tests are summarized by hydrogeologic unit in Table 11. The base-ten logarithm of the mean permeabilities listed in Table 11 also were used as observations in the calibration.

Parameter Estimation

PEST uses the Gauss-Marquardt-Levenberg algorithm to minimize the sum of the squared-weighted residuals between the measurements and the simulated values, a quantity also known as the objective function. Minimization of the objective function proceeds by systematically varying the model variables or parameters in a manner that is indicated by the derivative of the objective function with respect to the parameter, with appropriate constraints imposed on the process to ensure stability and speed convergence on an optimal set of parameter values. The details of the optimization procedure are given in chapter 2 of the PEST user manual (Watermark Computing, 1994).

PEST requires that weights be given to the various observations. In formal mathematical terms, these weights are inversely proportional to the standard deviations of the measurements to which they are applied (Watermark Computing, 1994, p. 2-5). Weights that are calculated in this manner compensate both for the uncertainty in the individual measurement and for differences in the units of measurement among the observations. In applying PEST to Española Basin, weights given to the observations

were based on more comprehensive considerations: (1) Data, particularly the ground-water head data, were highly clustered. A weighting method was applied that de-emphasized the importance of clustered data and emphasized measurements where the data was sparse. (2) The accuracy of the measurements was frequently unknown. In the case of hydraulic head data, the actual measurement error also was compounded with other sources of uncertainty, including whether ground-water conditions had been locally affected by development and whether or not the ground water was locally perched. (3) Differences between the scale of the permeability measurements and the scale at which the hydrogeologic units are modeled introduces uncertainty with regard to the representativeness of the measurements. (4) Accuracy of the model in certain areas, particularly in the vicinity of Los Alamos National Laboratory, was more important to the objectives of this study than in other areas. Thus, although automated parameter-estimation techniques such as those incorporated in PEST theoretically are objective in that they identify the parameter set that minimizes the objective function, a good deal of judgement is required in the correct assignment of weights to observations. Based on the considerations outlined above (1) relatively small weights were given to water-level measurements in the Valles Caldera, which may have been made in perched water; (2) relatively large weights were given to water-level measurements in the area of Los Alamos National Laboratory, where the accurate characterization of ground-water movement is critical to assessing the fate of chemicals in the ground water; and (3) relatively small weight was given to permeability measurements because of concern over the possible effects of scale.

Another limitation of using automated parameter-search techniques is that, although they excel at reducing the sum of the weighted-square differences, they can achieve this single-minded goal at the expense of hydrologic reality unless adequately constrained by limiting the allowable parameter ranges to be searched or by other methods. In the Española Basin study, a lack of hydrologic reality in the model sometimes became apparent in those areas that were poorly constrained by either head or flux data. Two areas that presented difficulties were the Embudo area and the lower part of the Pojoaque River. In Embudo area, a flux estimate of 0.35 cfs derived from a Darcy-law calculation was incorporated as a calibration target. In the lower Pojoaque River

area, the ground-water discharge of 7.5 cfs calculated by McAda and Wasiolek (1988) was included as a calibration target.

A final consideration in the optimization process was the incorporation of results from the transient analyses (see section "Transient Calibration"). Preliminary results from the transient model runs provided additional constraints for some model parameters that were not particularly sensitive to calibration targets established for the steady-state analyses. The parameter values identified in the transient model runs were used to further constrain the possible range of parameters to be searched, or, in some cases, were input as fixed parameters during the steady-state calibration.

Results

Of the three recharge cases presented in the section "Recharge estimates used in this Work", only the simulation results based on the case 1 recharge model were able to satisfactorily match the head, flux, and permeability data. The relative degree of success obtained with the case 1 recharge model, compared to the other recharge models, may have resulted more from the greater effort applied to this model because of promising early results than from the greater merit of the case 1 recharge model itself. Results are shown in this section for a simulation that uses the "optimal" permeabilities estimated by PEST for the case 1 recharge model and for a case in which these permeabilities were further adjusted using a trial-and-error approach.

The simulated potentiometric-surface contours and the residual hydraulic heads (predicted minus observed values) are shown for the case with PEST-optimized permeabilities in Figure 17 and for the case with best-fit trial-and -error permeabilities in Figure 18. The simulated potentiometric surface is similar for both sets of permeabilities, although simulated hydraulic heads are relatively higher in the Sangre de Cristos when the permeabilities were estimated by trial and error and relatively higher in the Valles Caldera when the permeabilities were estimated by PEST. The largest absolute residual for both simulations is in the northeast corner of the model area, although the sign of the residual differs between the simulations. The simulation using the permeabilities derived

by trial and error (Fig. 18) provides a better match to hydraulic heads near the Rio Grande and in the lower reaches of its tributaries, probably because vertical hydraulic gradients in these areas are better matched with the small horizontal-to-vertical anisotropy ratio (10:1) estimated from the trial-and-error fit. Using permeabilities estimated by PEST, residuals at wells located on the Pajarito Plateau near Los Alamos National Laboratory ranged from –200 to 100 feet but were generally between –25 and 25 feet. For the same area, residuals for the simulations that used permeabilities estimated by trial and error ranged from –100 to 100 feet, and were somewhat skewed toward positive values.

Histograms of hydraulic head residuals for the two simulations are shown in Figure 19. Despite their approximately normal distribution, the histograms show that both simulations had a few very negative residuals. The mean residuals were –36.5 feet for the PEST calibration and 20.0 feet for the trial-and-error calibration. In the PEST calibration, 50 percent of the residuals were between –111 and 75 feet, the maximum negative residual was –1377 feet, and the maximum positive residual was 430 feet. In the trial-and-error calibration, 50 percent of the residuals were between –39 and 79 feet, the maximum negative residual was –790 feet, and the maximum positive residual was 589 feet.

East-west cross-sections with the simulated hydraulic head contours and potentiometric surface are shown in Figures 20a and 20b. For both simulations, the simulated potentiometric surface generally coincides with the top of the aquifer, which was estimated from measured hydraulic heads. The upward gradients beneath the Rio Grande were larger in the case that used the PEST-derived permeability estimates, probably because of the larger horizontal to vertical anisotropy ratio (100:1) assumed in this case resulted in a smaller overall vertical permeability for the Western Santa Fe Group unit that lies beneath the river. Both simulations indicate that a ground-water divide exists beneath the western rim of the Valles Caldera, although both simulations also show a potentiometric surface that, unrealistically, is slightly above land surface.

Simulated ground-water fluxes along different basin boundary segments and river reaches are listed in table 12. The ground-water discharge calculated by the both models generally is in good agreement with the estimated discharge calculated from streamflow

data or other sources. The largest discrepancy is between the simulated and estimated flow to the Rio Grande between Española and Otowi, but the estimated mean discharge along this reach of 31.4 cfs has a standard error of 71.7 cfs (see table 12), so the estimate itself is subject to considerable uncertainty. The discharge to the Pojoaque River simulated with the permeabilities derived by trial and error is also large compared with the discharge estimated by McAda and Wasiolek (1988). Along the reach of the Rio Grande between Otowi and Cochiti Reservoir, which includes the part of the Rio Grande immediately east of Los Alamos National Laboratory, the calculated discharge is in very good agreement with baseflow estimates based on streamflow data.

The permeabilities estimated by PEST and the permeabilities derived through trial and error are listed in Table 11, which also summarizes the permeability data for the hydrologic units and the 95 percent confidence limits estimated by PEST. The permeabilities estimated both with PEST and by trial-and-error are in varying degree of agreement with the data. The permeability estimated by PEST for the Chaquehui is about an order-of-magnitude less than the measured mean permeability, whereas in the trial-and-error calibration the permeability of the Chaquehui was fixed at near its mean value. The permeability estimated by PEST for the Bandelier Tuff is about half its measured mean value, whereas in the trial-and-error calibration the permeability of the Bandelier Tuff was fixed at its mean value because of the extremely wide confidence limits indicated by the PEST run. The permeability of the Puye Formation in both the PEST calibration and the trial-and-error calibration is low compared to the mean measured value. The 95 percent confidence interval calculated by PEST indicates that the permeability of the Puye Formation is very poorly constrained by the observations. The Ancha Formation and the Tschicoma Formations are in poor agreement with the measured permeabilities, but the latter consist of only one measurement in each formation. The estimated permeabilities for the both the shallow Sangre de Cristo unit and the Eastern Santa Fe Group were in good agreement with the measured mean permeabilities in both the PEST and the trial-and-error calibrations. For the western Santa Fe Group, the permeability calculated with PEST was in good agreement with the measured mean permeability, whereas the permeability estimated by trial-and-error was low by a factor of about 4 compared to the mean value.

Sensitivity

The 95 percent confidence limits for the permeabilities estimated by PEST were listed in table 11. These confidence limits reflect the degree to which the weighted observations permit the permeabilities to be accurately estimated. Wide confidence limits can result from a number of factors, including the insensitivity of the observations to changes in the permeability value. This insensitivity may arise if the volume of the hydrogeologic unit is small, the hydrogeologic unit is isolated from the observation points by other units, or the hydrogeologic unit is far from the observation points. Wide confidence limits for a particular unit can also arise if model objectives can be met equally well by adjustments to the permeability of that unit or by adjustments to other units. In this second case, wide confidence limits convey information about model non-uniqueness.

The confidence limits listed in table 11 indicate that the estimated permeabilities are constrained by the observations to widely varying degrees: (1) The permeabilities of the Paleozoic/Mesozoic rocks, the Airport Area Santa Fe Group, the Cerros basalts, the Puye Formation, the Totavi Lentil, the Bandelier Tuff and the Southern Cerros basalts are completely unconstrained by the observations. (2) The permeabilities of the Pojoaque Area Santa Fe Group, the Aqua Fria Fault, the Ancha Formation, and the Chaquehui Formation are moderately constrained by the observations. And (3) The permeabilities of the Shallow Sangre de Cristo, the Deep Santa Fe Group, Eastern Santa Fe Group, Western Santa Fe Group, Northern Santa Fe Group, Tshicoma Formation, Pajarito Fault, the Penasco Formation and Ojo Caliente Formation are highly constrained by the observations. Again, the absence of constraints imposed by the observations on some of the permeability values do not necessarily imply that these permeabilities can be changed with no impact on the objective function, but rather that these permeabilities cannot be estimated accurately given the structure of the model and the associated observations.

It is important to note that even for those units whose permeabilities that are highly constrained by the observations, the optimal permeability value and its confidence

limits may be a function of other aspects of the model that were not explicitly examined during the optimization, such as the recharge distribution and the anisotropy ratios assumed for the model. Optimization runs using the case 2 and case 3 recharge models, although they did not produce realistic simulation results, did produce similar magnitude permeability confidence intervals as case 1. Mean estimates for permeabilities in some cases were well outside the 95 percent confidence intervals listed in Table 11.

The fact that some of the best-fit trial-and-error permeability values are outside the 95 percent confidence limits estimated by PEST (Table 11) also may indicate the dependence of the optimal permeability values and their confidence limits on the assumed anisotropy ratios: horizontal-to-vertical permeabilities of selected units were assumed to be 100:1 in the PEST optimization runs, whereas standard sensitivity analysis during the trial-and-error runs resulted in a best-fit anisotropy value of 10:1.

Transient simulations

The goal of transient modeling is to simulate the response of the aquifer to changes in groundwater withdrawals (pumping) and/or recharge rates. By doing so, the model captures features of the flow field that may have significant effect on fluxes, flow directions, and contaminant transport. In addition, through the process of calibrating a transient flow model we improve our understanding the aquifer and identify strengths and weaknesses of our numerical modeling approach.

In the Española Basin, significant pumping began in the 1940's and has increased steadily to the present. Water levels have declined significantly, up to several hundreds of feet in some areas. Water levels in the vicinity of LANL have declined as much as 100 feet; these changes have been well documented in numerous LANL water supply reports. Because of dropping water levels, increasing population (especially in the Santa Fe area), uncertain relationships between groundwater and surface water flow, and complex water rights appropriation processes, the topic of groundwater withdrawals, aquifer recharge, and water level fluctuations are becoming increasingly politically charged.

Compilation of hydrograph and pumping data

We have compiled annual pumping data for all municipal wells for City of Santa Fe and Los Alamos County from 1947 to present (Lewis, City of Santa Fe, pers.comm., 1999; McLin, LANL, pers.comm., 1999). We also have data for City of Española withdrawals from 1995 to present (Lewis, City of Santa Fe, pers.comm., 1999). We do not have data for pueblo lands; the significance of this omission is unknown. The pumping data we have compiled is presented in Figure 22, aggregated by wellfield. Pumping data are presented in Appendix II. In total, we have withdrawal, well construction, and location data for 39 municipal supply wells.

To examine aquifer response to pumping, we compiled hydrographs for 39 wells in the vicinity of Los Alamos, Buckman wellfield, and Santa Fe. The location of all wells with hydrographs are shown in Figures 23 and 24, along with the location of supply wells for reference. The value of the hydrograph data from the wells shown in this figure is varies considerably from well to well. In the vicinity of LANL, we have excellent period of record for all test wells. However, all the test wells were completed at considerably more shallow depths than supply wells. This limits their utility has indicators of aquifer response to pumping at depth. The same applies to several piezometer nests in the Buckman wellfield (SF 3, 4, and 5). However, both the Buckman wellfield and the Santa Fe wellfields contain one deep piezometer nest (SF-2 and SF-1, respectively). Data from these deep nests should be excellent indicators of aquifer response at similar depths that pumping occurs. Unfortunately, there is very little data available from these well nests. The U.S.G.S. has recently begun collecting data from these wells recently, and so future trends should be better documented.

Because of the scarcity of observation well data, particularly at depths well below the water table, we also use hydrographs (non-pumping water levels) from all the supply wells in the Los Alamos area. The disadvantage of this type of data is that it provides a sort of averaged head over a long vertical interval. The implications of this will be discussed below.

Compilation of aquifer properties

The two aquifer properties that affect water level response to pumping are transmissivity and storativity. Of these two, transmissivity has the most impact (Freeze et al. 1979, pg. 318). Our numerical model requires specification of aquifer permeability (K) for each element, rather than transmissivity (T, where T=Kb and b=aquifer thickness) for each layer. Our process for assigning permeability values to each stratigraphic unit, as described in the section above, relied primarily on values reported in the literature and, within reasonable ranges, upon calibration of the pre-development simulations to observed water levels for a given model of recharge.

Storage properties of aquifer rocks, while not as influential as permeability, are also important to assign correctly. The biggest issue regarding storage is whether an aquifer is unconfined (large storage) or confined (small storage). Evaluation of unconfined or confined conditions is often based on S (storativity) calculations from pump tests. Large values of storativity (0.01 – 0.3) indicate unconfined conditions; small values (.005 or less) indicate confined conditions. Confined aquifers typically respond rapidly to pumping; unconfined aquifers typically respond more gradually.

Storage parameters derived from pump tests, both on the Pajarito Plateau and elsewhere in the basin, are shown in Table 13. Also shown in this table are storage parameters used by other groundwater flow models in the region. For reported S values less than 0.01, S was converted to Ss (specific storage) by dividing by the screen interval in the well. By defining unconfined aquifers as those with S = 0.01 or greater, these data suggest that aquifers in Precambrian rocks and the Ancha formations are mostly unconfined. Data collected in the Santa Fe group rocks (including the Tesuque and "Chaquehui" formations) are mixed, although most pump tests indicate confining conditions. An intermediate case, a leaky confined aquifer, was described on the Pajarito Plateau at O-1. This type of aquifer response may be typical of Santa Fe group rocks (McLin, pers. comm., 1998). Frenzel (1995) assumed unconfined conditions in the uppermost 200' of the aquifer (Sy = 0.15) and confining conditions everywhere below (Ss = 1.E-6/ft). FEHM requires a specification of S for every grid element. For the simulations described below, we assume either confined conditions everywhere (very low S) or a mixed system with deep nodes having a low S and shallow nodes having a large S (approximating an unconfined conditions). Since we are not modeling the unsaturated zone, a process-level model of a dropping water table and draining of pore spaces cannot be directly simulated.

Simulating pumping

Pumping from wells is simulated as a source/sink terms in FEHM. Sources/sink are applied to individual nodes within the numerical mesh. Our first step was to identify all nodes corresponding to screened intervals within pumping wells, and to identify the

hydrostratigraphic units associated each node. The x-y resolution of the grid (250m) in the vicinity of Los Alamos and Santa Fe was sufficient to accurately map well locations onto the grid (see Figure 25). The z-resolution of the grid (50m) provided as many as 12 nodes within a typical water supply well screened over 610m (2000 '). The total withdrawal for a given year within a well was divided between each node within the screened interval. The water pulled from each node was assumed to be linearly proportional to the local permeability and to the spacing between the node and nearest nodes within the wellbore. For example, if the total pumping from a well is 10 kg/s and there are 5 evenly-spaced nodes associated with the open screened interval, the model will simulate 2 kg/s withdrawal from each node in a homogeneous permeability field. If, by contrast, the top node is in a hydrostratigraphic unit with a much higher permeability (K_1) than lower units (K_2=0.1*K_1), then the top node will be assigned a withdrawal rate of 7.1 kg/s and the lower 4 nodes will be assigned a rate of approximately 0.71 kg/s (10 times lower). A similar algebraic calculation is made to account for the effect of variable spacing between nodes. Apportioning pumping according to the vertical variations in permeability allows us to incorporate observations such as those made in the Guaje field, where over 90% of the flux is thought to occur in the uppermost, most permeable layers (McLin, pers.comm).

Because of grid resolution limitations, this method cannot predict water level variations within the pumping element (250m X 250m X 50m) and so cannot account for wellbore effects and drawdown within the well during pumping. The "averaging" of the pumping effects over the entire element associated with a node should not negatively impact our ability to simulate non-pumping water level changes on the scale of years.

In addition to this averaging caused by discritization of the flow field, we are also limited by the uncertain averaging process that influences a water level measured in a well with a long screened interval. Water levels in these wells may represent a simple average of heads at various depths, or, be more influenced by heads within some layers than by others. Many of the hydrographs with which we compare our model were constructed using water level data from such wells. For the sake of simplicity, we compare the head predicted by the model at the *mean elevation* of the screened wellbore

to water level measurements from that well. There is an unknown degree of error inherent in this comparison.

Simulating water level changes since 1945

We used FEHM to simulate pumping in all Los Alamos, Buckman, and Santa Fe wellfields from 1945 to 1997. For initial conditions, we used the steady-state model with "trial and error" permeability values described earlier and recharge model 1. To assess model performance, we compare predicted water level changes to those observed. As described above, the degree of agreement will depend largely on three factors: adequacy of hydrostratigraphic framework model, correct assignment of permeability values to each unit, and correct assignment of storage parameters to each unit. Since the permeability values in the model are largely dependent on the steady-state calibration process described in earlier sections, we did not vary these parameters except within small ranges that were compatible with the steady-state calibration. We also chose not to refine the hydrostratigraphic framework model to improve the transient calibration, in order to preserve some measure of independence between the hydrostratigraphic and groundwater flow models. Therefore, the only relevant parameter that was adjusted to improve model performance was storage.

To provide a systematic way to test approaches to storage in the aquifer, we began with a very simple model. This model assumed confined conditions throughout the aquifer, with $Ss = 2 \times 10^{-6}$/m, a typical value from Table 12. This model provided a remarkably reasonable match between predicted and observed hydrographs for a number of wells. This result was relatively insensitive to global changes in storage (Ss was varied between 1E-6/m and 1E-3/m).

One conspicuous exception was poor agreement between predicted and observed hydrographs in the PM wellfield. Our model greatly overpredicted water level declines in this area. To address this, we specified a much larger S value for the Chaquehui aquifer than for the underlying Santa Fe group sediments. This may be justifiable if since the "Chaquehui aquifer" is primarily sands and gravels which, lacking the fine beds of

silts and clays, may be less confined than Santa Fe group sediments that host the lower Los Alamos, Buckman, and Santa Fe wellfields. Specifying a larger S value (Ss = 0.15/m) for the Chaquehui formation greatly improved the match to some hydrographs from PM wells.

A comparison of predicted v.s. observed hydrographs for this shown in Figures 25 through 29. In many of these figures, discrepancies exists between the first water level observed and the first model prediction; this error is related to the steady state calibrations described in an earlier section. Since the goal of transient simulations is to correctly model aquifer responses to pumping, the effect of this initial error is unimportant. To better compare observed and predicted transients, on many hydrographs we present both model predictions (blue lines) and "adjusted" model predictions (green lines), which are offset from model predictions to account for initial condition errors. The discussions below pertain primarily to adjusted model predictions.

In the Guaje wellfield, the model performs reasonably well for those wells closest to the Rio Grande (G-1, 1A, 2, and 3) (see Figure 25). For wells higher on the plateau (G-4, G-5, and G-6), however, the model overpredicts drawdown. In the hydrostratigraphic model, these upper G wells penetrate a thick section of "Chaquehui formation". Since we define the storage term to be quite large for this unit, underestimation of storage is probably not the cause of the problem. More plausible explanations include 1) overestimating the relative proportion of Chaquehui to lower Santa Fe group in the borehole and/or 2) underestimating the permeability of the Chaquehui and/or the lower Santa Fe group.

Comparisons to observed water levels for Pajarito Mesa wells are shown in Figure 26. The model performs reasonably well at PM-4 and PM-5 and overpredicts drawdown in PM-1, PM-3. The performance at PM-2 is mixed; adequate in early years and inadequate in later years. The hydrostratigraphic model is very similar in all these wells, with a thick section of Chaquehui underlain by a small section of Santa Fe Group near the bottom of the wellbore. Therefore, adequately modeling differences in water level responses to pumping amongst the PM wells can only be accomplished by improvements in the hydrostratigraphic framework model.

Figure 27 shows predictions and observations for test wells. The model overpredicts drawdown for all the test wells. It is important to note that the test wells are shallower than the supply wells. This result implies either that the model underestimates permeability in the units penetrated by the test wells, or that the degree of hydraulic connection between deeper and shallower layers is overestimated. Since the latter type of error would have significant impact on transport calculations, we propose to focus on this solving this discrepancy in the future.

Comparisons for the Los Alamos Well field are shown in Figure 28. For those wells closest to the Rio Grande, the rapid changes in observed water levels are reasonably approximated by the model. The model correctly predicts more subtle changes in water levels in upper Los Alamos Canyon, although the model generally overpredicts the responsiveness of water levels in these wells.

Data collected from wells in the Buckman field are shown in Figure 29. Unfortunately, there are very few observations in these wells and it is difficult to evaluate the responsiveness of water levels to pumping. We can, however, compare the total decline in water levels. The largest decline in water levels in this wellfield (336 ft) was observed in SF-2B, a piezometer completed at a depth to similar to average depth of pumping wells. The model estimates a similar amount of water level decline (300 ft). The model also provides a reasonable match to water level changes in the two other deepest piezometers, SF-2A and SF-2C. Drawdown is underestimated, however, in a slightly shallower piezometer, SF-3A. Very little drawdown was correctly predicted in the other shallow piezometers, SF-3B, C, SF4A,B,C, and SF-5C.

We are just in the preliminary stages of interpreting model results and hydrographs in the Santa Fe area; these results should become available in the next few months.

Chapter 4. Model evaluation

The results of the steady-state model calibration generally compared well with the observations that were used to constrain the model. In the vicinity of Los Alamos National Laboratory, residual heads ranged between –200 and 100 feet and generally were between –25 to 25 feet for the model calibrated with PEST. For the model calibrated by trial-and-error, residual heads ranged from –100 to 100 feet, but were somewhat skewed toward positive values. Both calibration approaches resulted in simulated discharges to the rivers in the basin that agreed well with discharges estimated from streamflow data. The simulations matched the estimated discharge to reach of the Rio Grande downgradient from the Laboratory particularly well, a facet of the model that is important for predicting the rate of movement of chemicals in the ground water beneath the Laboratory. With some exceptions, both the trial-and-error calibration and the PEST calibration matched the head and discharge date without requiring permeabilities to have values that were outside the range of the permeability data. The PEST calibration did a somewhat better job than the trial-and-error calibration in this regard. The PEST calibration also provided 95 percent confidence limits on the estimated permeabilities in the model, a feature that identified the permeabilities that were well constrained by the data and the permeabilities that were not. The permeabilities of units with wide confidence limits cannot be estimated with the model and their permeabilities in the model will need to be fixed at values determined from field measurements or by analogy with similar geologic media. Many hydrogeologic units with large uncertainty in their permeability values are not expected play a large role in the movement of ground water near the Laboratory, either because they are only partly saturated, very deep, or far from the Laboratory boundaries. However, some of the hydrogeologic units whose estimated permeabilities are poorly constrained, such as the Totavi Lentil, are expected to play a central role in the ground-water hydrology near the Laboratory. For these units, permeability values in the model need to be fixed near the values determined from field measurements or estimated with the model from the transient head data.

The results presented for transient simulations indicate that, while reasonable predictions are achieved for wells completely entirely within the Santa Fe Group (primarily Tesuque Formation), considerable disagreement between predictions and observations existed for some wells that penetrate multiple formations, particularly those that penetrate both the lower Santa Fe Group and the "Chaquehui aquifer". Some improvement was achieved by specifying different storage parameters for these two units. The higher storage parameter we assumed for the "Chaquehui aquifer" is somewhat in conflict with pump test results for O-1 and O-4. Pump test results from O-4 (Stoker et al. 1989), which is reported to penetrate layers of the Chaquehui, indicate very low storativity. In contrast, pump test results from O-1 (Purtymun et al. 1990), which does not penetrate the Chaquehui, indicate a much higher storativity (apparent "phreatic conditions"). There are at least two ways to interpret this. One, that the apparent "phreatic conditions" at O-1 reported by Purtymun et al. (1990) may reflect wellbore effects (as the authors suggest) and not fundamental characteristics of the aquifer. Or two, that our simple assumptions about the relative storage characteristics of these two hydrostratigraphic units are incorrect. In any case, it is clear that improved model performance for transient predictions on the Pajarito Plateau will require some measure of refinement in both the hydrostratigraphic framework model and exploring alternative approaches to estimating storage parameters.

As noted in the transient calibration discussion above, drawdowns in several wells on the plateau were overestimated. In addition to refining our approach to estimating storage, we should also investigate increasing the permeability values for several units on the plateau. After importing the updated hydrostratigraphic framework model (October, 1999), as we re-calibrated both the steady-state and transient models we will evaluate this possibility.

By continuing to optimize permeability parameters (with both the pre-development and transient simulations) it is likely that the agreement between simulated and observed hydrographs will continue to improve. However, in the near future we will surely reach a point where no further improvement can occur without a change in the hydrostratigraphic model. Frenzel (1995) introduced new hydrostratigraphic units (for example, a small unit defining the Los Alamos wellfield) for the sole purpose of better

matching the hydrograph data. We have not taken this approach, however. By keeping hydrostratigraphic definitions independent of model calibration we make the resulting flow and transport models more credible. In October, we expect to introduce a new hydrostratigraphic framework model (Carey, pers. comm, 1999). We will re-calibrate our models at that time and results may change.

Chapter 5. Suggestions for future work

Hydrostratigraphic framework model

We expect the hydrostratigraphic framework model to become more detailed and accurate as new data is collected as part of the deep drilling program. Better definition of the Pajarito Fault zone and volcanics to the west of LANL, however, is outside the scope of the deep drilling program. Our ability to accurately model fluxes to the aquifer from the west and to evaluate alternative conceptual models of the water table in the western portion of LANL is limited by the lumping of all silicic volcanics into one large hydrostratigraphic unit (called the Tschicoma formation) and the simplistic modeling of the fault zone. We propose that cross-sections published by Goff (1988) be used to refine the current hydrostratigraphic model, and that a preliminary, simplistic representation of intra-caldera Bandelier Tuff and alluvium also be introduced to the model. Alternative geometric realizations of the Pajarito fault zone would also be helpful.

It is premature to evaluate the existing hydrostratigraphic model within LANL boundaries until the latest update is incorporated (October 1999). After this model is incorporated and new calibrations are achieved, we may have recommendations for further modifications.

Permeability modeling

Although it is widely recognized that geologic factors influence hydrologic properties of rocks, permeability variations used in groundwater flow models are rarely based exclusively upon geologic framework models. This is due to a number of factors, including 1) permeability variations within a given stratigraphic unit may be as large or

larger than permeability variations between stratigraphic units, 2) permeability variations within a stratigraphic unit such as an alluvial fan deposit may be so complex as to preclude explicit geometric modeling, and 3) pump test and water level data may strongly indicate hydrostratigaphic boundaries where no known geologic boundaries exist.

As described in earlier sections, to date we have avoided ad-hoc introduction of new permeability zones in the vicinity of LANL in order to more clearly evaluate our conceptual models of flow and transport. If we are to provide realistic estimates of travel times of contaminants and associated uncertainty, we must introduce a heterogeneous permeability field within each of the sedimentary units (Puye Formation and rocks of the Santa Fe group, at minimum). Although some increased refinement is expect to occur as new wells are drilled, the spatial extent of individual facies is likely to be smaller than spacing between wells and so we probably will never be able to create discreet maps of individual facies within the Puye Formation and Santa Group. Therefore, we propose to develop a stochastic-based model of permeability for these units. The model should be based on spatial statistics of hydrofacies rather than purely random variation. To do this requires estimating length scales associated with distinctive facies within the deposit. We propose to incorporate wellbore data, new outcrop-based data (if feasible), and results of other studies in sedimentary deposits (Koltermann et al. 1996; Weissmann et al. 1999).

References

Anderholm, S. K. (1994).Ground-water recharge near Santa Fe, north-central New Mexico.94-4078.

Duffy, C. J. and S. Al-Hassan (1988). "Groundwater circulation in a closed desert basin: topographic scaling and climatic forcing." Water Resources Research **24**(10): 1675-1688.

Freeze, R. A. and J. A. Cherry (1979). Groundwater. Englewood Cliffs, New Jersey, Prentice-Hall, Inc.

Frenzel, P. F. (1995).Geohydrology and simulation of ground-water flow near Los Alamos, North Central New Mexico.95-4091.

Goff, F., L. Shevenell, J. N. Gardner, F. D. Vuataz, et al. (1988). "The hydrothermal outflow plume of Valles Caldera, New Mexico, and a comparison with other outflow plumes." J.Geophys.Res. **93**: 6041-6058.

Keating, E., E. Kwicklis and B. Robinson (1999).Simulated transport of HE in the regional aquifer from TA-16.LANL.

Keating, E., G. Zyvoloski, C. Gable, M. Witkowski, et al. (1998).A Steady-state regional flow model for the saturated zone in the Espanola Basin.Los Alamos National Laboratory.

Koltermann, C. E. and S. M. Gorelick (1996). "Heterogeneity in sedimentary deposits: a review of structure-imitating, process-imitating, and descriptive approaches." Water Resources Research **32**(9): 2617-2658.

Landmark (1998). Stratamodel- Stratigraphic Geocellular Modeling, Landmark Graphics.

Lewis, A. (1994).Santa Fe County water resource inventory.1.Daniel B. Stephens and Associates Inc.

McAda, D. P. and M. Wasiolek (1988).Simulation of the regional geohydrology of the Tesuque aquifer sytem near Santa Fe, New Mexico.87-4056.U.S. Geological Survery.

Purtymun, W. D. and H. Adams (1980).Geohydrology of Bandelier National Monument, New Mexico.LA-8461-MS.LANL.

Purtymun, W. D., S. McLin and A. Stoker (1990).Water supply at Los Alamos during 1990.LA-12471-PR.Los Alamos National Laboratory.

Purtymun, W. D., S. McLin and A. Stoker (1992).Water supply at Los Alamos during 1992.LA-12926-PR.Los Alamos National Laboratory.

Purtymun, W. D., R. J. Pters and J. W. Owens (1980).Geohydrology of White Rock Canyon of the Rio Grande from Otowi to Frijoles Canyon.LA-8635-MS.LANL.

Purtymun, W. D., A. K. Stoker and S. G. McLin (1993).Water supply at Los Alamos during 1993.LA-12951-PR.Los Alamos National Laboratory.

Shaull, D. A., M. R. Alexander and R. P. Reynolds (1996a).Surface water data at Los Alamos National Laboratory, 1995 Water Year.LA-13177-PR.Los Alamos National Laboratory.

Shaull, D. A., M. R. Alexander, R. P. Reynolds and C. T. McLean (1996b).Surface water data at Los Alamos National Laboratory, 1996 Water Year.LA-13234-PR.Los Alamos National Laboratory.

Shaull, D. A., M. R. Alexander, R. P. Reynolds and C. T. McLean (1998).Surface water data at Los Alamos National Laboratory, 1997 Water Year.LA-13403-PR.Los Alamos National Laboratory.

Shaull, D. A., M. R. Alexander, R. P. Reynolds and C. T. McLean (1999).Surface water data at Los Alamos National , 1998 Water Year.LA-13403-PR.Los Alamos National Laboratory.

Spiegel, Z. and B. Baldwin (1963).Geology and water resources of the Santa Fe area.1525.U.S. Geological Survey.

Stoker, A. K., S. G. McLin, W. D. Purtymun and M. N. Maes (1989).Water supply at Los Alamos during 1989.LA-12276-PR.LANL.

Trease, H., D. George, C. W. Gable, J. Fowler, et al. (1996). The X3D grid generation system. Numerical grid generation system in computational fluid dynamics and related fields. B. K. Soni, J. F. Thompson, H. Hausser and P. R. Eiseman.

Vautaz, F. D., F. Goff, C. Fouillac and J. Y. Calvez (1986). "Isotope geochemistry of thermal and nonthermal waters in the Valles Caldera, Jemez Mountains, northern New Mexico." J. Geophysics Res. **91**: 1835-1853.

Wasiolek, M. (1995).Subsurface recharge to the Tesuque Aquifer system from selected drainage basins along the western side of the Sangre de Cristo mountains near Santa Fe, New Mexico.94-4072.U.S. Geological Survey.

Watermark Computing (1994).PEST Model-Independent parameter estimation: user's manual, Watermark Computing.

Weissmann, G., C. SF and F. GE (1999). "Three dimensional hydrofacies modeling based on soil surveys and transition probability geostatistics." Water Resources Research **35**(6): 1761-1770.

List of Figures

1. Stratigraphic framework model for Española Basin, with boundary conditions indicated.
2. Numerical grid in the vicinity of the Pajarito Plateau.
3. Numerical grid, with colors according to hydrostratigraphic units (undifferentiated Santa Fe Group)
4. Numerical grid, with colors according to hydrostratigraphic units (differentiated Santa Fe Group)
5. Area considered in the pre-development water-budget analysis.
6. Conceptual framework for the pre-development water-budget analysis
7. Relation between precipitation and elevation in the Española Basin
8. Locations of stream gaging stations in the water-budget study area.
9. Locations of stream gaging stations in the Española Basin.
10. Yearly baseflow gains along various reaches of streams and rivers in the Española Basin.
11. Data from Blake et al. (1995) showing the relation between (a) chloride and δ^2H and (b) chloride and $\delta^{18}O$ in selected spring and ground-water samples.
12. Relations between (a) the fraction of precipitation that becomes recharge and estimated recharge elevation, and (b) recharge magnitude and estimated recharge elevation, based on selected chloride, δ^2H, and $\delta^{18}O$ data.
13. Fit of the recharge model to the recharge estimates of Wasiolek (1995).
14. Recharge versus elevation for (a) case 1, (b) case 2, and (c) case 3.
15. Areal distribution of recharge for (a) case 1, (b) case 2, and (c) case 3.
16. Pre-development water table
17. Simulated potentiometric surface and residuals using best-fit trial-and-error permeabilities.
18. Simulated potentiometric surface and residuals using PEST-derived permeabilities
19. Histogram of residuals for (a) PEST calibration and (b) trial-and-error calibration
20. Cross-section showing simulated hydraulic head contours and potentiometric surface for (a) PEST calibration and (b) Trial-and-error calibration.
21. Withdrawals from wellfields in the Española Basin
22. Location of pumping wells and wells with hydrographs in the vicinity of the Pajarito Plateau
23. Location of pumping wells and wells with hydrographs in the vicinity of Santa Fe
24. Location of water supply wells and nearest grid node
25. Comparison of predicted and observed water level changes, Guaje well field
26. Comparison of predicted and observed water level changes, Pajarito Mesa well field
27. Comparison of predicted and observed water level changes, test wells
28. Comparison of predicted and observed water level changes, Los Alamos well field
29. Comparison of predicted and observed water level changes, Buckman well field

List of Tables

1. Model Domain in Polar Stereographic Coordinates (Kilometers) and Grid Statistics
2. Total volume of each hydrostratigraphic unit, in $m^3 \times 10^{10}$, for 3 numerical grids
3. Summary of the recharge estimates of Anderholm (1994) and Wasiolek (1995).
4. Water-budget used in the pre-development steady-state simulation of McAda and Wasiolek (1988).
5. Precipitation and evapotranspiration (ET) calculated with the Wasiolek (1995) ET model.
6. Yearly streamflow losses and gains ($S_o - S_I$) in the water-budget study area.
7. Average discharge of perched springs within the water-budget study area.
8. Yearly baseflow gains along various reaches of streams and rivers in the Española Basin.
9. Recharge parameters used in the three recharge cases considered in the regional modeling.
10. Water levels used in pre-development calibration
11. Comparison of permeability estimates from calibration with measured permeabilities.
12. Comparison of simulated ground-water flux with estimates based on streamflow measurements or other calculations
13. Compilation of storage characteristics data for the regional aquifer

Table 1: Model Domain in Polar Stereographic Coordinates (Kilometers) and Grid Statistics

Grid Name and Version	Grid Dimension	Grid Spacing	Minimum Extent	Maximum Extent	Difference	Number of Unique Materials Modeled
Version 6, 1998	X(West-East)	1.000	-15.00	85.00	100.00	20
	Y(South-North)	1.055	-166.00	-60.50	105.50	
	Z > 1.3 KM	0.050	-1.30	2.75	4.05	
	Z < 1.3 KM	0.500				
Version 1, 1999	X(West-East)	1.000	-15.00	85.00	100.00	21
	Y(South-North)	1.055	-166.00	-60.50	105.50	
	Z > 1.3 KM	0.050	.100	2.75	2.65	
	Z < 1.3 KM	0.500				
Version 2, 1999	X(West-East)	Variable	-15.00	85.00	100.00	21
	Y(South-North)	Variable	-166.00	-60.50	105.50	
	Z > 1.1 KM	0.050	-.400	2.75	3.15	
	Z < 1.1 KM	0.500				

Table 2. Total volume of each hydrostratigraphic unit, in $m^3 \times 10^{10}$, for 3 numerical grids

Rock type	Hydrostratigraphic unit	Version 6, 1998	Version 1, 1999	OMR
Crystalline rocks	Deep basement (Precambrian)	1249.7	248.7	400.8
	Shallow rocks (fractured Paleozoic/Mesozoic)	319.0	220.5	214.2
	Paleozoic/Mesozoic	0.0	144.8	181.7
	Cerros del Rio basalts	0.1	0.1	0.4
	Cerros del Rio basalts, southern	3.6	2.0	2.2
	Tschicoma formation	42.8	50.1	57.1
Fault zones	Fault zone	36.3	20.7	17.6
	Agua Fria fault zone	0.2	0.1	0.1
Sedimentary rocks	Santa Fe group, east	28.1	38.9	47.4
	Santa Fe group, west	58.4	140.5	171.2
	Ancha formation	1.6	2.9	3.4
	Santa Fe group, north	39.3	68.4	90.3
	Ojo Caliente sandstone	24.6	37.7	48.0
	Penasco embayment	15.8	33.3	38.5
	Santa Fe group, deep	175.2	170.0	162.4
	Ojo Caliente sandstone	30.5	11.4	13.0
	Santa Fe group, near SF airport	12.3	7.6	8.2
	Santa Fe group, "Chaquhui formation"	2.2	2.1	2.6
	Puye, fanglomerate	0.3	0.1	0.4
	Puye, Totavi Lentil	0.2	0.1	0.5
	Bandelier Tuff	0.0	0.0	0.1
Total model volume		2040.0	1200.0	1620.0

Table 3. Summary of the recharge estimates of Anderholm (1994) and Wasiolek (1995).

Drainage Basin	Annual Recharge (Acre-feet) Anderholm (1994)	Recharge Percentage[1] Anderholm (1994)	Annual Recharge (Acre-feet) Wasiolek (1995)	Recharge Percentage[1] Wasiolek (1995)
Rio Nambe	No estimate	No estimate	5,520	12.2
Rio en Medio	No estimate	No estimate	1,710	15.4
Tesuque Creek	690[2]	3.2	1,530[3]	10.6
L. Tesuque Creek			1,790[3]	19.1
Santa Fe River	2,320	7.7	4,170	11.5
Arroyo Hondo	830	9.7	No estimate	No estimate

[1]Recharge percentage refers to the percentage of precipitation that is estimated to become recharge.

[2]Anderholm (1994) estimated only the combined recharge for the Tesuque Creek and Little Tesuque Creek drainage basins.

[3]The sum of Wasiolek's (1995) estimates for Tesuque Creek and Little Tesuque Creek drainage basins is 3,320 acre-feet, which is 13.9 percent of the precipitation falling on the basins.

Table 4. Water-budget used in the pre-development steady-state simulation of McAda and Wasiolek (Modified from McAda and Wasiolek (1988, Table 3).

Description	Flow: Cubic feet per second	Flow: Acre-feet per year
Sources		
Areal recharge	10.6	7,700
East mountain-front and stream-channel recharge	38.5	27,900
West mountain-front recharge	18.6	13,500
Recharge from Rio Grande	1.9	1,400
Subsurface inflow at south specified-flux boundary	2.2	1,600
Subsurface inflow at north constant-head boundary	2.0	1,400
Total	73.8	53,500
Discharges		
Discharge to Pojoaque River and tributaries	7.3	5,300
Discharge to Rio Grande	39.3	28,500
Discharge to Santa Fe River	6.5	4,700
Subsurface outflow at south specified-flux boundary	0.3	200
Subsurface outflow at north constant-head boundary	3.0	2,200
Subsurface outflow at southwest constant-head boundary	17.4	12,600
Total	73.8	53,500

Table 5. Precipitation and evapotranspiration (ET) calculated with Wasiolek (1995) ET model

Avg. Elev. (ft)	Area (mi^2)	Fract-ional Area	Winter Precip (inches)	Winter ET (inches)	Spring Precip. (inches)	Spring ET (inches)	Sum/Fa Precip. (inches)	Sum/Fa ET (inches)	Annual Precip. (inches)	Annual ET (inches)	Winter P-ET (inches)	Spring P-ET (inches)	Sum/Fa P-ET (inches)	Annual P-ET (inches)
5500	3.52	.0202	2.97	1.8	1.98	1.7	3.47	7.0	8.42	10.5[a]	1.17	0.28	-3.53	-2.08[b]
5750	24.64	.1414	3.39	1.8	2.40	2.1	4.17	7.9	9.96	11.8[a]	1.59	0.30	-3.73	-1.84[b]
6250	35.20	.2020	4.06	1.8	2.87	2.7	5.00	8.2	11.93	12.7[a]	2.26	0.17	-3.20	-0.77[b]
6750	47.52	.2727	4.62	1.8	3.26	3.1	5.68	8.5	13.56	13.4	2.82	0.16	-2.82	0.16
7250	26.40	.1515	5.61	1.8	3.96	3.9	6.93	9.1	16.5	14.8	3.81	0.06	-3.17	1.70
7750	12.32	.0707	6.22	1.8	4.38	4.2	7.78	9.25	18.38	15.25	4.42	0.18	-1.47	3.13
8250	8.80	.0505	7.33	1.8	5.15	4.9	9.12	9.25	21.60	15.95	5.53	0.25	-0.13	5.65
8750	10.56	.0606	7.92	1.8	5.61	5.0	9.74	9.25	23.27	16.05	6.12	0.61	0.49	7.22
9250	5.28	.0303	8.91	1.8	6.27	5.7	11.22	9.25	26.40	16.75	7.11	0.57	1.97	9.65
Total	**174.24**	**.9999**	**5.03**	**1.8**	**3.51**	**3.33**	**6.21**	**8.57**	**14.75**	**13.25[a]**	**----**	**----**	**----**	**1.54[b]**

[a] Elevation intervals in which average annual ET exceeded average annual precipitation were assumed to have average annual ET equal to average annual precipitation when computing total annual ET.

[b] Elevation intervals in which the difference in average annual precipitation minus evapotranspiration is negative had this difference set to zero when computing total annual (P-ET).

Table 6. Yearly streamflow losses and gains ($S_o - S_i$)

Note: where headwaters of stream are within LANL boundary, $S_I = 0$ even when streamflow near headwaters is nonzero.

Los Alamos Canyon:	E042 (94.0 acre-ft)	–	E025 (224.5 acre-ft)	= -130.5 acre-ft
Sandia Canyon:	E125 (0.95 acre-ft)	-	0	= + 0.95 acre-ft
Mortandad Canyon:	E204 (0 acre-ft)	-	0	= 0.0 acre-ft
Canyon del Buey:	E230 (0 acre-ft)	-	0	= 0.0 acre-ft
Pajarito Canyon:	E250 (4.9 acre-ft)	-	E240(95.0 acre-ft)[1]	= >-90.1 acre-ft
Portillo Canyon:	E255 (0.07 acre-ft)	-	0	= +0.07 acre-ft
Water Canyon:	E265(0 acre-ft)	-	E252(10.8 acre-ft)	= -10.8 acre-ft
Ancho Canyon:	E275 (1.4 acre-ft)	-	0	= +1.4 acre-ft

Within LANL boundary, the net recharge due to streamflow is 231.4 acre-ft/yr – 2.42 acre-ft/yr = 229 acre-ft/yr.
[1] does not include inflow on ungaged tributary
Flow on Frijoles Creek is 1543 acre-ft/yr and flow on Santa Clara Creek is 2901 acre-ft/yr

Table 7. Average discharge of perched springs within the water-budget study area. Flow measurements are in gallons per minute.

Spring name	Discharge (gpm)	Spring Name	Discharge (gpm)
American Spring	----	Hamilton Bend Spring	1.9[1]
Apache Spring	4.0	Homestead Spring	5.0
Armistead Spring	3.5	Los Alamos Spring	----
Basalt Spring #1	4.0	Pine Spring	1.0
Basalt Spring #2	1.0	Sawyer Spring	1.0
Burning Ground Spring	----	Spr. above LA Canyon	---
Chaque Spring	----	Spring at Blue Dot Trail	---
DP site, Cold Spring	----	Turkey Springs	16.0
DP Spring, DP Canyon	1.8	Unnamed cold spring	16.0
Frijoles Spring #49	3.0	Spr. near Apache Spring	8.0
Frijoles Spring #50	5.0	Spring north of ice rink	0.26
Frijoles Spring #51	----	Water Canyon Gallery	8.0
----	----	**Total**	**83.5**[2]

[1]Average does not include measurement of 600 gpm on March 21, 1958. If this measurement were included, the average flow at Hamilton Spring would become 41.9 gpm.

[2]83.5 gallons per minute is 0.2 cubic feet per second

Table 8. Yearly baseflow gains along various reaches of streams and rivers in the Espanola Basin. Flow measurements are in cubic feet per second.

	Reach #1 Otowi to Cochiti	Reach #2 Espanola to Otowi	Reach #3 Rio Grande north of Espanola[1]	Reach #4 Chama River	Reach #5 Santa Fe River	Reach #6 Jemez River at East Fork
Mean	12.93	31.44	28.58	19.31	8.08	14.86
Std. Error	4.34	71.66	1.04	3.18	0.54	0.90
Median	13.70	-5.7	29.49	19.2	8	14
Mode	-8.3	---	---	14.7	8	12
Std. Dev.	28.81	343.65	4.99	19.36	2.88	4.65
Variance	829.8	118096.8	24.96	374.9	8.27	21.63
Kurtosis	2.70	1.55	0.50	1.83	-0.24	2.58
Skewness	-0.61	0.41	0.11	0.21	0.51	1.45
Range	166	1530.9	22.3	107.7	10.6	20.6
Minimum	-87.3	-687.8	18.3	-30.6	3.8	9
Maximum	78.7	843.1	40.65	77.1	14.4	29.6
Sum	568.8	723.1	657.3	714.4	226.3	401.3
Count	44	23	23	37	28	27

[1]The baseflow estimate for this reach includes the flow measured at station 8279000 on Embudo Creek at Dixon.

Table 9. Recharge parameters used in the three recharge cases considered in the regional modeling.

Parameter	Case 1	Case 2	Case 3
$z_{max\ (feet)}$	9,000	6,001	14,000
$z_{min\ (feet)}$	6,000	6,000	5,500
α	0.051	0.0295	0.10

Table 10. Pre-development heads, in feet, used for model calibration. (note: 15 digit numbers correspond to USGS data).

Well	screen elev.	head	Well	screen elev.	head
TW-1	5740	5773	354052105582101	6711	6744
TW-2	5865	5884	354103105574401	6652	6799
TW-3	5822	5842	354113105561801	6858	6940
TW-4	6058	6075	354113105575701	6836	6822
H-1	8246	8554	354133105571501	6829	6858
H-2	8243	8554	354135105561701	6931	6954
H-3	8243	8551	354135105561702	6931	6950
H-4	8364	8489	354135105562401	6980	6973
H-5	8239	8449	354139105563501	6954	6921
H-6	8243	8574	354338105571301	6783	6744
H-7	8059	8207	354347105565601	6672	6717
H-8	7911	8207	354404105582401	6796	6711
H-9	7911	8207	354418105583201	6678	6691
H-10	7908	8285	354419106022601	5789	6143
H-11	7911	8259	354427106060601	5979	5842
H-12	7911	8334	354442105550001	6885	6924
G-1	4848	5756	354627105560601	6652	6672
G-1a	5127	5743	354800105551601	6754	6681
G-2	4936	5760	354849105543101	6878	6875
G-4	5061	5865	355228105570501	6160	6147
G-5	5212	5891	355235106002701	5888	5901
LA-1	5159	5586	355318106031001	5704	5710
LA-2	5163	5563	355321106011301	5802	5829
LA-5	4749	5697	355324106024801	5697	5727
LA-3	5186	5589	355331106025501	5704	5727
LA-4	4615	5710	355337106054801	5583	5592
LA-6	4671	5678	355337106063701	5537	5553
G-3	5025	5825	355339106055701	5569	5560
353337106075001	5727	5878	355350106051001	5625	5612
353547106045901	6147	6173	355352106011201	5802	5825
353818106004901	6301	6360	355353105581701	6019	6042
353844105572201	6616	6685	355353105583401	6006	6006
353845105574101	6458	6694	355354105593701	5720	5963
353850106001801	6488	6540	355358106010001	5835	5848
353855106061501	6111	6134	355400105584301	6065	6055
353907105583701	6721	6721	355411106074001	5487	5517
353908105573201	6744	6708	355418106005201	5809	5855
353913106011701	6130	6291	355445105584201	6038	6048
353916105573201	6767	6701	355445106002701	5934	5934
353917106011501	6403	6291	355457106070901	5517	5520
353918105563101	6901	6862	355635106041901	5583	5553
353922105570801	6829	6747	355648106042801	5566	5537
353922106045301	6258	6176	355715106040201	5576	5546
353924106004101	6567	6580	355736106011101	5701	5753
353924106010801	6419	6304	355744106041201	5540	5514
353931106003701	6570	6583	355818106041301	5566	5569
353933105575601	6366	6721	355818106041302	5553	5569
353933105585101	6734	6721	355819106052001	5543	5602

353936105552701	7059	7085	355823106041301	5569	5579
353942105560401	7000	6990	355844106051101	5546	5573
353947105590801	6711	6698	355855106035201	5599	5592
354005106013501	6357	6163	355913106002901	5783	5779
354013105580601	6350	6717	355917106040501	5576	5583
354018105590701	6688	6711	355939106045401	5524	5576
354019105550701	7190	7101	355950105554501	6117	6104
354019105590801	6688	6714	360018105555601	6124	6117
354020105562001	6931	6990	360031105510601	6885	6957
354023105593101	6488	6511	360104106024801	5651	5632
354025105555501	6993	7052	360109106053501	5717	5710
354026105563401	6967	6980	360117106052901	5556	5655
354032105562001	7026	7022	360222106060001	5628	5628
354033105583701	6747	6747	360242105482201	7879	7902
354034105574301	6409	6776	360242105483001	7846	7892
354034105585201	6731	6724	360553106030701	5599	5628
354038105572101	6754	6763	360620106034001	5625	5642
354038105580301	6776	6744	360652106082101	5733	5753
354039105560301	7016	7019	360657106014601	5684	5701
354041105581301	6340	6737	360813105593001	5720	5730
354046105570601	6862	6806	360950105404001	7629	7695
354051105573601	6760	6717	361159105523401	6016	6022
354051105575101	6786	6750	361233105563601	5956	5983
354051105583901	6770	6724	361249105535801	5760	5845
354052105570201	6816	6918	361255105542101	5845	5852
361804106025001	6212	6209	361502106030801	6071	6084
362114106113301	6944	6940	361755106025501	6160	6173

Table 11. Comparison of permeability estimates from calibration with measured permeabilities.

|---------- PEST Results ----------| |---------- Data ---------
--------|

Hydrogeologic unit	Permeability (m^2)	Lower 95% Confidence Limit (m^2)	Upper 95% Confidence Limit (m^2)	Best-fit trial and error permeability (m^2)	Mean measured Permeability (m^2)	Number Of Samples	Permeability Range (m^2)
Basement rocks	5.00×10^{-16}	-----	-----	5.00×10^{-16}	-----	-----	-----
Paleozoic/ Mezozoic Rocks	2.00×10^{-17}	1.03×10^{-76}	$9.75 \times 10^{+41}$	2.00×10^{-17}	-----	-----	-----
Shallow Sange de Cristo	1.85×10^{-14}	1.45×10^{-14}	2.36×10^{-14}	1.00×10^{-14}	4.24×10^{-14}	16	1.08×10^{-15} to 1.30×10^{-11}
Deep Santa Fe Group	1.21×10^{-14}	2.09×10^{-15}	6.96×10^{-14}	1.00×10^{-15}	-----	-----	-----
Eastern Santa Fe Group	2.07×10^{-13} [a]	1.24×10^{-13}	3.45×10^{-13}	1.90×10^{-13} [b]	1.65×10^{-13}	15	2.91×10^{-14} to 5.19×10^{-12}
Western Santa Fe Group	1.40×10^{-13} [a]	1.14×10^{-13}	1.71×10^{-13}	6.00×10^{-14} [b]	2.44×10^{-13}	7	1.45×10^{-13} to 4.49×10^{-13}
Northern Santa Fe Group	1.50×10^{-14}	6.89×10^{-15}	3.25×10^{-14}	3.00×10^{-14}	-----	-----	-----
Pojoaque area Santa Fe Group	7.14×10^{-15} [a]	1.20×10^{-17}	4.26×10^{-12}	1.00×10^{-14}	-----	-----	-----
Aqua Fria Fault	4.49×10^{-15}	1.18×10^{-19}	1.71×10^{-10}	4.49×10^{-15}	-----	-----	-----
Airport Area Santa Fe Group	1.00×10^{-11} [a]	7.13×10^{-20}	1.40×10^{-03}	1.00×10^{-11} [b]	-----	-----	-----
Ancha Formation	1.34×10^{-13} [a]	1.52×10^{-15}	1.18×10^{-11}	4.00×10^{-14} [b]	6.27×10^{-15}	1	-----
Tshicoma	7.10×10^{-16}	1.02×10^{-16}	4.94×10^{-15}	1.25×10^{-15}	9.17×10^{-13}	1	-----
Pajarito Fault	2.13×10^{-15}	1.52×10^{-15}	2.97×10^{-15}	2.50×10^{-15}	-----	-----	-----
Cerros basalts	1.00×10^{-15}	1.00×10^{-315}	$1.00 \times 10^{+285}$	1.00×10^{-15}	-----	-----	-----
Puye Formation	2.38×10^{-13}	7.66×10^{-37}	7.38×10^{10}	4.70×10^{-14}	1.59×10^{-12}	14	1.93×10^{-13} to 1.16×10^{-11}
Totavi Lentil	1.00×10^{-13}	3.69×10^{-45}	2.71×10^{18}	1.00×10^{-12}	-----	-----	-----
Chaquequi	1.00×10^{-13}	3.36×10^{-15}	2.97×10^{-12}	1.00×10^{-12}	9.14×10^{-13}	16	2.56×10^{-13} to 8.63×10^{-12}
Bandelier Tuff	3.95×10^{-14}	9.42×10^{-161}	$1.65 \times 10^{+133}$	1.00×10^{-13}	1.02×10^{-13}	?	4.06×10^{-14} to 2.56×10^{-13}
Southern Cerros Basalts	1.00×10^{-16}	2.42×10^{-48}	$4.13 \times 10^{+15}$	1.00×10^{-16}	-----	-----	-----
Penasco	4.67×10^{-13}	2.51×10^{-13}	8.68×10^{-13}	1.50×10^{-13} [b]	-----	-----	-----
Ojo Caliente Formation	2.20×10^{-14}	1.31×10^{-14}	3.67×10^{-14}	3.25×10^{-14}	-----	-----	-----

[a] The vertical permeability for this unit was two orders of magnitude less than the value listed.
[b] The vertical permeability for this unit was one order of magnitude less than the value listed.

Table 12. Comparison of simulated ground-water flux with estimates based on streamflow measurements or other calculations.

Zone	Simulated Discharge (PEST-derived permeabilities) kg/s (cfs)	Simulated Discharge (Trial-and-error permeabilities) kg/s (cfs)	Estimated ground-water Discharge kg/s (cfs)
Basin boundary At Embudo	-79 (-2.8)	-5 (-0.18)	-10 (-0.35) [a]
Basin boundary near Rio Chama	-16 (-0.56)	-42 (-1.5)	----
Basin boundary near Jemez River	295 (10.4)	246 (8.7)	420.8 (14.9) [b]
Basin boundary with Albuquerque Basin	246 (8.7)	176 (6.2)	----
Rio Grande between Embudo and Espanola (includes Rio Embudo)	682 (24.1)	641 (22.6)	809.8 (28.6) [b]
Rio Grande between Espanola and Otowi	334 (11.8)	291 (10.3)	890.4 (31.4) [b]
Rio Grande between Otowi and Cochiti Reservoir	382 (13.5)	365 (12.9)	366.2 (12.9) [b]
Rio Grande below Cochiti Reservoir	-3 (0.11)	-5 (0.18)	----
Rio Chama	455 (16.1)	505 (17.8)	546.9 (19.3) [b]
Lower Pojoaque River	280 (9.9)	398 (14.1)	212.0 (7.5) [c]
Lower Santa Fe River	147 (5.2)	144 (5.1)	228.8 (8.1) [b]
Beneath Cochiti Reservoir	-20 (0.71)	-12 (0.42)	----

[a] Estimated from a Darcy's Law calculation using the measured hydraulic gradient and an assumed value of permeability.

[b] Estimated from streamflow data

[c] Estimated by the flow model of McAda and Wasiolek (1988).

Table 13 here

Appendix I.

Grid Generation Process for Orthogonal Structured Grids

The grid generation strategy is to create an orthogonal structured grid, with a constant x and y grid spacing and variable z spacing. To resolve the high aspect ratio of the geologic layers requires higher resolution in the z dimension than in the x and y dimensions. A cell dimension of 1000 meters in the x-dimension and 1055 meters in the y-dimension is adequate to resolve lateral geologic and hydrologic gradients on the regional scale. However, to resolve key geologic and hydrologic gradients in the areas of interest and in an effort to cut down on the number of nodes, two distinct vertical zones of resolution are used. In the upper elevations of the model, defined at >1300 meters, a resolution of 50 meters in the z-dimension is used. In the lower elevations of the model, defined at < 1300 meters, a resolution of 500 meters in the z dimension is used. For the OMR grid the two distinct verticals zones of resolution occur at the 1100 meter level. (See Table 1).

Material properties that relate to the stratigraphic framework model must be assigned and parts of the grid which are outside the Espanola basin or above the water table removed. Material properties are assigned by superimposing the computational grid and the surfaces from the framework model. Each node of the computational grid is located within the layer sequence and assigned a material number. For example, if a node is located between the top and bottom surface of stratigraphic unit 4, then the node would have a material number of 4. A similar process is used to determine which nodes are above the water table or outside the Espanola basin. Once determined these nodes are removed from the grid. The resulting computational grid contains 110,284 nodes.

Grid Generation Process to create Octree (OMR) grid

The grid generation process for the OMR grid starts with determining what the initial point distribution/resolution will be for the majority of the nodes in the grid. The initial point distribution is highly dependent on what resolution will be sufficient to capture the coarse sections of the model and adequate, after refinement, to capture geologic features at a greater resolution in the areas of interest. The initial X,Y cell resolution of the OMR grid was exactly the same as the orthogonal grid (Table 1).

Once an initial point distribution for the grid is established, we then determine where increased resolution is needed. Based on previous modeling efforts for the Espanola Basin and the need to capture site-scale process within the basin, more resolution is needed for areas encompassed by the LANL boundary, the Buckman well field, and the Santa Fe well field. One polygon is defined that encompasses those areas within both the LANL boundary and the Buckman well field and another that encompasses the Santa Fe well field. OMR is used to refine elements with at least one node that falls within the polygons to four times the initial resolution in the horizontal dimensions. After employing the OMR technique horizontal cell resolution is approximately 250 meters in those areas refined (See Figure 2).

Once the OMR is used and a desirable point distribution is achieved for the grid, the next step in the process is to read in all of the geologic surface information from the geologic framework model. The elements are hexahedra when the geologic materials are assigned. Once hexahedral elements and nodes are assigned material numbers, the OMR grid is converted into a tetrahedral grid. Although this tetrahedral grid does not satisfy all criteria for grid quality, it can be used to set the correct geologic materials.

A parallel process to the one listed above for the OMR grid starts with the OMR grid produced after running the OMR commands on the initial point distribution. The nodes are copied and are reconnected to establish element connectivity using a command in LaGriT to ensure a Delaunay grid. At this point in the grid process there are two different grids, one which has the elements identified with the correct geologic materials, and another that is a Delaunay grid but without geologic materials established. Because the former grid has the correct element materials set, it is used as a source to interpolate the element materials numbers and set element material numbers correctly on the Delaunay grid. The algorithm in LaGrit loops though each of the elements in the

sink grid, computes the centroid of the sink element, finds the element of the source grid element and assigns the material number from source to sink grid. After the interpolation procedure occurs the non-Delaunay grid is no longer used in the grid generation process.

At this point it is possible to remove all of the elements that are identified as being above the water-table surface. Then the geologic surfaces must be re-read into LaGrit to establish the correct node materials for the grid. Since equivalent materials in the geologic model building process are artificially broken-out into separate materials they are recombined at this point in the grid generation process. In addition to recombining units, unique hydrostratigraphic zones are created using various three-dimensional polygons that define which nodes belong to which zones. As listed above the Tesuque unit is broken into 7 distinct hydrostratigraphic zones. The Santa Fe group is broken into six unique hydrostratigraphic zones and two unique zones are created for the Pajarito and Agua Fria faults. There is also a zone defining the Paleozoic/Mesozoic boundary. The last step was to create a unique hydrostratigraphic zone that delineates the Pajarito fault. Using LaGriT, the existing surface trace of the fault was extruded to the bottom of the computational grid creating a vertical surface. Offsetting a copy of the existing fault 1200 meters east created a duplicate vertical surface. The offset surface and the original surface were connected in such a way to create a 3-D polygon. Any nodes in the computational grid that fall within the fault polygon were identified as part of the Pajarito fault hydrostratigraphic zone.

Once the nodes are correctly identified, LaGriT is used to create all of the files required by FEHM for flow and transport computations. The OMR grid is composed of 301,436 nodes, 1,688,457 elements, and 21 unique hydrostratigraphic materials.

Appendix II. Withdrawal data

Note regarding Tables 1 and 2: For a subset of years, only total pumping rates were supplied for Buckman and Santa Fe well fields. To apportion total pumping amongst individual wells in the wellfield, we used ratios derived from years when detailed data was available to assigned estimated withdrawal rates for each well. These estimates are indicated in red. When more detailed records become available for these years, we will substitute these numbers for the estimates.

Table 1. Withdrawal rates for Buckman wellfield, in kg/s

Year/Well	1	2	3	4	5	6	7	8	Total
1972	4	5	2	4	1	7	4	5	32
1973	11	14	5	11	4	18	12	13	88
1974	15	20	7	16	5	26	17	19	125
1975	11	14	5	12	4	19	13	13	90
1976	12	16	6	13	4	21	14	15	103
1977	14	19	7	15	5	25	16	18	118
1978	7	10	4	8	2	13	8	9	61
1979	2	3	1	3	1	4	3	3	19
1980	2	3	1	2	1	4	3	3	19
1981	39	56	6	13	4	20	14	14	166
1982	22	27	3	6	2	10	7	7	83
1983	0	0	0	0	0	0	0	0	
1984	4	8	1	1	0	2	1	2	20
1985	17	25	2	5	2	8	5	6	70
1986	22	36	3	7	2	11	8	8	99
1987	21	34	3	7	2	11	7	8	92
1988	21	28	3	18	1	22	11	12	117
1989	21	48	10	39	6	48	20	22	213
1990	13	32	10	39	6	46	17	18	181
1991	7	21	7	24	4	31	11	14	119
1992	7	28	4	20	1	46	38	36	181
1993	27	28	6	24	6	46	41	36	213
1994	27	28	4	25	10	39	24	29	187
1995	36	31	14	29	14	38	32	29	224
1996	35	27	24	24	17	36	22	29	215
1997	35	31	20	17	6	39	20	13	180
1998	31	32	20	15	6	39	25	34	202

Table 2. Withdrawal rates for City of Santa Fe wellfield, in kg/s

Year	Agua Fria	Alto	Ferguson	Osage	Santa Fe	Torreon	St Michaels	Total
1950	2	1	1	0	1	0		4
1951	37	11	9	1	10	7		74
1952	13	4	3	0	3	2		26
1953	11	3	3	0	3	2		22
1954	30	9	7	1	8	5		60
1955	30	9	7	1	8	6		61
1956	48	14	12	1	13	9		96
1957	18	5	4	0	5	3		37
1958								
1959	23	7	6	0	6	4		46
1960	10	3	2	0	3	2		20
1961	9	2	2	0	2	2	1	18
1962	6	2	2	0	2	1	10	22
1963	11	3	3	0	3	2	5	27
1964	40	11	10	1	11	7	37	117
1965	4	1	1	0	1	1	0	7
1966	3	1	1	0	1	0	2	7
1967	46	13	11	1	12	8	29	121
1968	20	6	5	0	5	4	5	45
1969	25	7	6	1	7	5	0	49
1970	67	19	16	1	18	12	26	160
1971	60	17	15	1	16	11	30	150
1972	59	17	14	1	16	11	21	139
1973	16	5	4	0	4	3	3	36
1974	29	8	7	1	8	5	23	82
1975	8	2	2	0	2	1	1	17
1976	24	7	6	0	6	4	18	67
1977	27	8	6	1	7	5	22	75
1978	10	3	2	0	3	2	11	30
1979	21	6	5	0	5	4	3	44
1980	29	8	7	1	8	5	0	58
1981	39	13	8	0	15	3	22	101
1982	32	10	10	0	17	8	7	84
1983	53	14	3	0	21	15	0	107
1984	51	17	11	0	21	6	5	110
1985	38	13	14	0	17	0	4	86
1986	32	14	15	0	17	0	2	81
1987	58	13	17	0	18	0	2	107
1988	51	17	13	1	11	0	17	110
1989	59	20	14	1	3	1	22	120
1990	58	15	11	1	13	0	15	113
1991	52	15	11	1	11	0	2	93
1992	53	11	11	1	3	0	5	85
1993	53	11	10	1	0	0	1	77
1994	51	0	15	1	0	8	3	79
1995	49	0	15	0	0	8	4	77
1996	49	0	13	1	1	7	25	97
1997	27	0	11	1	0	0	8	47

1998	42	0	14	0	0	20	7	83

PuO_2^+

$$> FeOH + PuO_2^+ => FeOHPuO_2^+ \qquad \log K = 4.79 \quad K_{lump} = K[> FeOH] =$$

$$> FeOH + PuO_2^+ + H_2O => FeOHPuO_3^- + 2H^+ \qquad \log K = -10.66 \quad K_{lump} = \frac{K[> FeOH]}{[H^+]^2} =$$

$$> Ca^{+2} + PuO_2^+ => PuO_2^+ + Ca^{+2} \qquad \log K = 1.85 \quad K_{lump} = \frac{K[> Ca^{+2}]}{[Ca^{+2}]} =$$

$$> AlOH + PuO_2^+ => AlOPuO_2 \qquad \log K = -3.09 \quad K_{lump} = K[> AlOH] =$$

$$> SiOH + PuO_2^+ => SiOPuO_2 \qquad \log K = -6.43 \quad K_{lump} = K[> SiOH] =$$

$$> SiOH + PuO_2^+ + H_2O => SiONpO_3H^- + 2H^+ \qquad \log K = -14.80 \quad K_{lump} = \frac{K[> SiOH]}{[H^+]^2} =$$

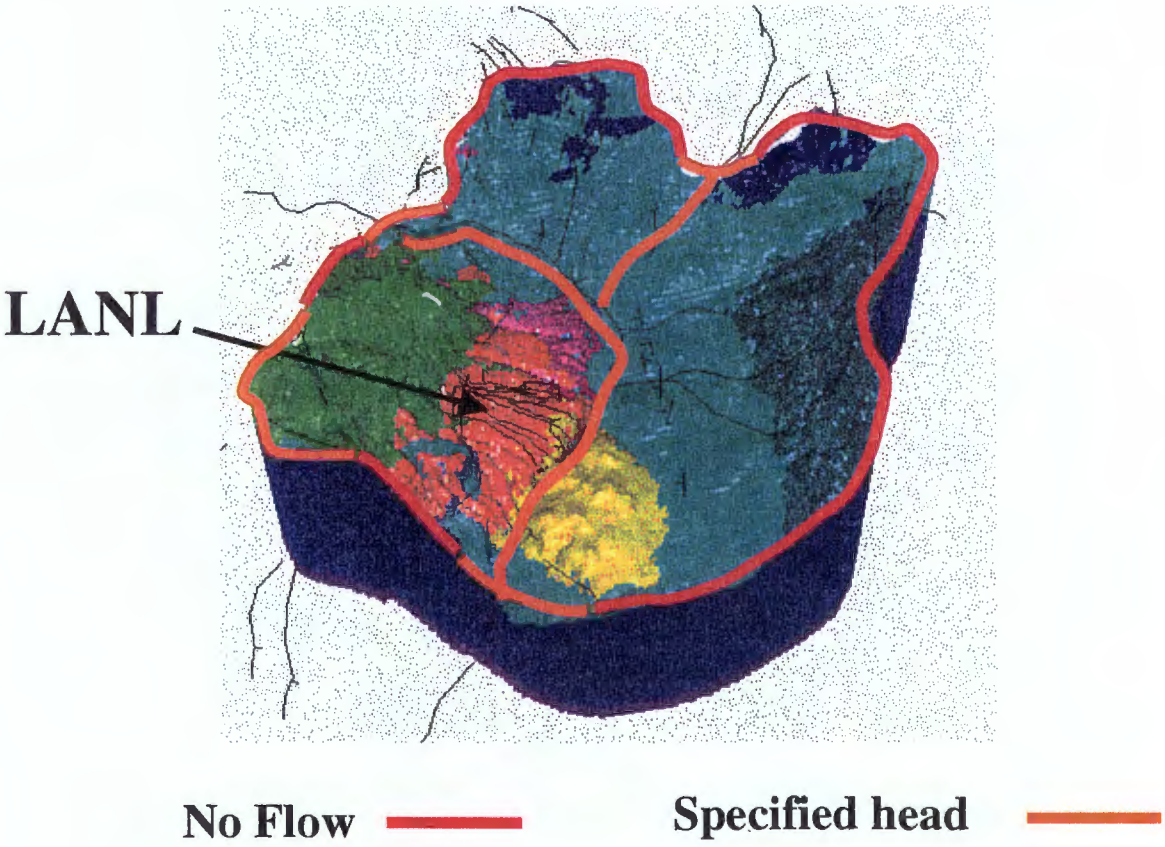

Figure 1. Location of model boundaries and type of flow conditions specifies at those boundaries in FEHM

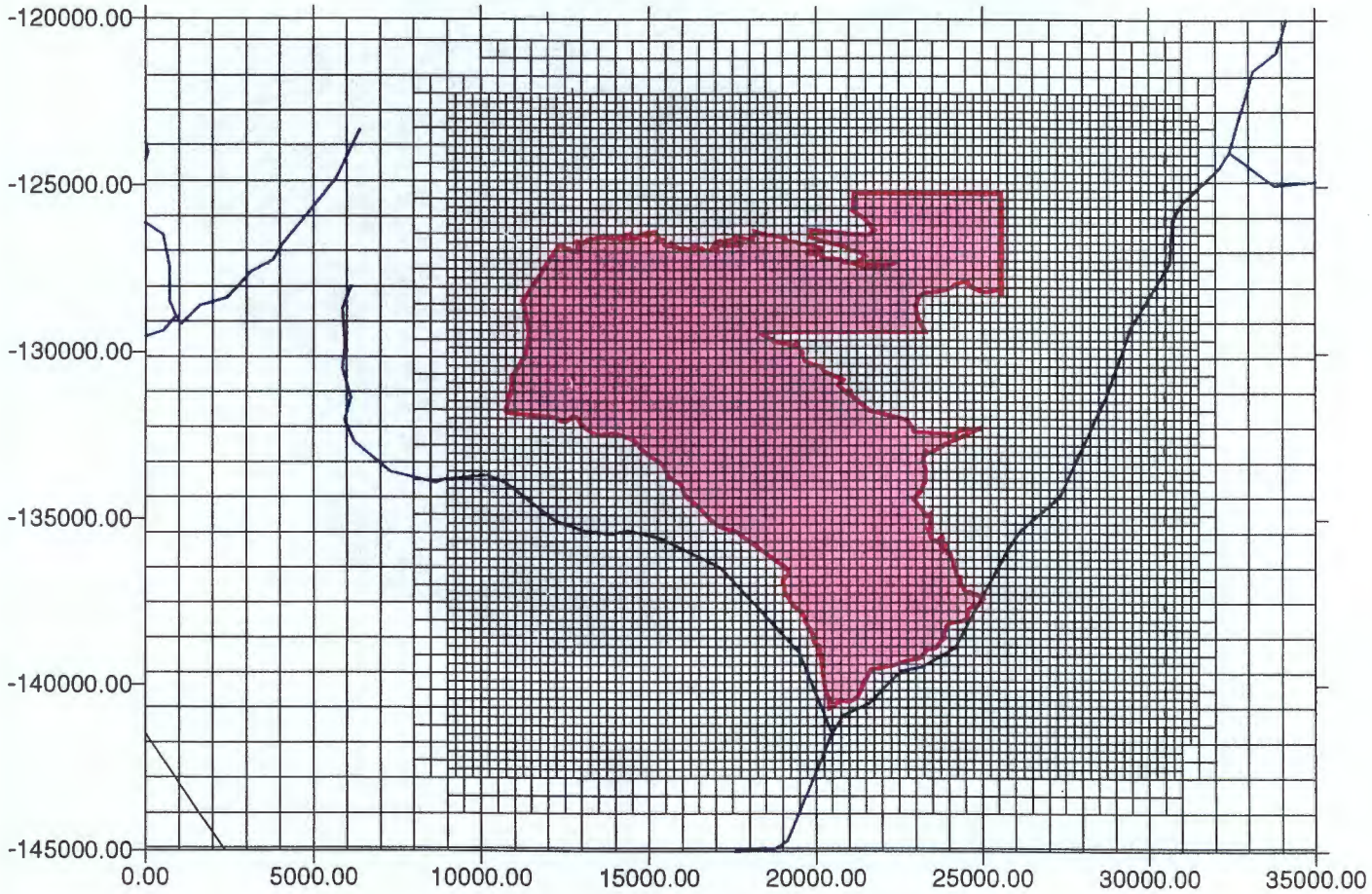

Figure 2. Computational mesh, showing grid refinement near LANL. Units are meters.

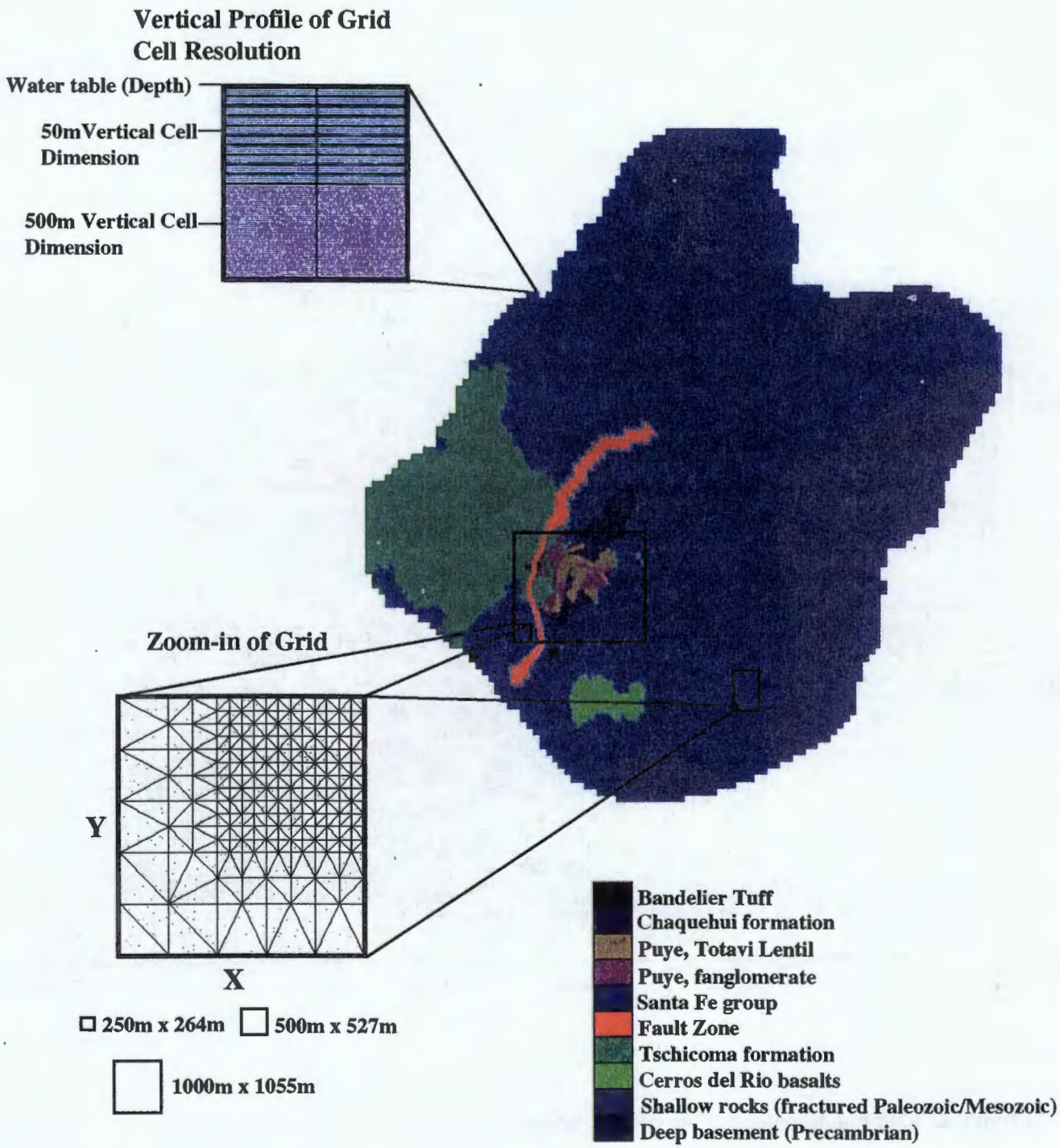

Figure 3. Numerical grid, showing hydrostratigraphic units (undifferentiated Santa Fe Group) and zones of increased grid resolution

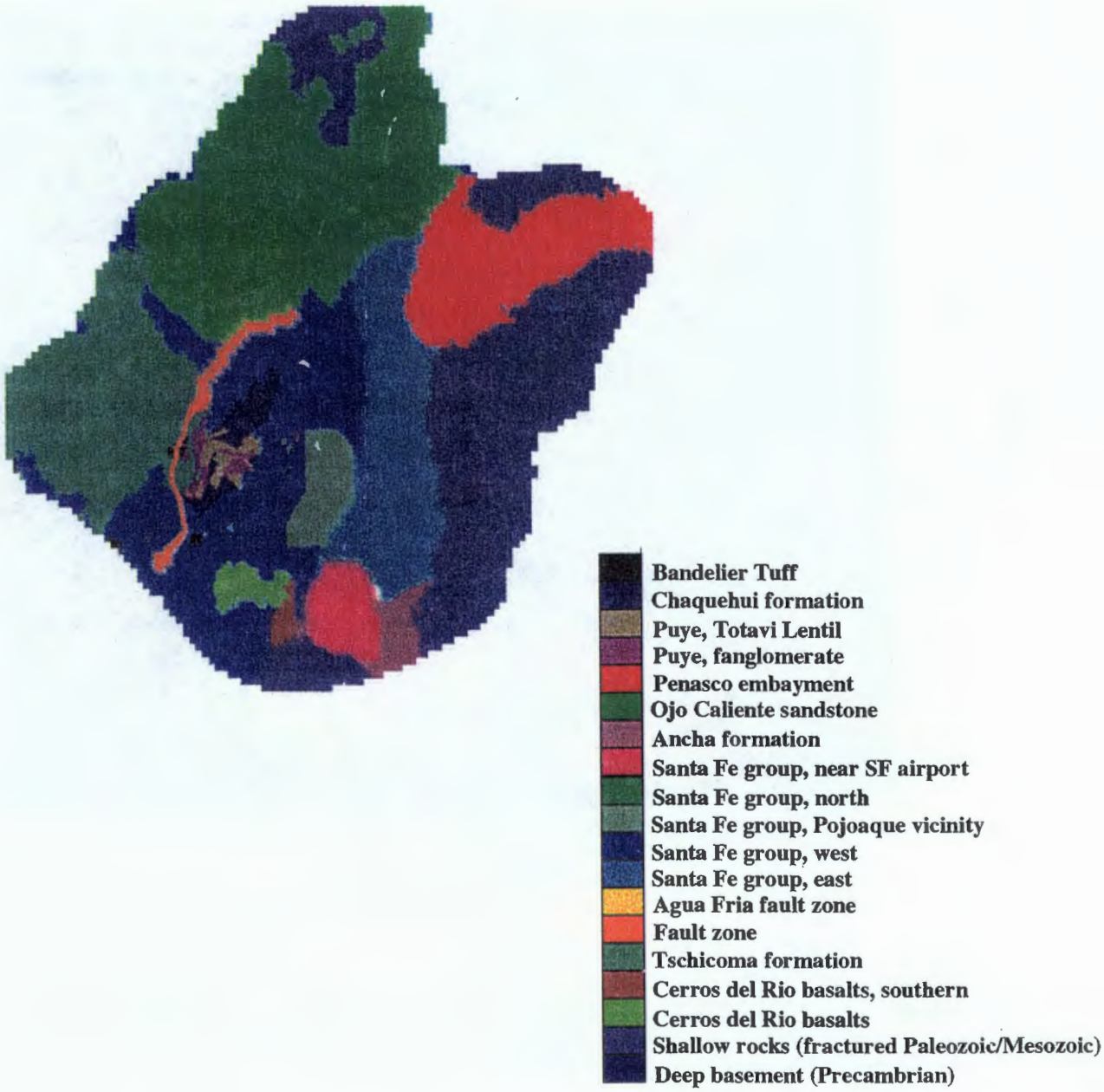

Figure 4. Hydrostratigraphic framework model, with Santa Fe Group sub-units colored

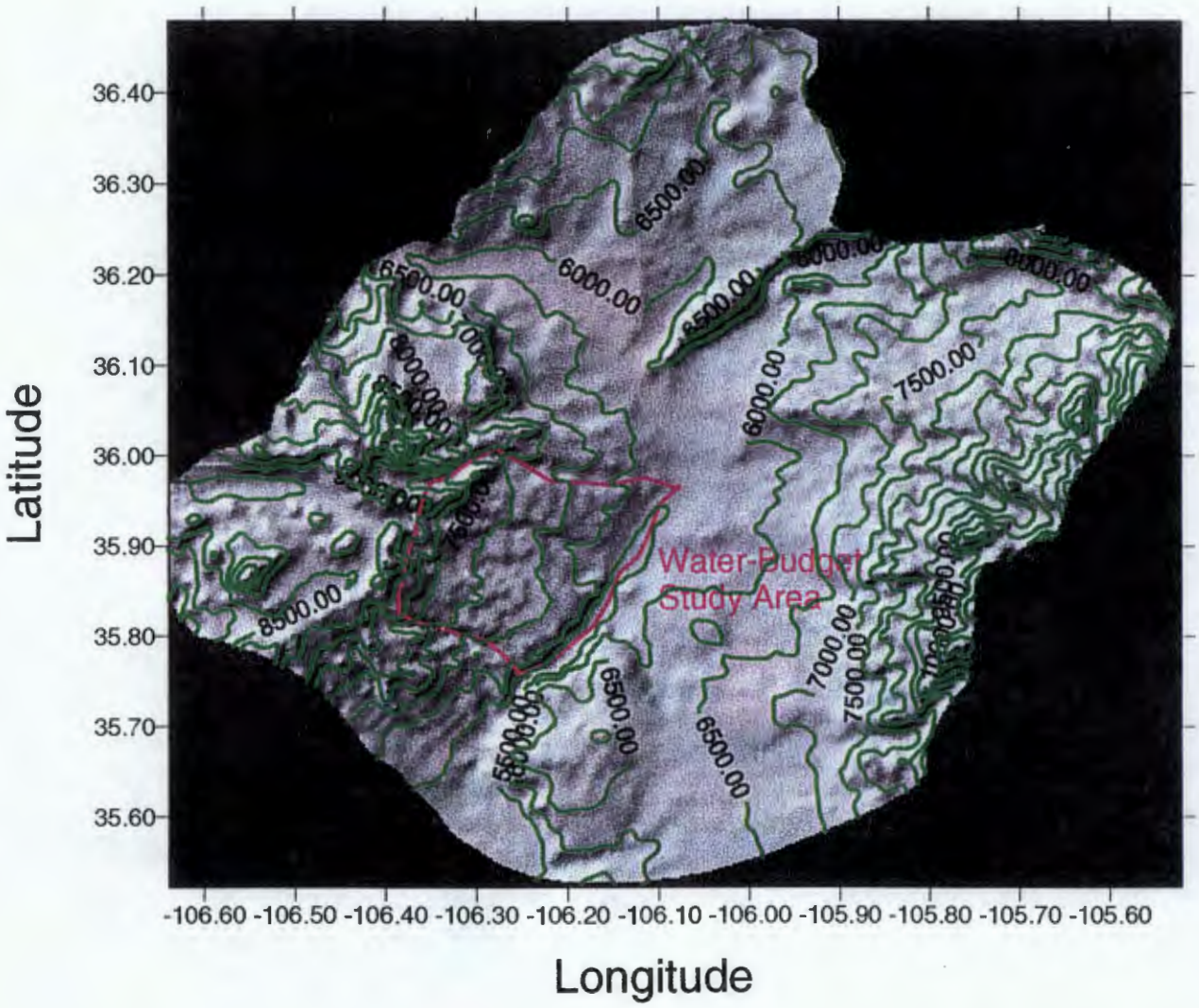

Figure 5. Area considered in pre-development water-budget analysis. Elevation contours in the Espanola Basin are shown in feet.

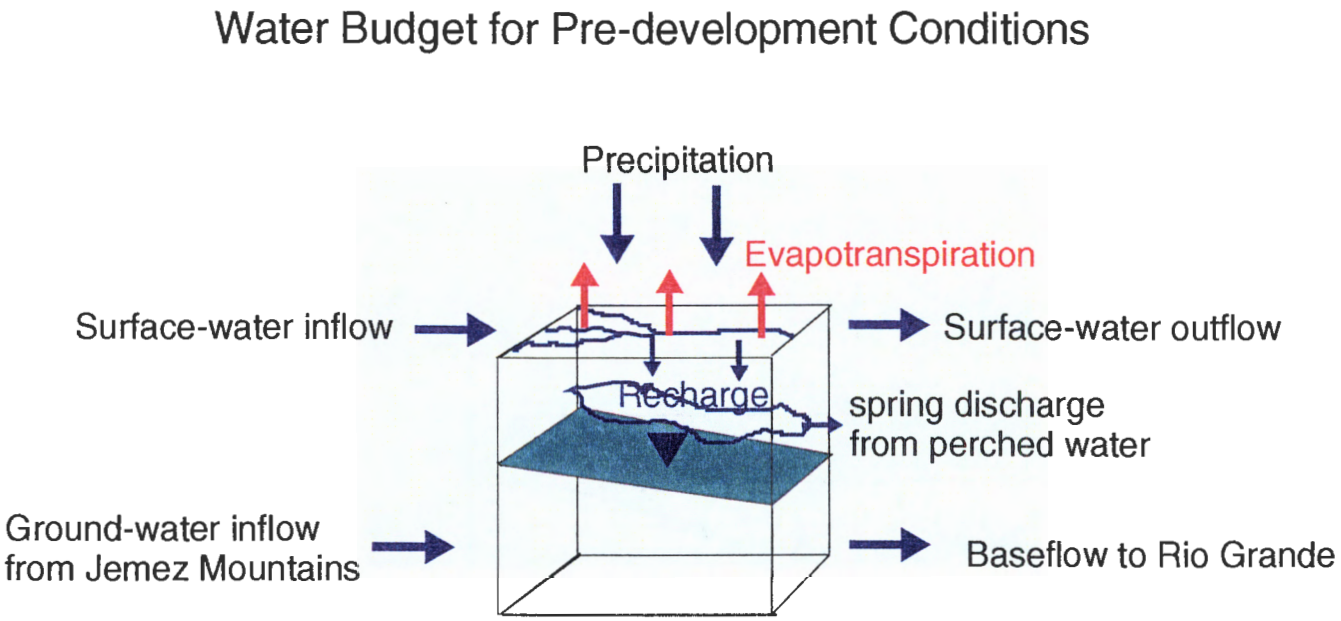

Figure 6. Conceptual framework for pre-development water-budget analysis.

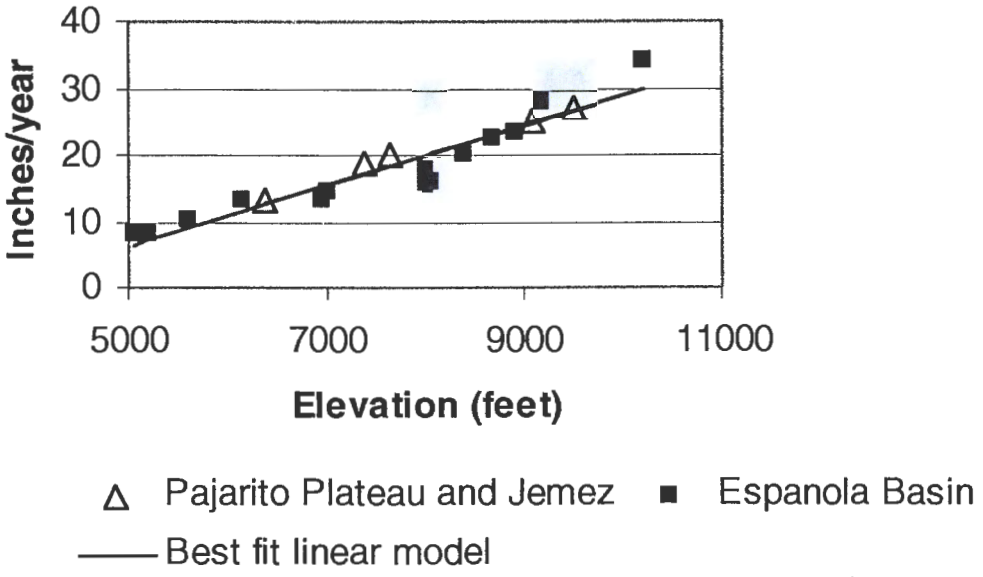

Figure 7. Precipitation data for the Espanola Basin

Figure 8. Location of stream gaging stations within the water budget study area

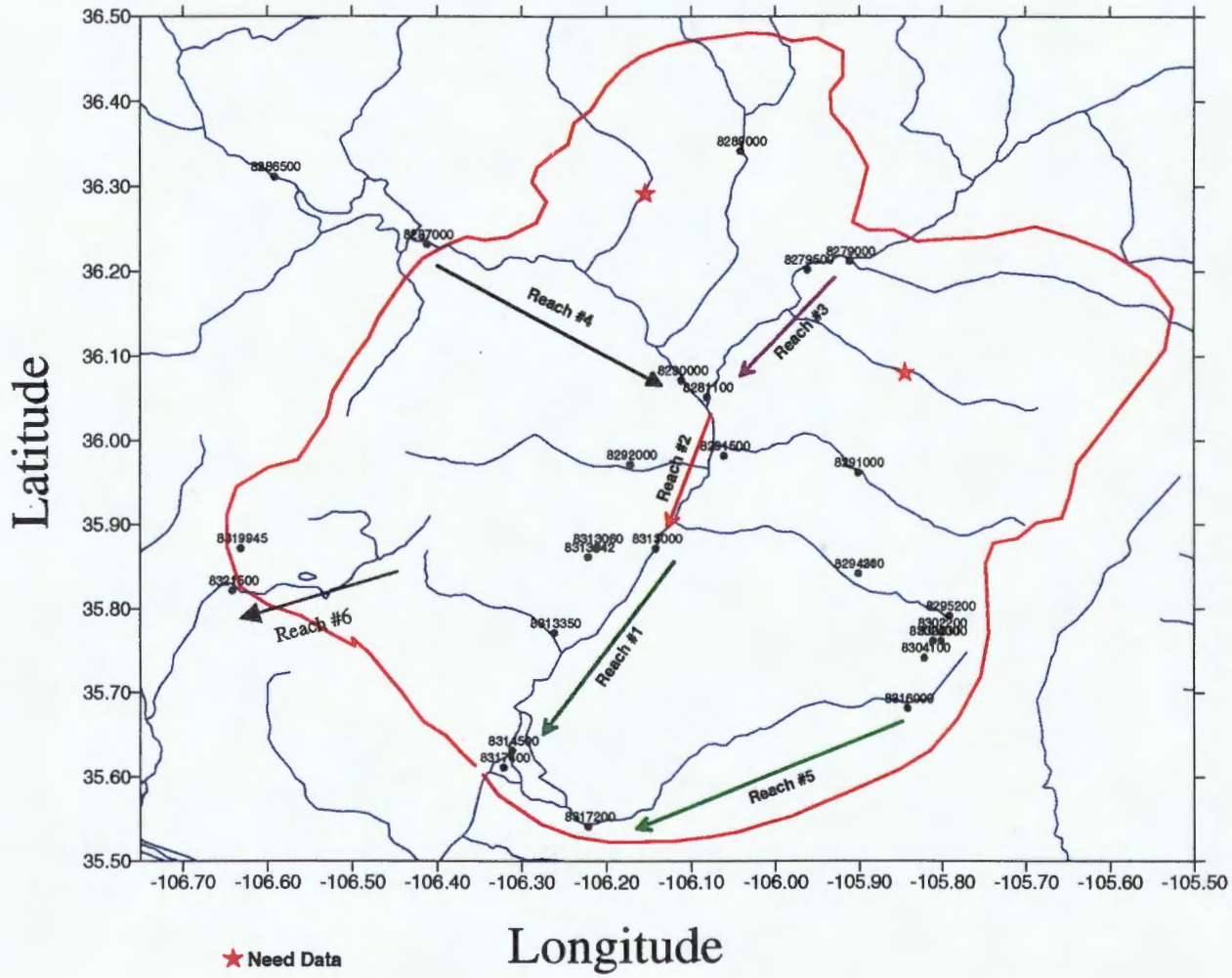

Figure 9. Locations of stream gaging stations in the Espanola Basin

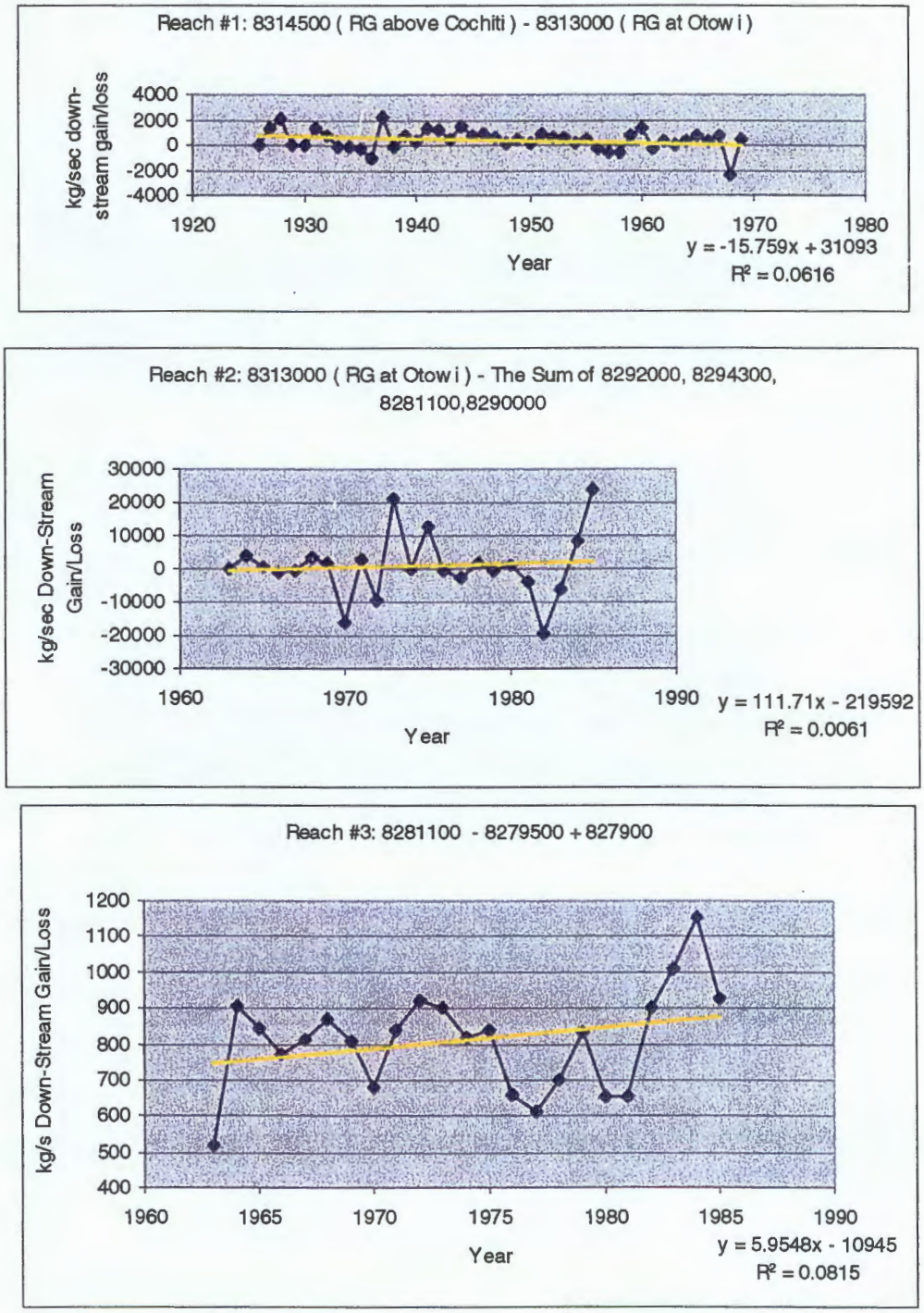

Figure 10. Yearly baseflow gains along various reaches of streams and rivers in the Espanola Basin

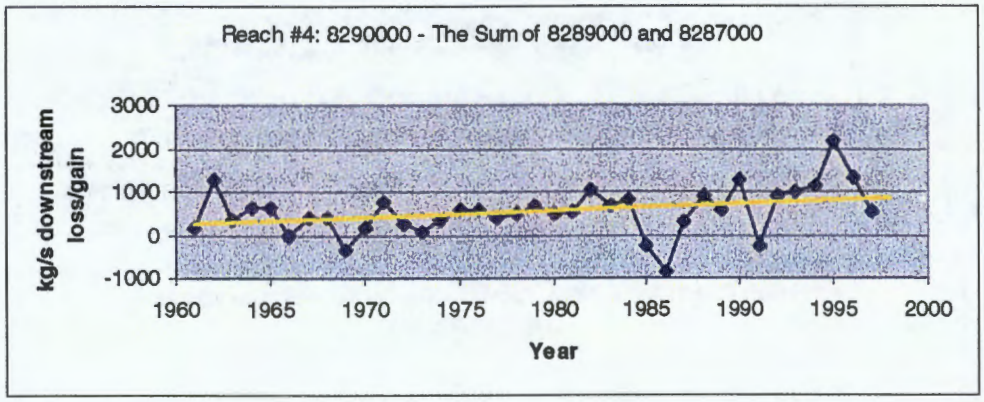

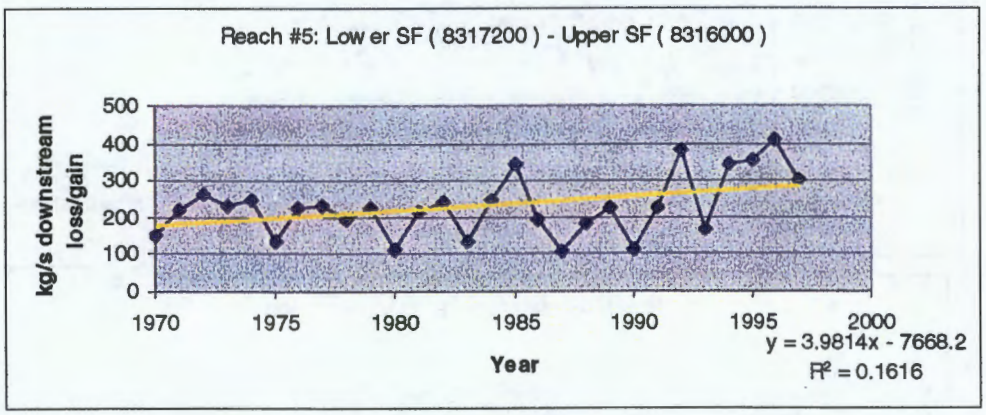

Figure 10 (continued). Yearly baseflow gains along various reaches of streams and rivers in the Espanola Basin

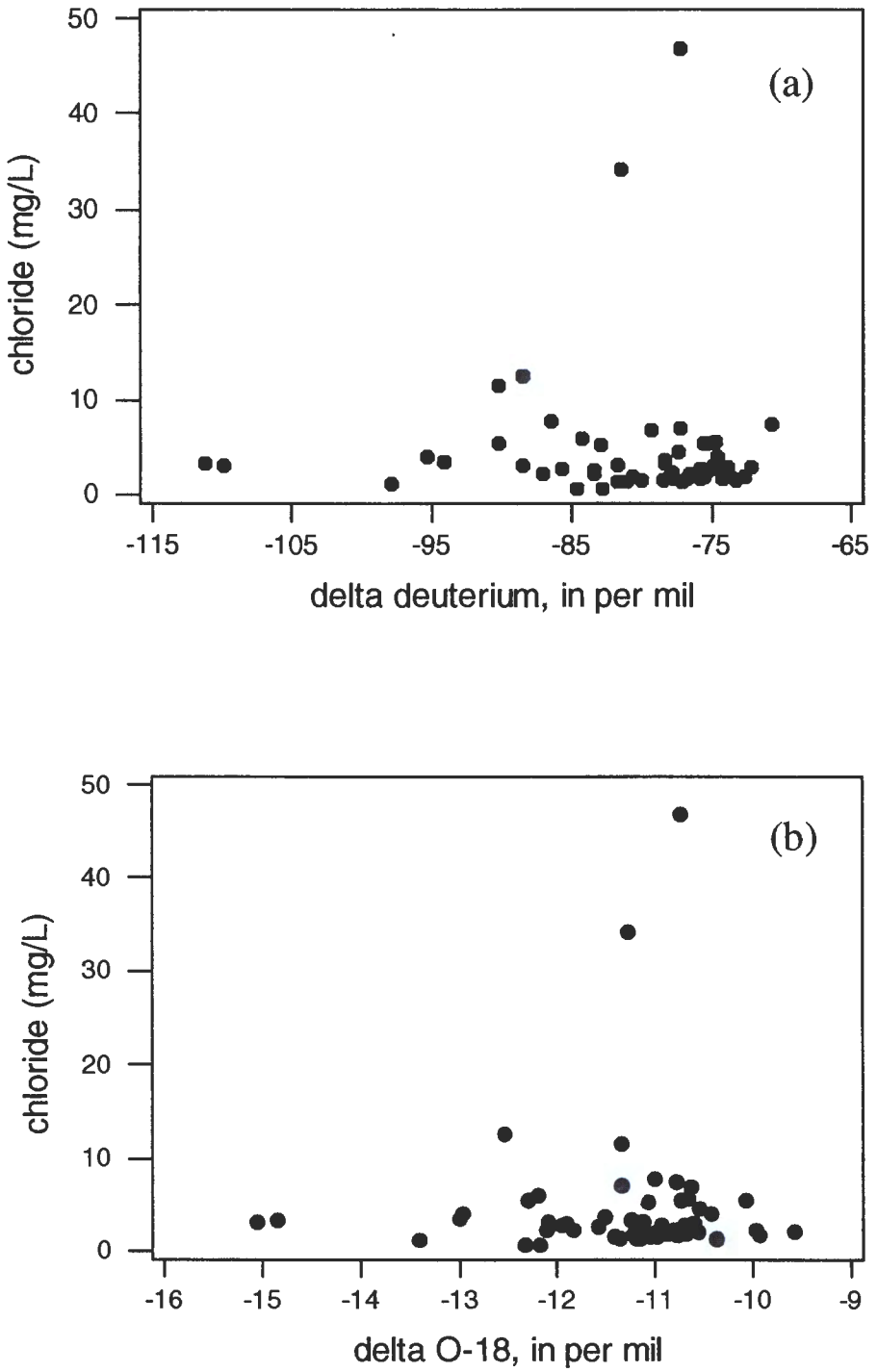

Figure 11. Data from Blake et al. (1995) showing the relation between (a) chloride and delta deuterium and (b) chloride and oxygen-18 in selected spring and ground-water samples.

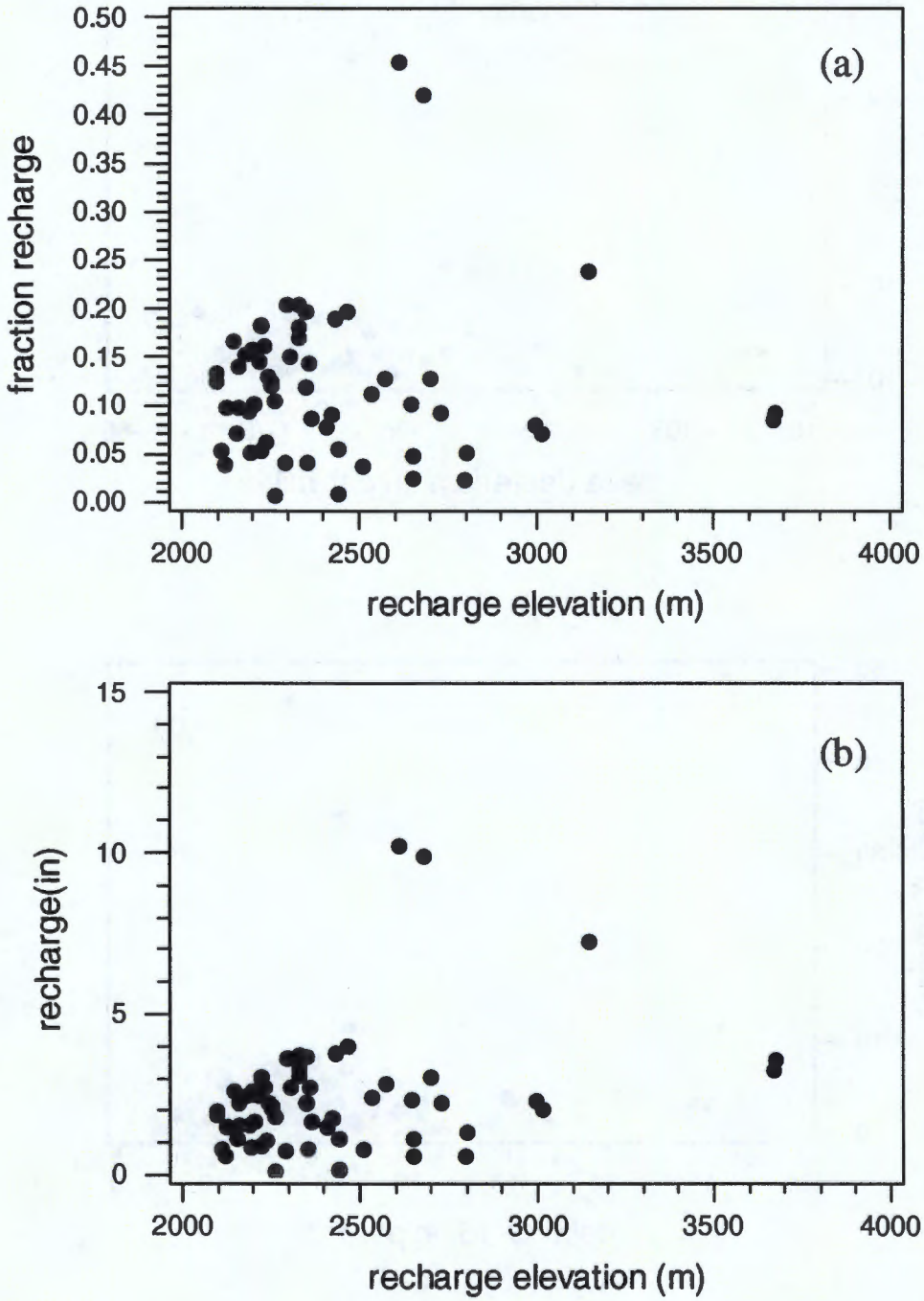

Figure 12. Relations between (a) the fraction of precipitation that becomes recharge and estimated recharge elevation, and (b) recharge magnitude and estimated recharge elevation, based on chloride, delta deuterium and delta oxygen-18.

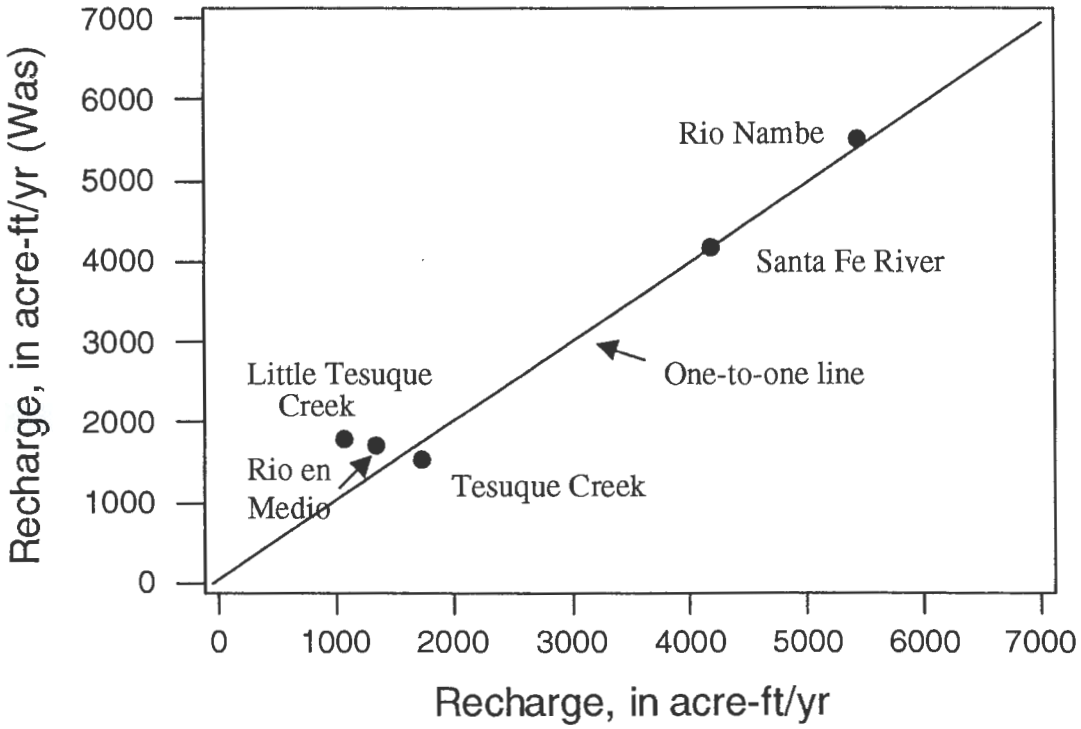

Figure 13. Fit of the recharge model to the recharge estimates of Wasiolek (1995)

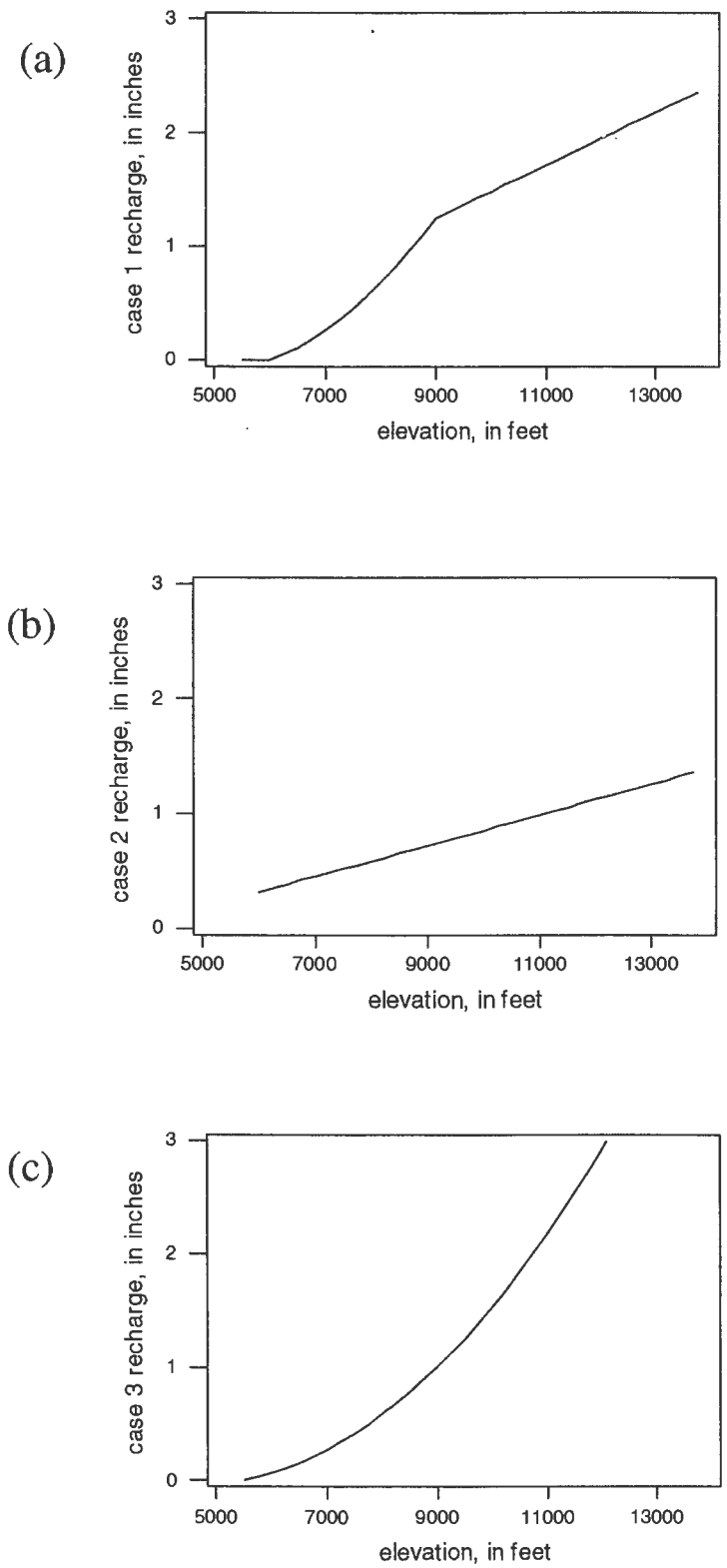

Figure 14. Recharge versus elevation for (a) case 1, (b) case 2, and (C) case 3.

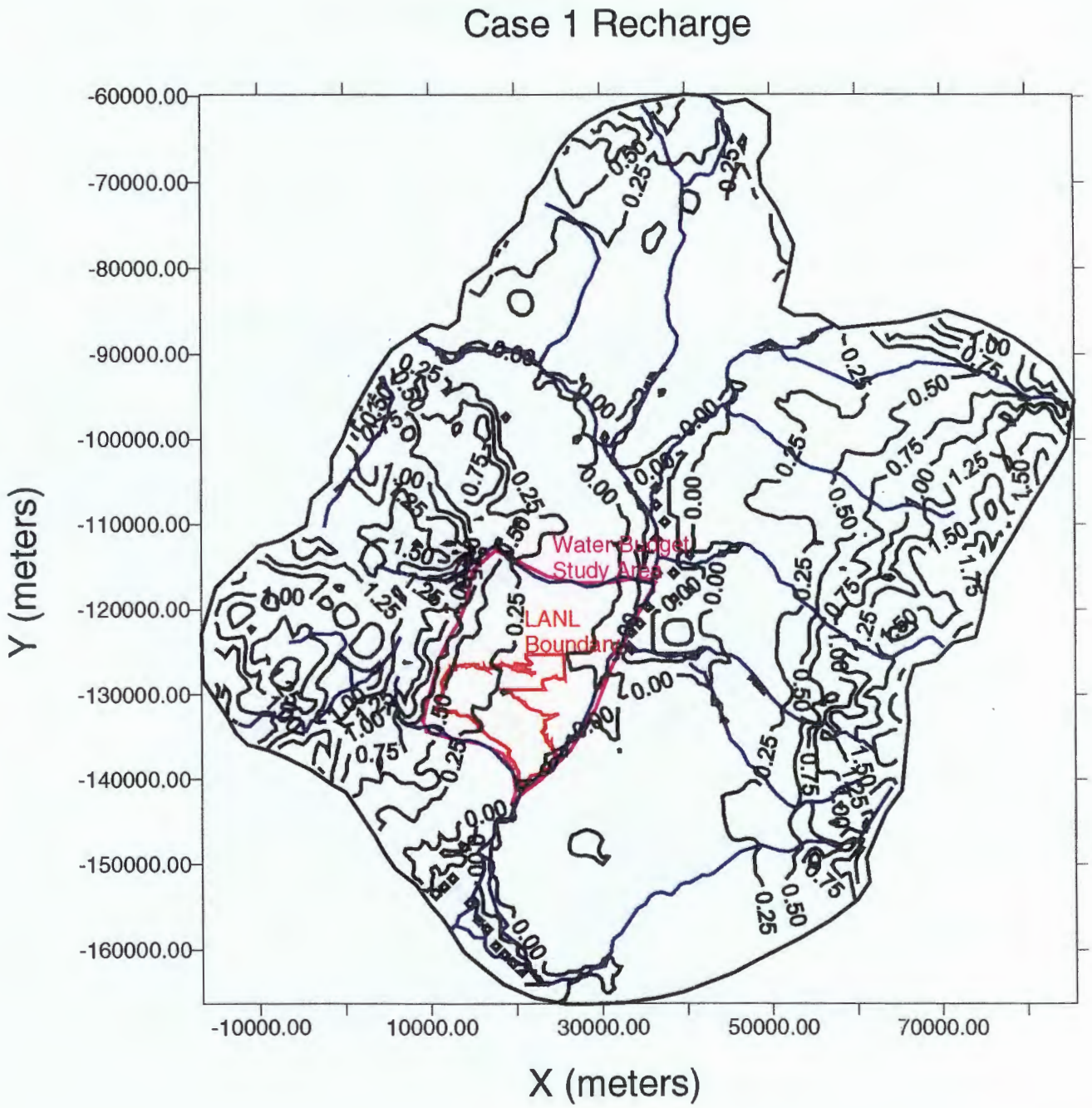

Figure 15a. Areal distribution of recharge for Case 1

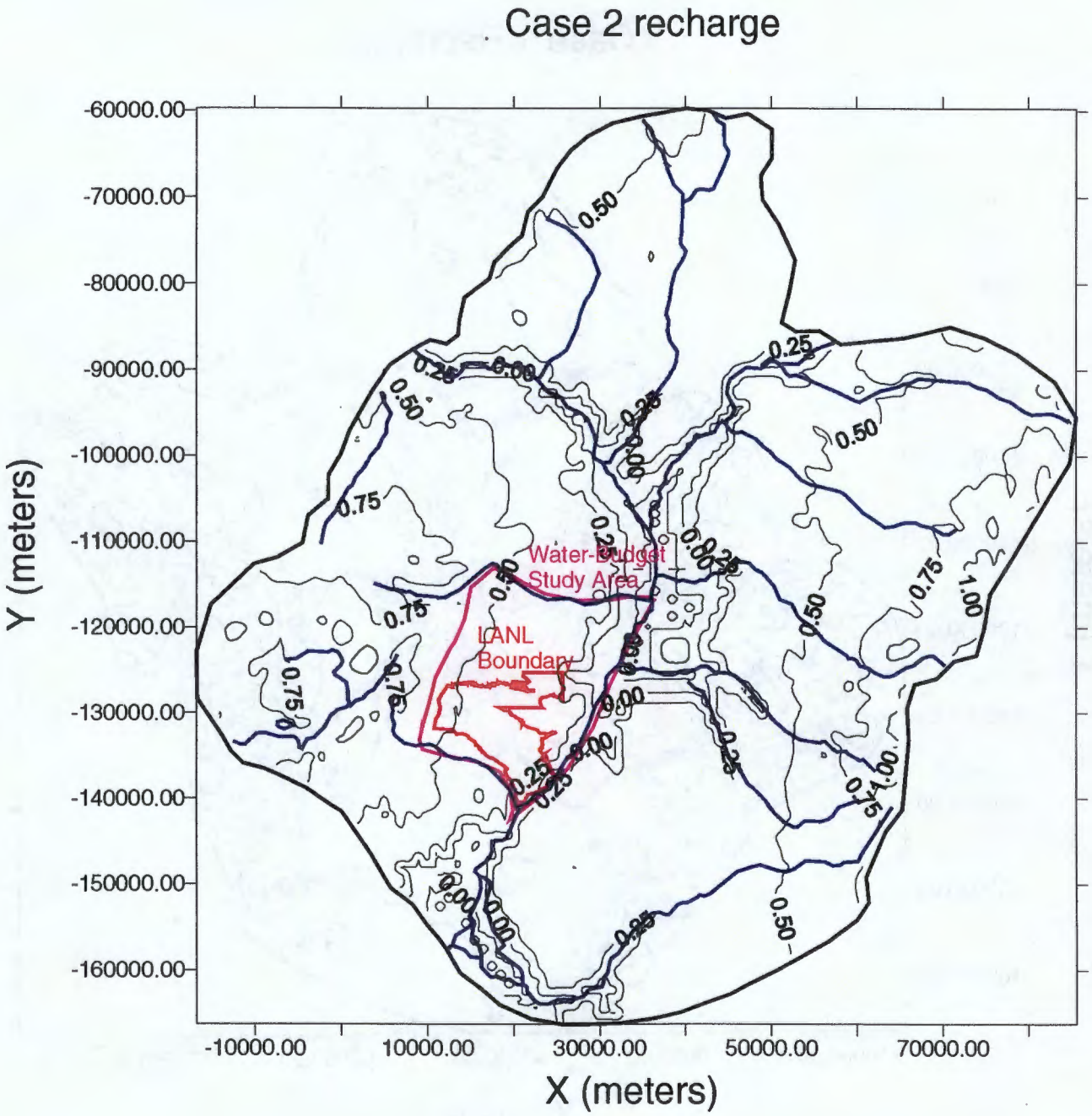

Figure 15b. Areal distribution of recharge for case 2.

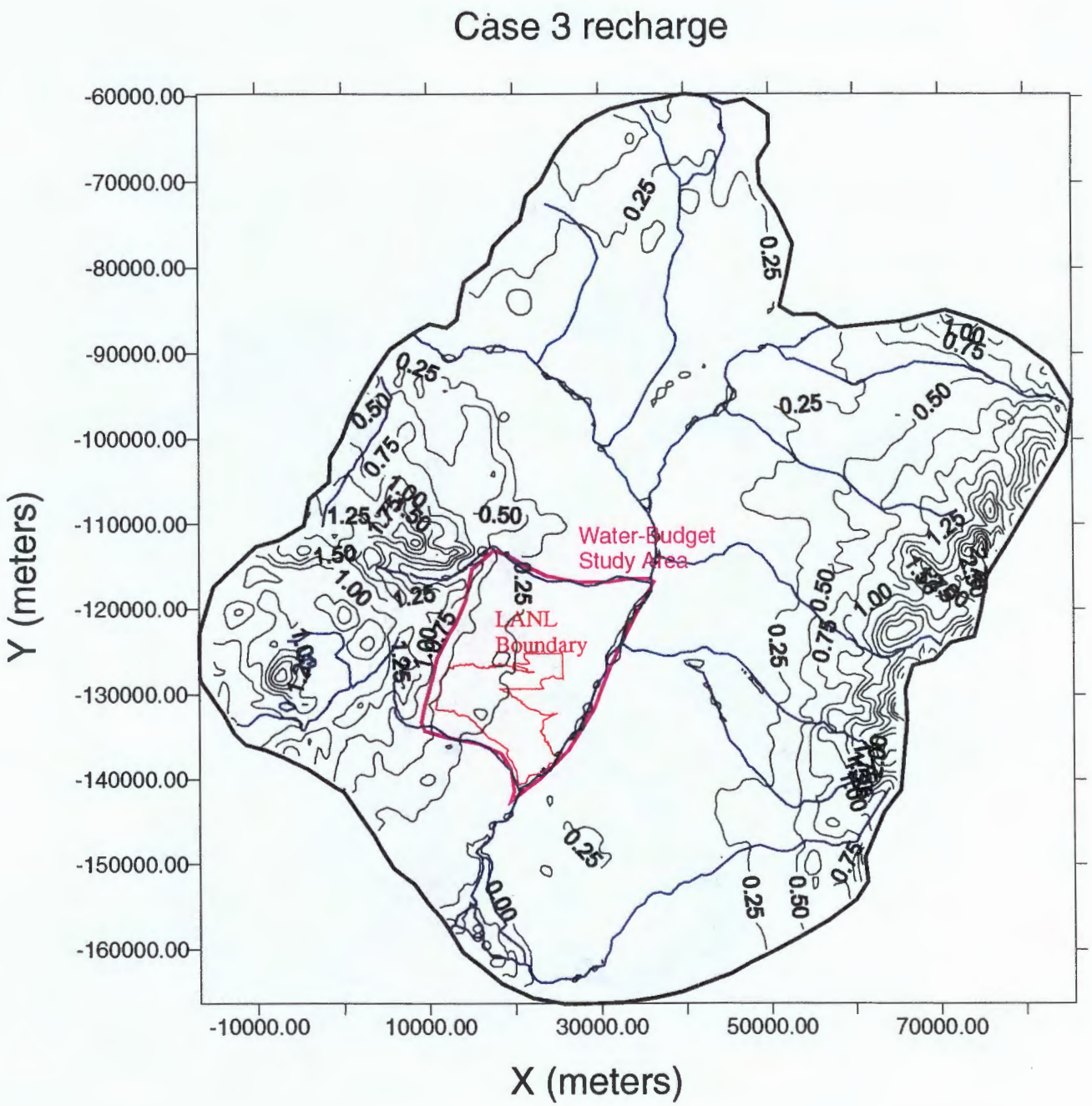

Figure 15c. Areal distribution of recharge - Case 3

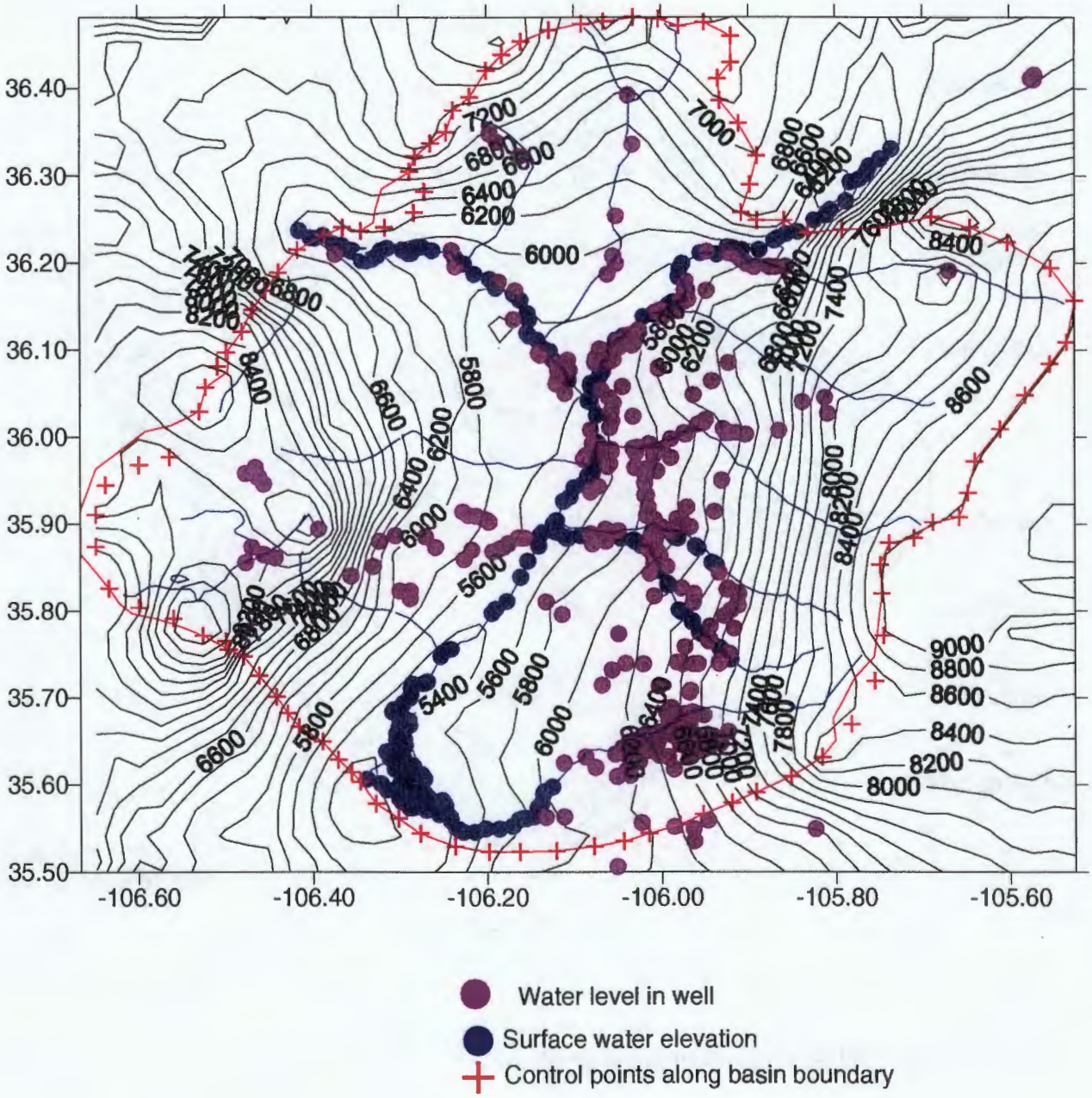

Figure 16. Approximation to pre-development water table. Red crosses are points added for the purpose of illustration and do not enter into model calculations

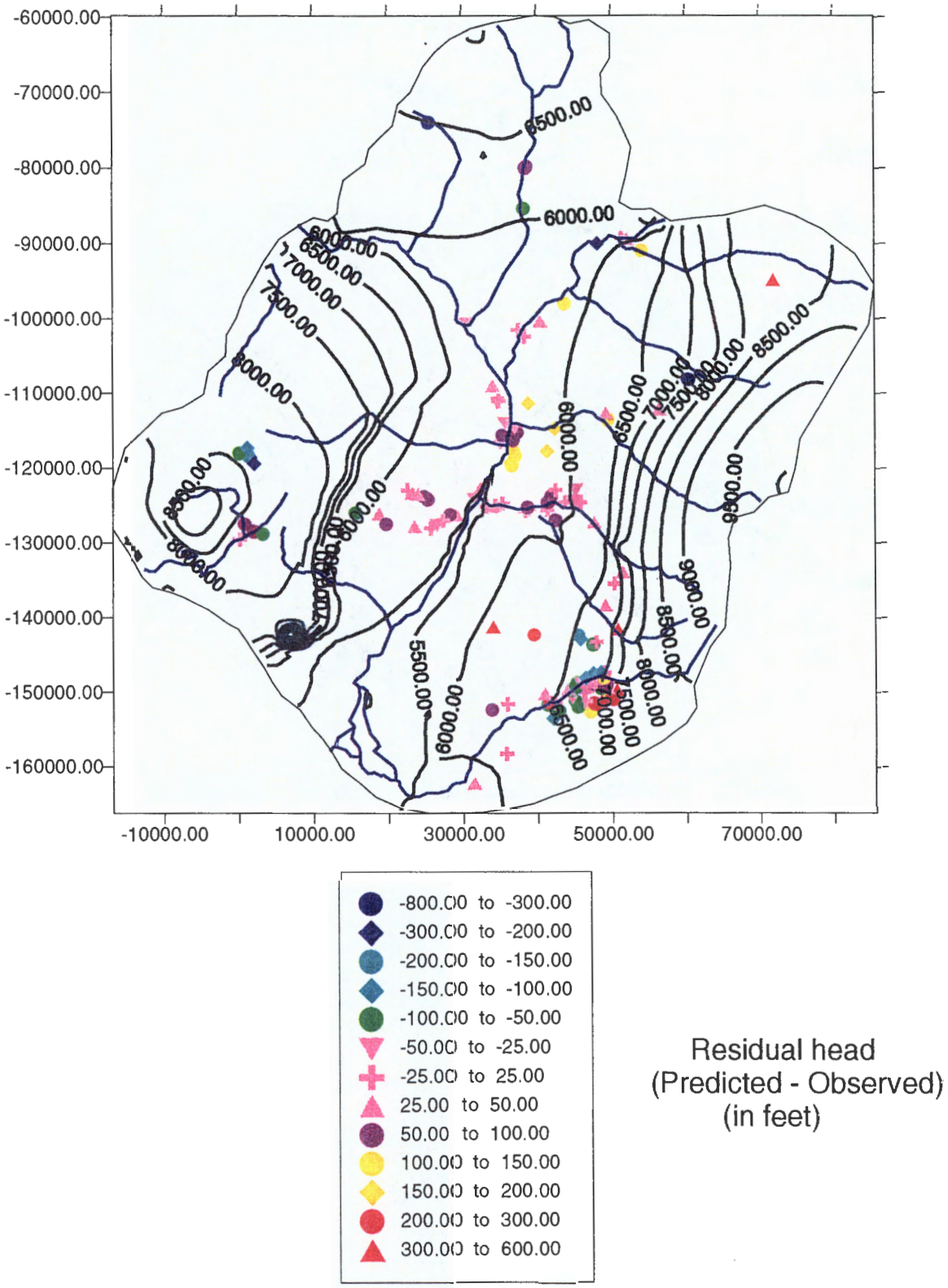

Figure 17. Simulated potentiometric surface and residuals using best-fit trial-and-error permeabilities.

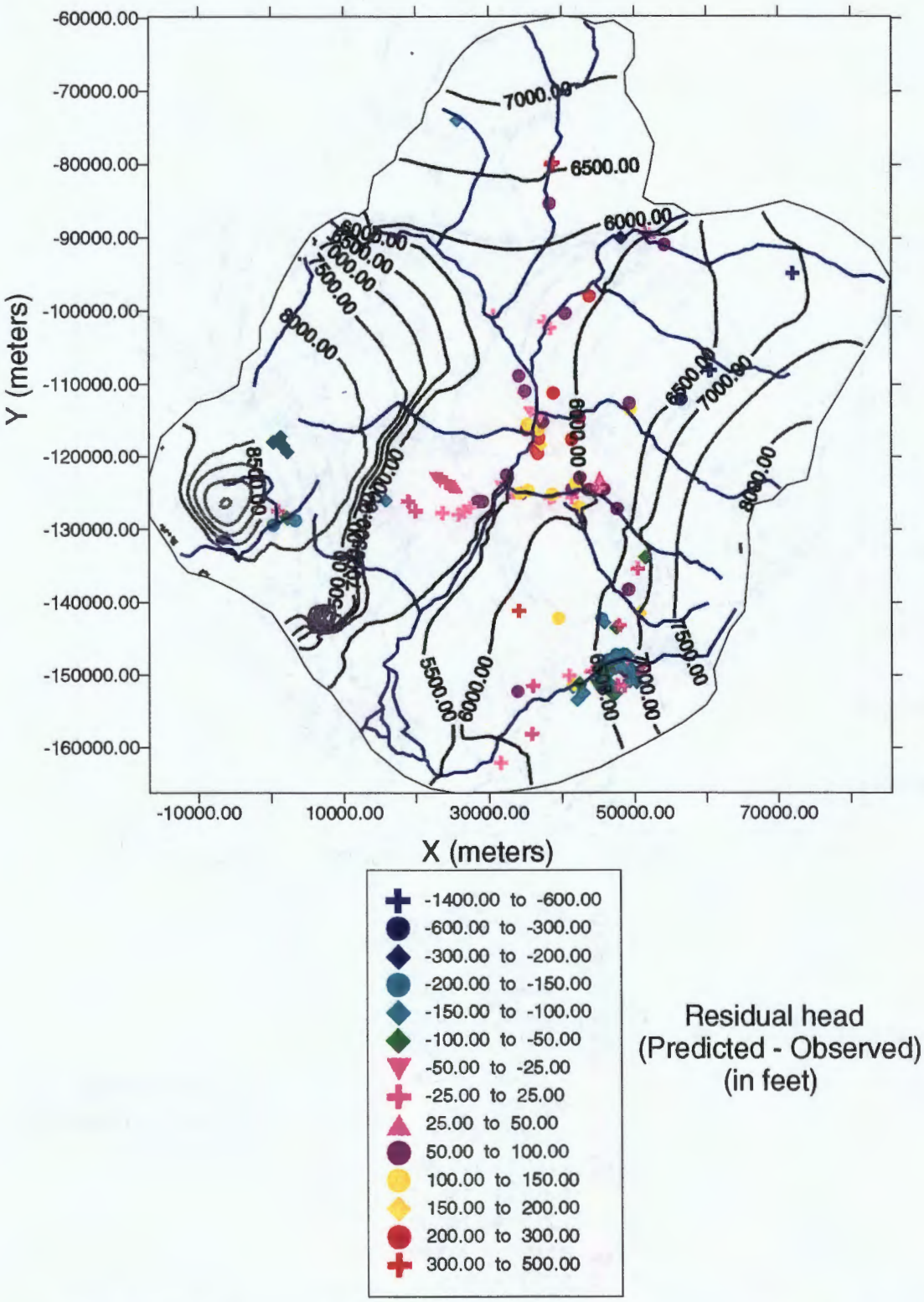

Figure 18. Simulated potentiometric surface and residuals using PEST-derived permeabilities

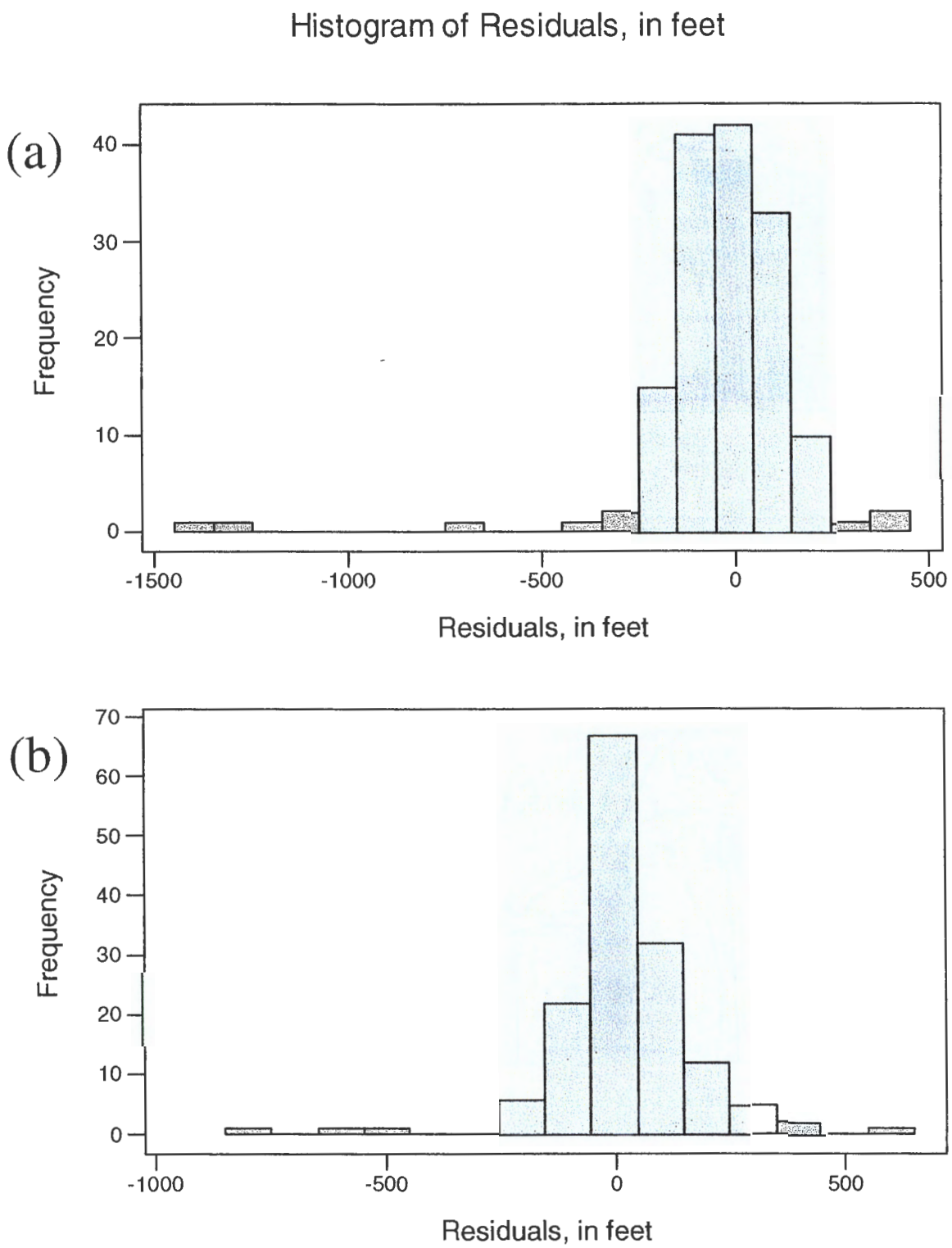

Figure 19. Histogram of residuals for (a) PEST calibration and (b) trial-and-error calibration

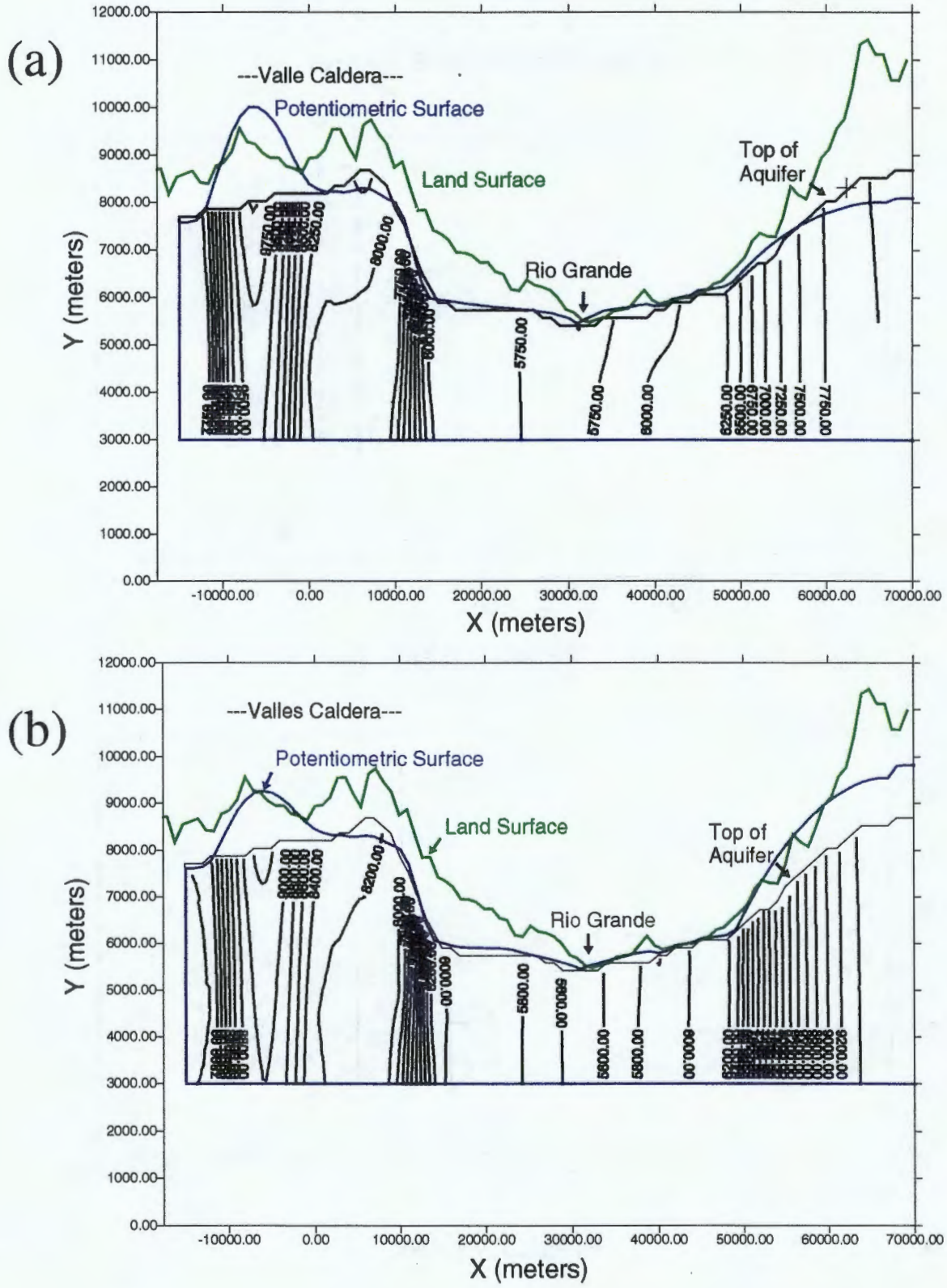

Figure 20. Cross-section showing simulated hydraulic head contours and potentiometric surface for (a) PEST calibration and (b) Trial-and-error calibration.

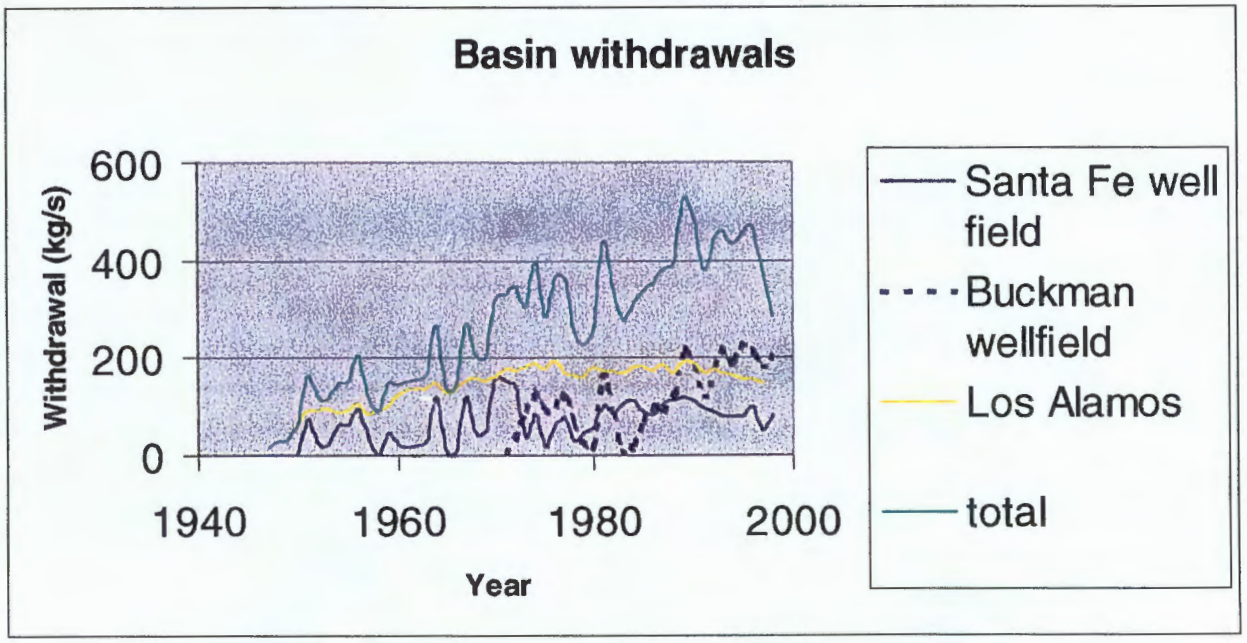

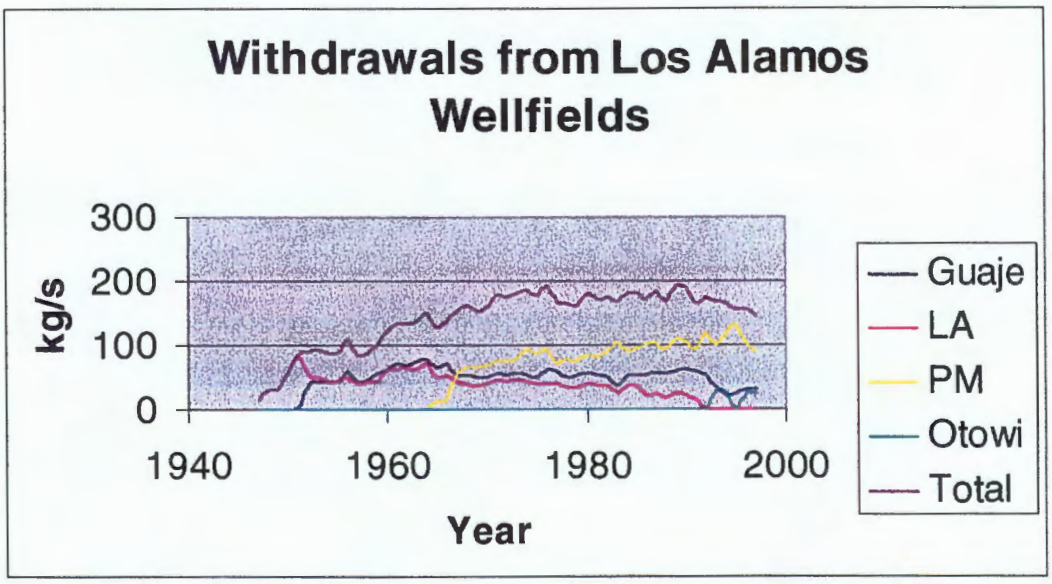

Figure 21. Withdrawals from wellfields within the Espanola Basin

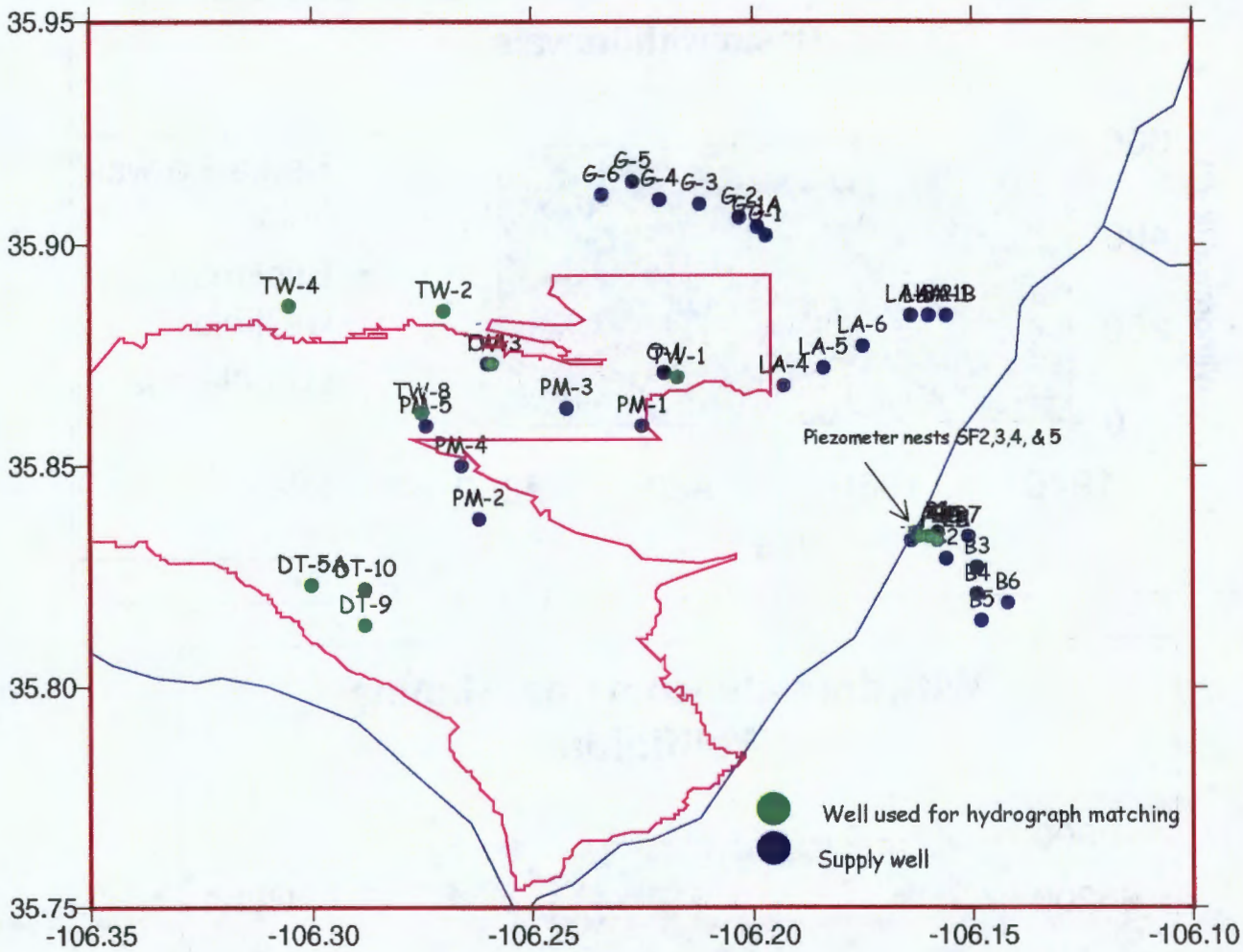

Figure 22. Location of pumping wells and wells with hydrographs in the vicinity of the Pajarito Plateau

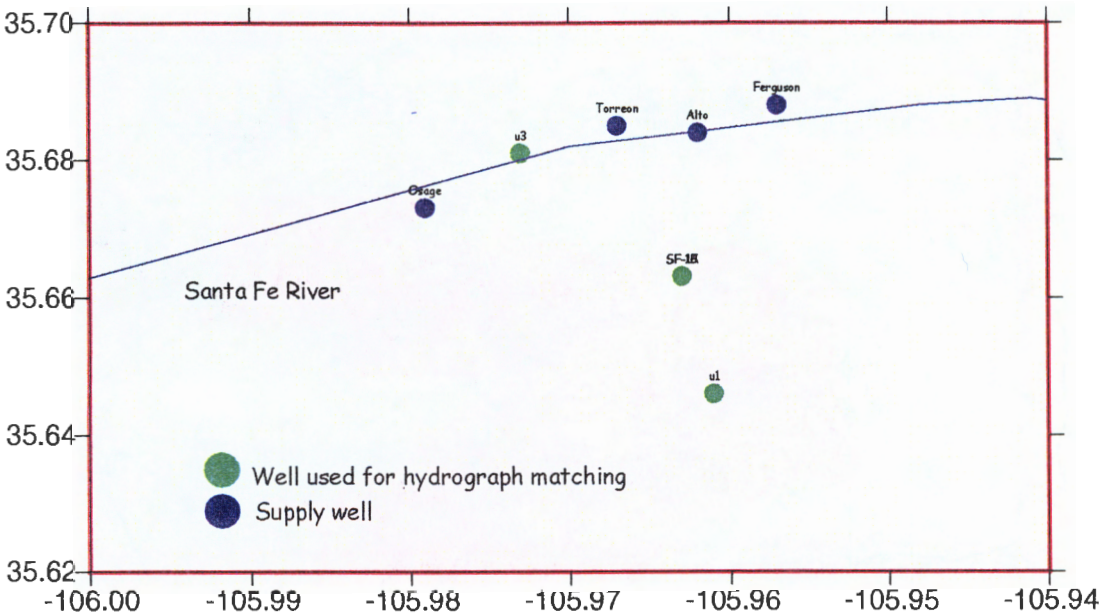

Figure 23. Location of pumping wells and wells with hydrographs in the vicinity of Santa Fe

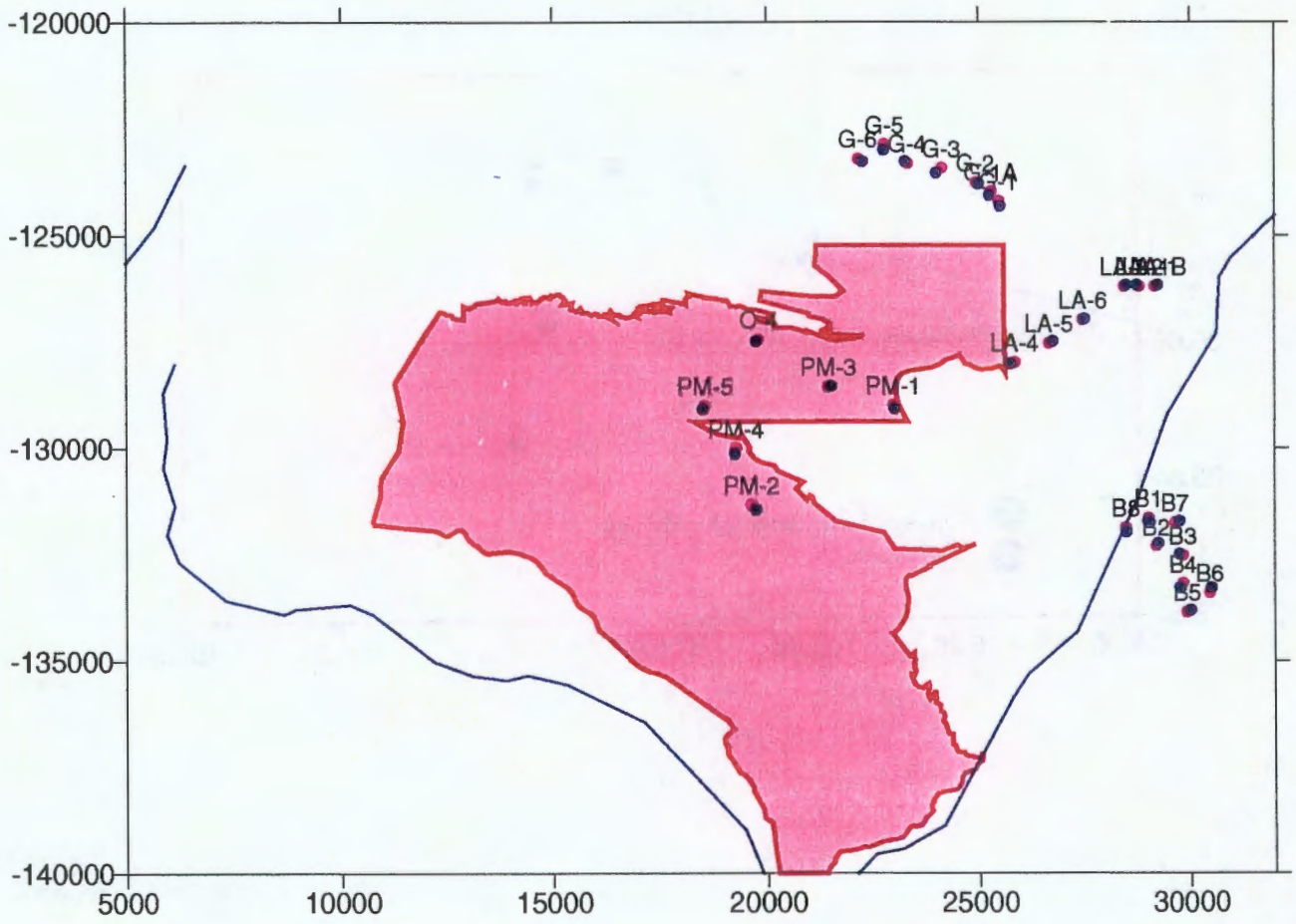

Figure 24. Water supply locations (pink) and grid nodes where pumping is simulted (blue)

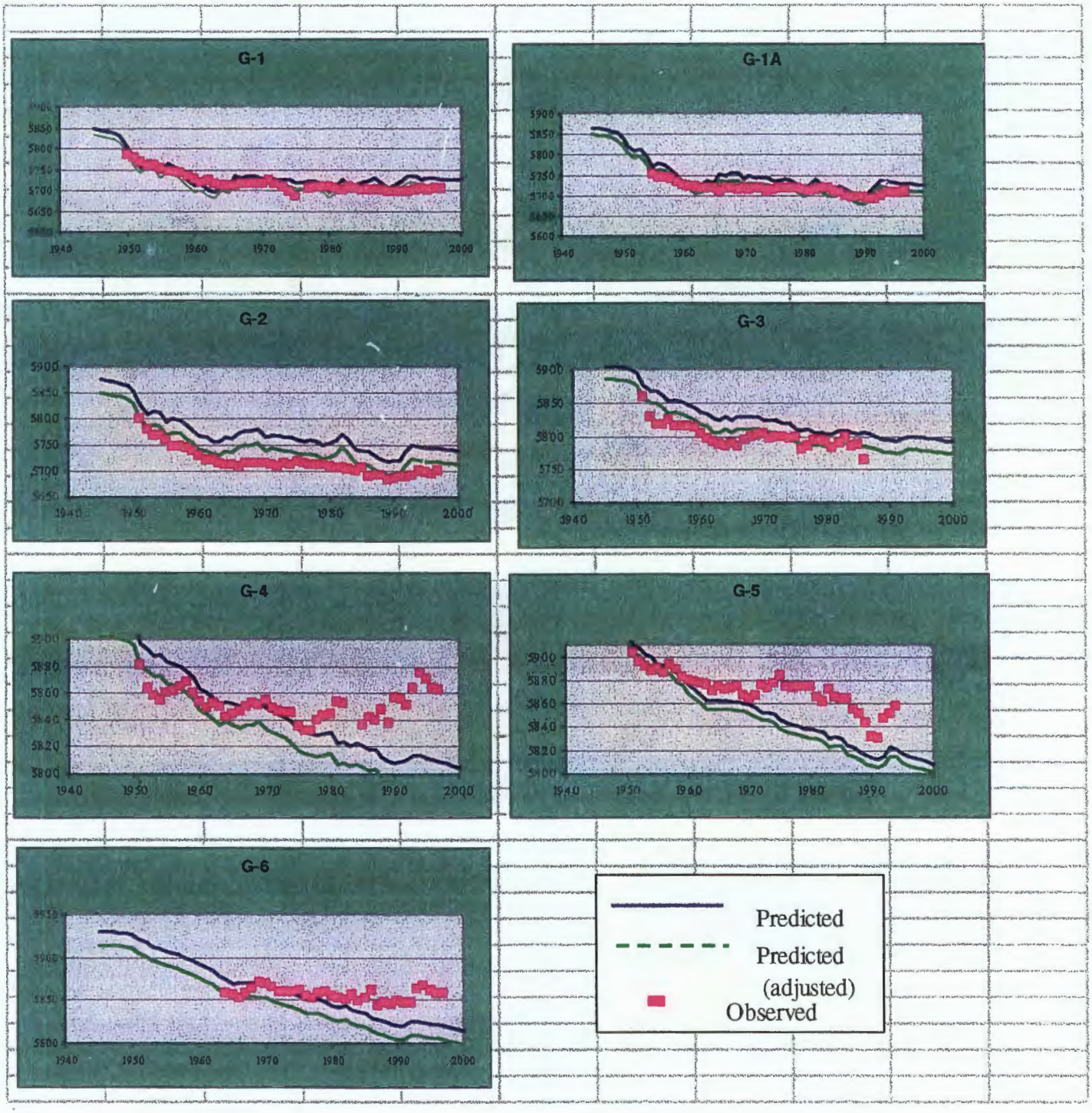

Figure 25. Comparison of predicted and observed water level changes in the Guaje well field. Green lines are model predictions offset to pass through the first data point.

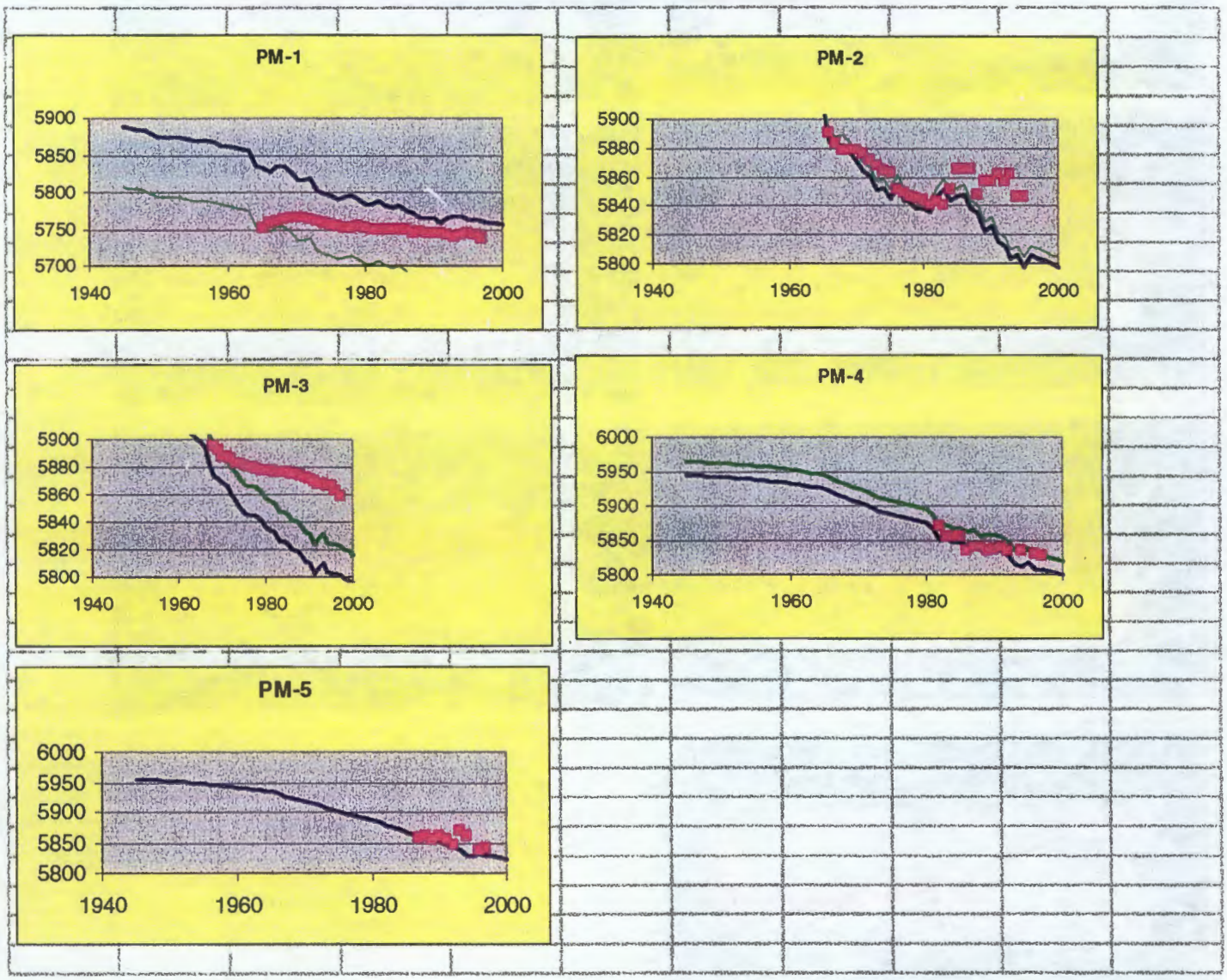

Figure 26. Comparison of predicted and observed water level changes in the Pajarito well field. Green lines are model predictions offset to pass through the first data point.

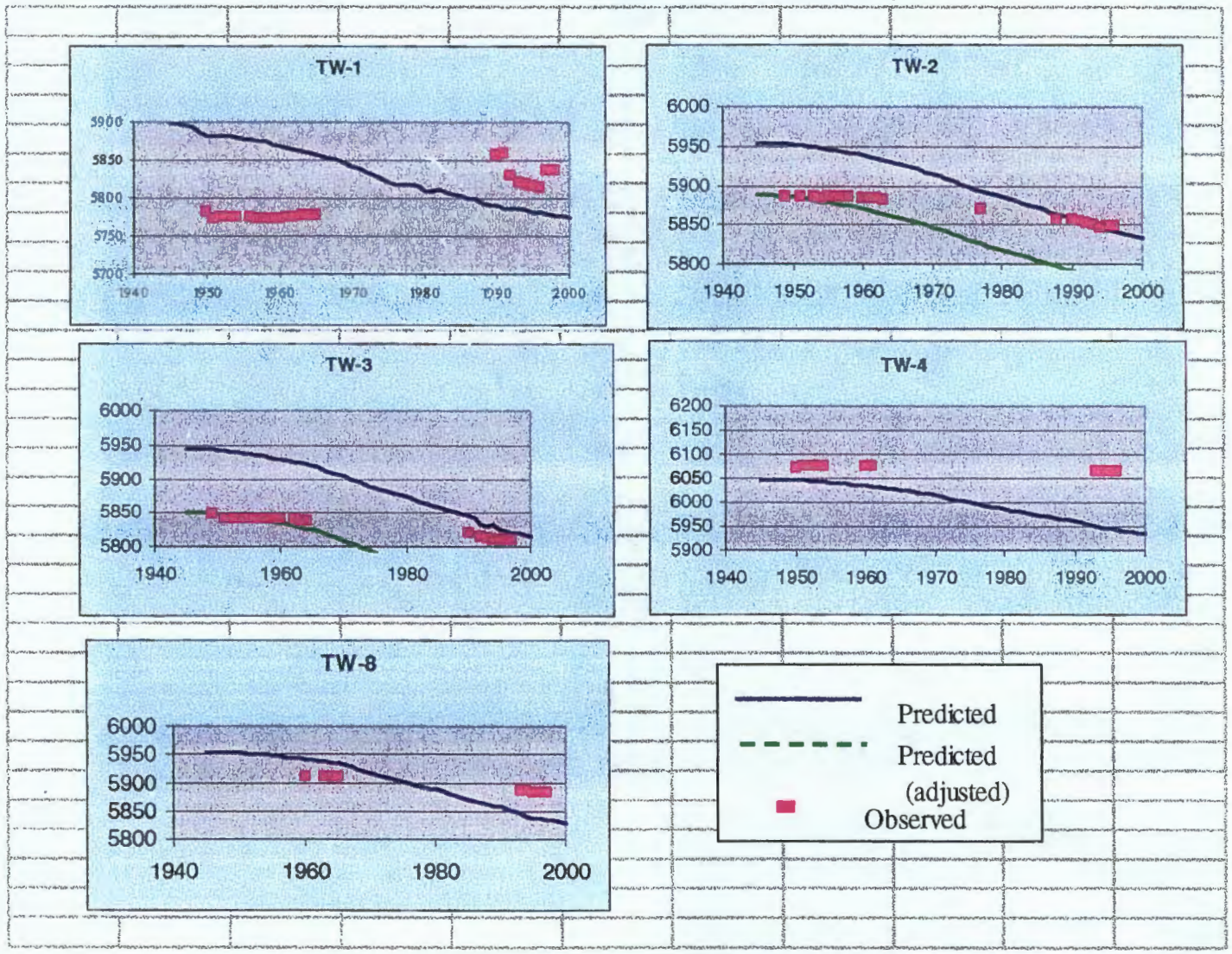

Figure 27. Comparison of predicted and observed water level changes in the test wells. These wells are all more shallow that the screened intervals in water supply wells. Green lines are model predictions offset to pass through the first data point.

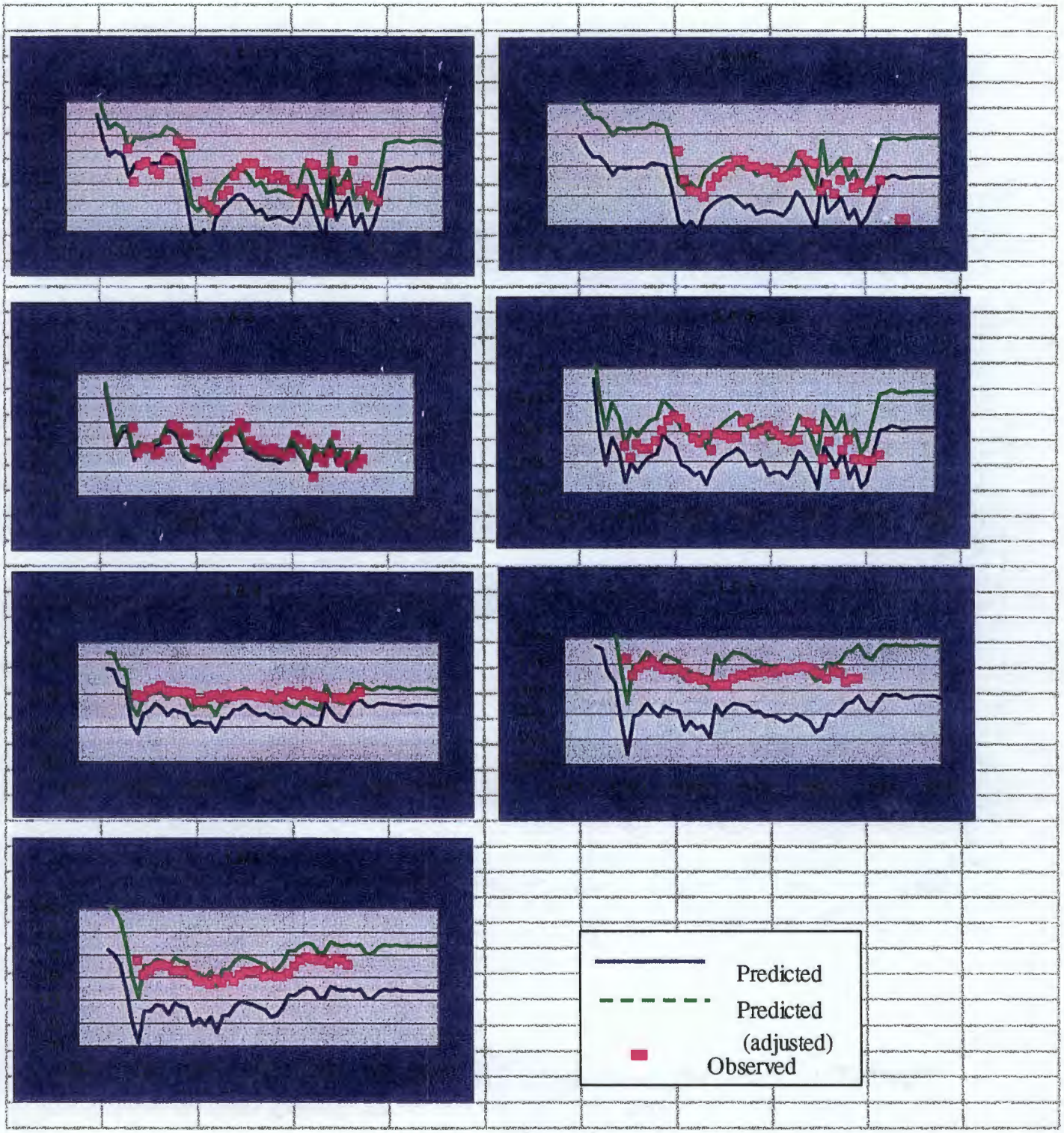

Figure 28. Comparison of predicted and observed water level changes in the Los Alamos well fields. Green lines are model predictions offset to pass through the first data point.

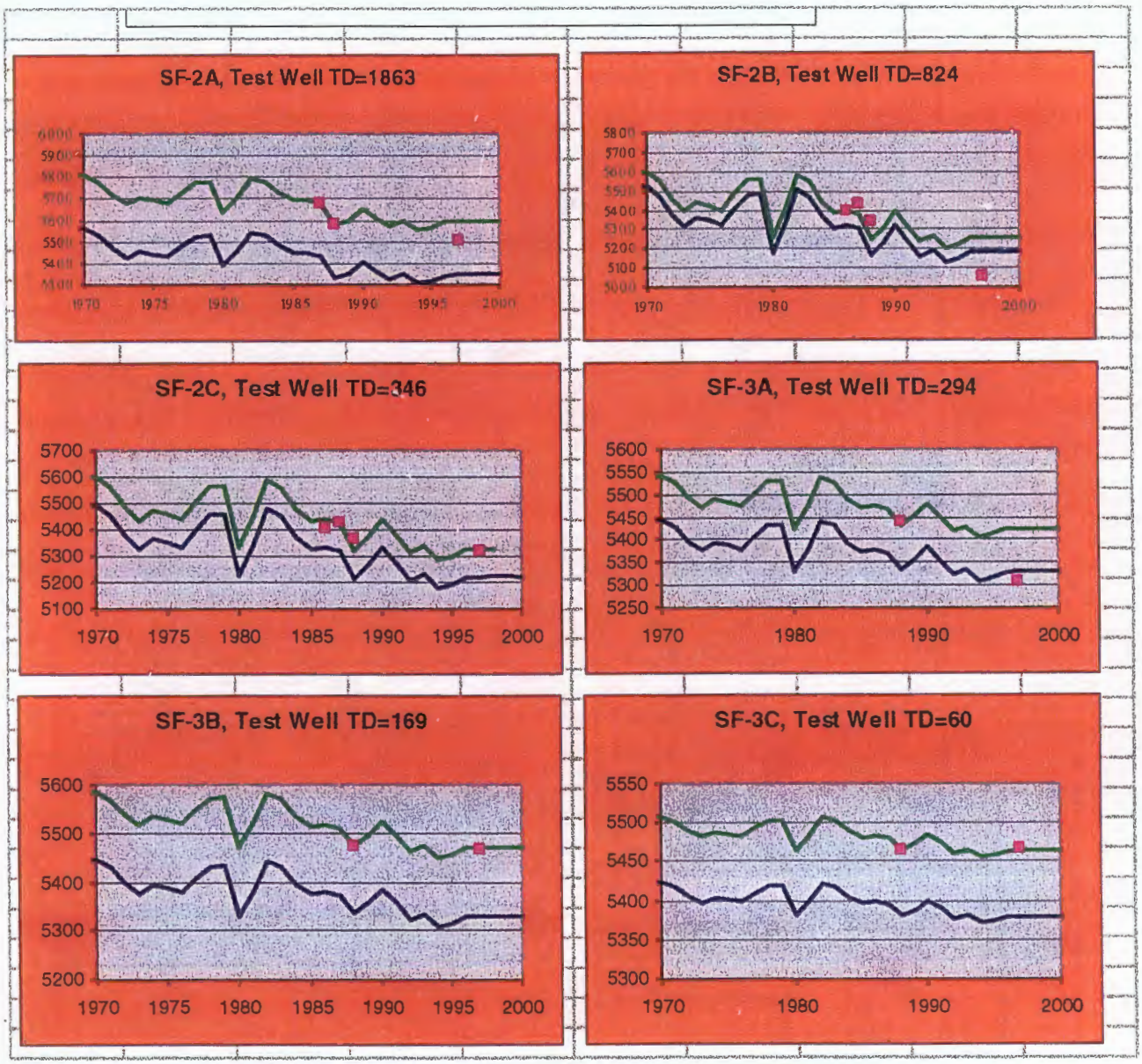

Figure 29(a). Comparison of predicted and observed water level changes in the Buckman well field.

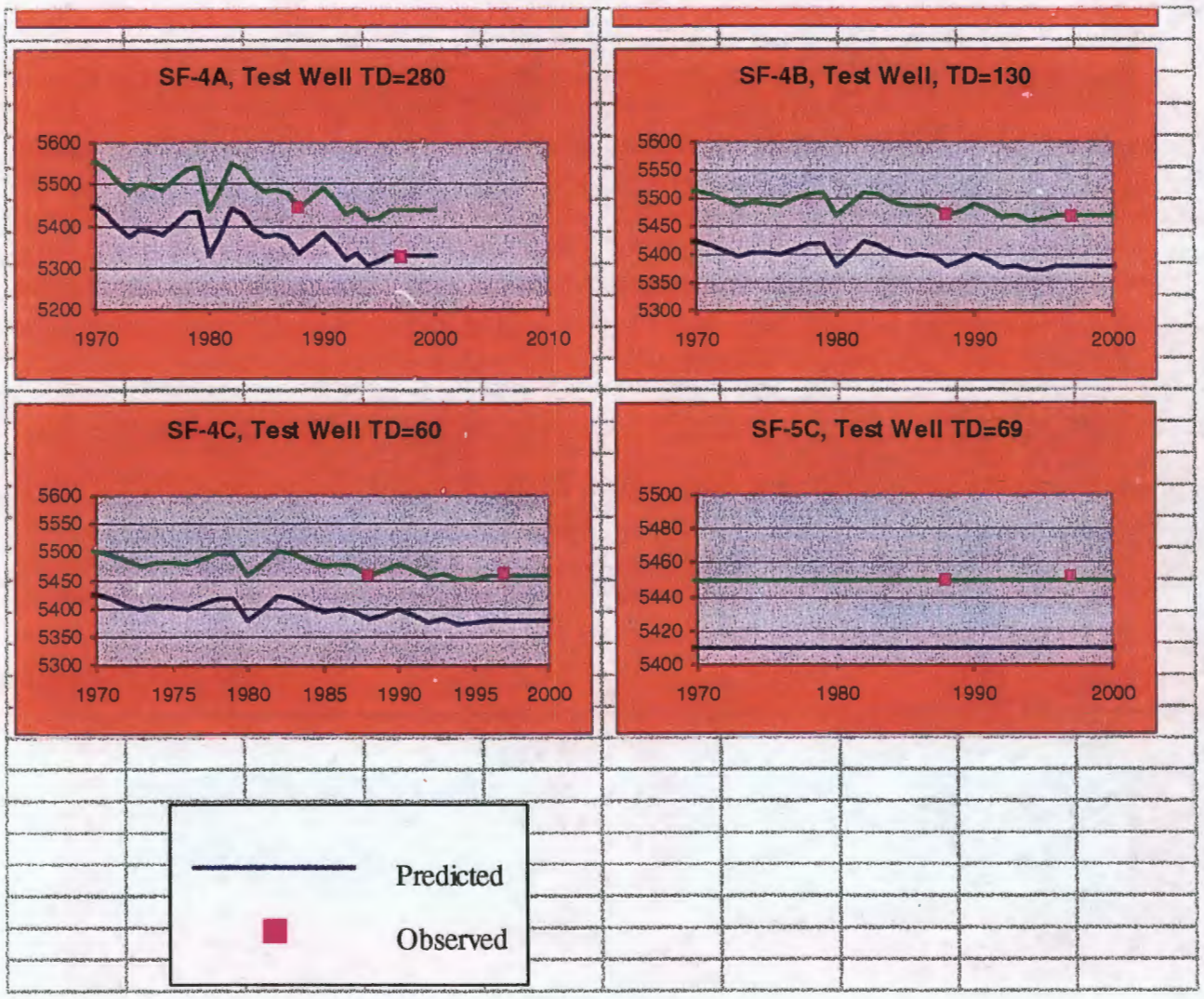

Figure 29(b). Comparison of predicted and observed water level changes in the Buckman well field.